KAUNAS UNIVERSITY OF TECHNOLOGY

YAN DANYLIV

SYNTHESIS AND INVESTIGATION OF PROPERTIES OF DONOR-ACCEPTOR MATERIALS EXHIBITING AGGREGATION-INDUCED EMISSION ENHANCEMENT

DOCTORAL DISSERTATION

Technological Sciences, Materials Engineering (T 008)

2019, Kaunas

KAUNAS UNIVERSITY OF TECHNOLOGY

YAN DANYLIV

DONORINES IR AKCEPTORINES GRUPES TURINČIŲ MEDŽIAGŲ, PASIŽYMINČIŲ AGREGACIJOS SUSTIPRINAMA EMISIJA, SINTEZĖ IR SAVYBIŲ TYRIMAS

TABLE OF CONTENTS

LIST OF ABBREVIATIONS

(fbi)$_2$Ir(acac)	Bis(2-(9,9-diethyl-fluoren-2-yl)-1-phenyl-1H-benzo[d]imidazolato)(actylacetonate)iridium(III)
(pq)$_2$Ir(acac)	Iridium(III)bis(2-phenylquinoline-N,C2′)acetylacetonate
ACQ	Aggregation-induced quenching
AIE	Aggregation-induced emission
AIEE	Aggregation-induced emission enhancement
BODIPY	Boron-dipyrromethene derivative
Btp$_2$Ir(acac)	Bis(2-(2'-benzothienyl)pyridinato-N,C3') iridium (acetylacetonate)
CBP	4,4′-Bis(N-carbazolyl)-1,1′-biphenyl
CE	Current efficiency
CELIV	Charge extraction by linearly increasing voltage technique
CT	Charge Transfer
CV	Cyclic voltammetry
D-A/D-A-D	Donor-acceptor/donor-acceptor-donor
DF	Delayed fluorescence
DPEPO	Bis[2-(diphenylphosphino)phenyl] ether oxide
DSC	Differential scanning calorimetry
EA$_{CV}$	Electron affinity measured by CV
EA$_{PE}$	Electron affinity measured by photoelectron emission method
EBL	Electron-blocking layer
E$_g{}^{CV}$/ E$_g{}^{opt}$	Electrochemical/optical band gap
EIL	Electron-injection layer
EL	Emissive layer
EQE/ η_{ext}	External quantum efficiency
E$_S$	Energy of singlet state
E$_T$	Energy of triplet state
ETL	Electron-transporting layer
FIrpic	Iridium(III)bis(4,6-di-fluorophenyl)-pyridinato-N,C2')picolinate
FT-IR	Fourier-transform infrared spectroscopy
HBL	Hole-blocking layer
HIL	Hole-injection layer
HOMO	Highest occupied molecular orbital
HTL	Hole-transporting layer
ICT	Intramolecular charge transfer
IP$_{CV}$	Ionization potential measured by CV
IP$_{PE}$	Ionization potential measured by photoelectron emission method
IQE	Internal quantum efficiency
Ir(piq)$_3$	tris(1-phenylisoquinoline)iridium(III)
Ir(ppy)$_2$(acac)	bis(2-phenylpyridine)iridium(III)acetylacetonate
Ir(ppy)$_3$	tris(2-phenylpyridine)iridium
ISC	Intersystem crossing

ITO	Indium-tin oxide
LED	Light-emitting diode
LUMO	Lowest unoccupied molecular orbital
mCP	1,3-Bis(N-carbazolyl)benzene
Me	Methyl
MS	Mass spectrometry
NMR	Nuclear magnetic resonance
OFET	Organic field-effect transistor
OLED	Organic light-emitting diode
OMe	Methoxy
OPVC	Organic photovoltaic cell
PE	Power efficiency
Ph	Phenyl
PhOLED	Phosphorescent OLED
PLQY	Photoluminescence quantum yield
PtOEP	2,3,7,8,12,13,17,18-Octaethyl-21H,23H-porphine platinum(II)
RIR/RIV/RIM	Restricted intramolecular rotation/vibration/motion
RISC	Reversed intersystem crossing
TADF	Thermally activated delayed fluorescence
T_c	Temperature of crystallization
T_d	Temperature of degradation (5% weight loss)
TD-DFT/DFT	Time-dependent density functional theory
T_g	Glass-transition temperature
TGA	Thermogravimetric analysis
T_m	Melting temperature
TOF	Time-of-flight
T_{s-s}	Temperature of solid-solid phase transition
TTA	Triplet-triplet annihilation
t_{tr}	Transit times
UV-VIS	Ultraviolet-visible
$\lambda_{abs}/\lambda_{em}$	Wavelength of maximum absorption/emission
τ	Excited-state lifetime
χ	Estimated error
Φ	Quantum yield
ΔE_{S-T}	Singlet-triplet energy gap

1. INTRODUCTION

"Edison's electric light did not come about from the continuous improvement of the candles."

— *Dr. Oren Harari*

Since ancient times mankind was curious about the construction of the world. In that time people were frightened of natural phenomena and, considering this, even believed that they had supernatural origin. However, with the evolution of consciousness, humanity started intensive investigation of the laws of nature. In the middle ages, many great scientists lightened the path of knowledge with their important investigations. In the very beginning of the 19th century, a new era in science started with the construction of the first electric cell performed by Volta[1]. Further investigation of the electricity phenomenon performed by Nikola Tesla, increasing popularity and affordability of electrical power made possible the development of such technical innovations as the telephone and radiotelegraphy[2]. Starting from 20th century, the speed of development of technologies increased considerably and, as a result, many inventions were developed in the field of electronics, such as: the diode (1904)[3], the triode (1906)[4], the light-emitting diode (1927)[5], and the transistor (1947)[6]. Parallel progress in organic chemistry, the rising price of manufacturing and materials and public interest in environmentally-friendly electronics led to the creation of the first organic transistor and the first organic light-emitting diode in 1987[10].

As a result, during last thirty years, organic materials appeared among the most important components of devices of organic electronics. Organic compounds are used in organic light-emitting diodes (OLED), organic photovoltaic cells (OPVC), organic field-effect transistors (OFET), and lasers[7]. Many commercial companies have utilized these technologies to develop important consumer products, such as smartphones, smartwatches and wearable healthcare electronics, medical equipment and environmentally-friendly energy sources

Currently, researchers are highly interested in the development of novel organic materials suitable for application in OLEDs and other optoelectronic devices, due to a high interest from the industry. To achieve state-of-the-art OLED performance, organic materials have to fulfill a number of requirements, such as: thermal and electrochemical stability, suitable morphological properties of their layers and appropriate photophysical and charge-transporting properties. The implementation of recently discovered phenomena of thermally activated delayed fluorescence (TADF)[47] and aggregation-induced emission enhancement (AIEE)[72] are highly recommended to achieve the best performance and cost-effectiveness of organic-light emitting devices. In addition, the costs of fabrication are of great importance in utilizing organic materials in electronics. Due to high demands of the industry, the production cost of OLEDs still remains relatively high and any possible solution of

this issue is crucial for a wide application of OLED technology. Taking these considerations into account, the importance of investigations related to the design and synthesis of novel materials with improved physical properties, cost-effectiveness and suitability for application in highly efficient OLEDs is very high.

The aim of this work was to design, synthesize and investigate the physical properties of new low-molar-mass donor-acceptor heterocyclic organic electroactive compounds demonstrating aggregation-induced emission enhancement with the potential application in OLEDs.

The tasks set to achieve the above stated aim:

• To design, synthesize and investigate the physical properties of carbazole-substituted chloropyridines and analyze the influence of the number of carbazolyl-moieties on the physical properties.

• To design, synthesize and investigate the physical properties of phenyl-linked carbazole-imide derivatives with different acceptor nature.

• To investigate the photophysical and electrochemical properties and the structure-properties relationship of the 1,3-thiazole-based organoboron complexes.

• To perform theoretical quantum chemical calculations and structural analysis of abovementioned materials and estimate the applicability of the studied materials in electroluminescent devices.

The key statements of the doctoral dissertation:

• The presence of a strong acceptor with structural units which restricts intramolecular rotations and vibrations in low-molar mass donor-acceptor materials allows to achieve a combination of thermally-activated delayed fluorescence (TADF) and aggregation-induced emission enhancement.

• 1,3-Thiazole-based organoboron complexes exhibit very high photoluminescence quantum yields with sharp peaks of emission.

• Carbazole-imide donor-acceptor materials demonstrate thermally-activated delayed fluorescence and aggregation-induced emission enhancement properties with intramolecular charge-transfer implemented through space.

The novelty of the work:

• New carbazole-chloropyridine donor-acceptor TADF/AIEE materials with deep-blue photoluminescence were designed, synthesized and characterized.

• Novel carbazole-imide conjugates displaying through-space charge transfer and exhibiting TADF and AIEE phenomena, were designed, synthesized, characterized and applied in OLEDs.

• Structure-properties relationship, photophysical and electrochemical properties of new 1,3-thiazole-based organoboron complexes were investigated with theoretical and experimental tools for the first time.

Personal input of the author

The author has designed, synthesized and purified the compounds described in Chapters 4.1 and 4.2. Organic materials described in Chapter 4.3. were synthesized by Dr. Potopnyk (Institute of Organic Chemistry, Polish Academy of Sciences). The author has performed theoretical calculations, structure analysis, UV-VIS absorption, photoluminescence including quantum yield and excited-state lifetime and cyclic voltammetry measurements. Measurements of thermal properties were done by Dr.

2. LITERATURE REVIEW

2.1 Organic materials for application in electronic devices

Over the past few decades, organic electronics became one of the most important fields of science for the humanity. Due to rapid evolution of microelectronic technologies, particularly, from classic inorganic semiconductors and transistors to their organic alternatives, the development of excellent consumer products such as: smartphones, smartwatches, affordable and portable solar cells, curved TV display panels, etc. became possible[8,9]. Huge consumer success and impressive technical abilities of novel electronic devices resulted in the necessity of further scientific investigations and developments in the field of organic electronics.

Nowadays, investigations and development in the scientific field of organic electronics mostly concentrated on three main types of possible applications: solar cells, transistors, and light-emitting devices. Light-emitting devices, in particular, are today definitely the fastest progressing branch of organic electronics. The first demonstration of effective and thin light-emitting electronic device — an organic light-emitting diode was presented to the public in 1987 by Tang and van Slyke[10]. Since that time, the efficiency of organic light-emitting diodes raised constantly. OLEDs became great alternatives to inorganic LED technology due to their unique advantages such as low-cost production, flexibility, and functionality.

Organic materials for application in electronic light-emitting devices can be divided into two groups: non-polymer materials or low-molar-mass compounds, and polymers. While low-molar-mass materials have a known and defined molecular weight and structure, the molecular weight of polymers is not precisely defined and the structure can be different in case of using copolymers. Also, the application of non-polymers and polymers in organic light-emitting devices is different; while non-polymers usually are vacuum deposited to obtain thin films, and the thickness of films is fully controllable, polymers are only applicable *via* solution-processed techniques such as the spin-coating method and, thus, the thickness of polymer films are usually uncontrollable. On the other hand, films constructed from low-molar-mass materials can demonstrate unexpected crystallization and molecular packing defects, while polymers have more predictable morphological properties.

A huge variety of applications of organic materials requiring a massive quantity of organic materials with different physical properties which can be achieved with a high tunability of organic materials. The high tunability of organic materials and their properties can be obtained by applying different electron-donating and electron-withdrawing fragments into an organic semiconductor structure. A combination of donating and accepting units allows to modify the photophysical, electrochemical and photoelectrical properties, chemical and thermal stability, morphology and many other parameters[11]. The nature and strength of donating and accepting units affects intramolecular charge-transfer properties, as well as π-electron delocalization, triplet energy value, etc.

Summarizing, organic compounds are multifunctional electronic semiconducting materials with great advantages, such as tunability and flexibility, and low-cost production. The impressive photophysical, charge-transporting and

morphological properties are achieved with a complex design of the chemical structure and an implementation of various electron-donating and electron-withdrawing moieties in the construction of the chemical structure. All these factors allow to create materials for application in very different electronic devices and as a result – in consumer products.

Recent achievements in the structural design and investigation of physical properties of the organic materials for the applications in organic light-emitting devices will be discussed in this review.

2.2 Approaches to improve OLED efficiency

Nowadays, OLED technology has become very commercialized, since such technical "giants" as Samsung, Apple and LG create many electronic products with OLED displays. Because of that, the improvement of OLED technology and the development of OLEDs with higher efficiency is the key point for researchers in the field of materials science all over the world. Generally, an OLED is assembled from a layer of organic electroluminescent material placed between the anode and cathode, all located on a substrate[12]. The organic molecules of EL material have semiconducting properties, thus, after current transmission through the OLED, holes and electrons are recombining inside the semiconducting electroluminescent material, which results in the emission of light[13].
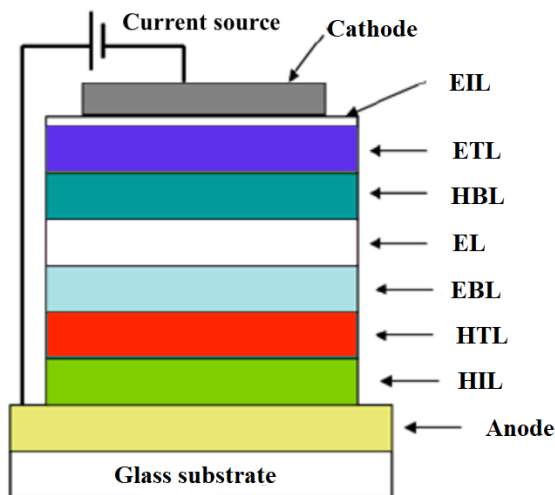
Fig. 2.1. A schematic diagram of a multilayer OLED structure

However, modern OLEDs evolved from a single-layer structure to a complicated multilayer structure (Fig. 2.1.), the construction of which is possible due to advance vacuum deposition techniques. This evolution occurred due to the low efficiency of single-layer OLEDs and, thus, a necessity of efficiency improvement. To boost the efficiency of organic light-emitting diode, the quantity of excitons recombined in the emissive layer has to be increased. The inclusion of additional layers of semiconducting materials, such as electron-injection (EIL), electron-transporting, (ETL), hole-blocking (HBL), electron-blocking (EBL), hole-

transporting (HTL) and hole-injection (HIL) will result in better charge transporting to the emissive layer (EL) followed by a higher conversion efficiency of excitons to light[14,15]. On the other hand, a multilayer structure of the OLED has some disadvantages as well. The accretion of layer quantity lead to an increase in device production cost, complicated production process and increased the thickness of a device. As a result, the design and synthesis of multifunctional materials for additional layers in OLEDs remains to be an important objective.

Introducing additional layers into an OLED structure is important to the OLED efficiency enhancement. However, another approach to enhance the efficiency of organic light-emitting diodes is utilizing the physical phenomena of thermally activated delayed fluorescence (TADF), aggregation-induced emission enhancement (AIEE) and phosphorescence emission. In recent years, a considerable amount of attention has been drawn to studying and investigating this physical phenomena.

2.2.1. Utilization of phosphorescent emitters for OLED efficiency enhancement

One of the most important approaches to improve device efficiency is the utilization of phosphorescent emission. It is a known fact that, during the recombination of electrons and holes in the emissive layer in an OLED formation ratio of excitons is 25% of singlet excitons and 75% of triplet excitons. Triplet excitons commonly decay non-radiatively at room temperature. However, several rare metal organometallic complexes with a heavy metal element such as Pt and Ir demonstrate the phenomenon of intersystem crossing implemented *via* strong spin-orbit coupling[16], thus singlet-triplet energy transfer became possible.

PtOEP   Btp$_2$Ir(acac)   Ir(piq)$_3$

Ir(ppy)$_3$ Ir(ppy)$_2$(acac)   FIrpic
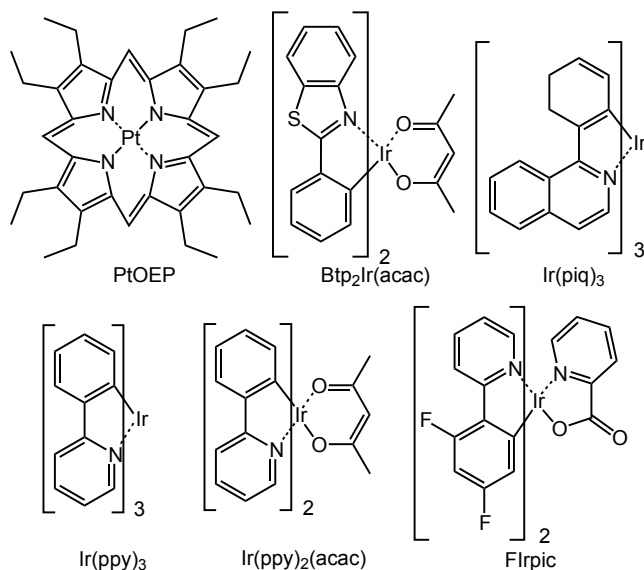
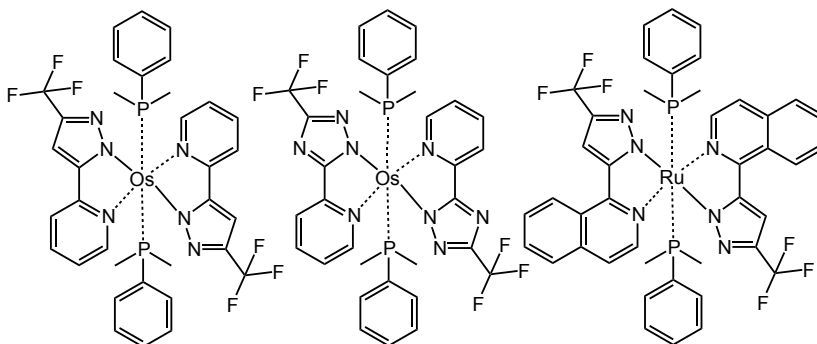**Fig. 2.2.** Pt- and Ir-containing phosphorescent emitting organometallic complexes

Hence, a red phosphorescent OLED were demonstrated by using 2,3,7,8,12,13,17,18-octaethyl-21H,23H-porphine platinum(II) (PtOEP)[17] and bis(2-

(2'-benzothienyl)pyridinato-N,C3') iridium (acetylacetonate) (Btp$_2$Ir(acac))[18] (Fig. 2.2.) as guest emitting materials achieving EQE value of 4% and 2.5%, respectively. Long operation lifetime red PhOLED presented by Meerheim *et al.*[19], based on tris(1-phenylisoquinoline)iridium(III) (Ir(piq)$_3$) emitter (Fig. 2.2.), exhibited impressive 10^7 hours of working time with initial brightness of 100 cd/m^2. Iridium(III)bis(4,6-di-fluorophenyl)-pyridinato-N,C2')picolinate (FIrpic) (Fig. 2.2.) is well known as an efficient blue emitter, with a photoluminescence emission peak at 470nm.

Efficient PhOLEDs using FIrpic as an emitter were reported to achieve 6%, 14% and 21% EQE[20,21,22]. However, it should be noted that the stability of FIrpic is relatively low, which results in a limitation of using this material in commercial applications due to short operating lifetime of the constructed devices. In addition, sky-blue electroluminescent emission of FIrpic does not fulfill the requirements for full color OLED displays.

Adachi *et. al.* report obtaining efficient green PhOLEDs based on bis(2-phenylpyridine)iridium(III)acetylacetonate (Ir(ppy)$_2$(acac)) (Fig. 2.2.) emitter achieving an EQE value of 19%[23], and those based on tris(2-phenylpyridine)iridium (Ir(ppy)$_3$) (Fig. 2.2.) which achieve a value of 15% of external quantum efficiency[24].

Sometimes, not only Pt and Ir organometallic complexes are investigated for use as emitting materials in PhOLEDs. It is also possible to use Osmium and Ruthenium complexes in phosphorescent emitting devices[25]. Effective red PhOLEDs with EQE of 13% and 20% were constructed[26] based on Osmium complexes (Fig. 2.3.). In addition, a red PhOLED was created using Ruthenium organometallic complexes achieving a promising EQE value of 7%[27] (Fig. 2.3.).

Fig. 2.3. Os- and Ru-containing phosphorescence emitting organometallic complexes

Recently, copper-containing organometallic complexes attracted some attention as potentially useful for application in PhOLEDs. Several studies investigate Cu-based complexes, particularly, their interesting properties – cuprophilic interactions inside the complex followed by an exhibition of both phosphorescence emitter properties and TADF[28] (Fig. 2.4. (a)). Another work, published by Wu *et. al.*[29], relates to the construction of a PhOLED based on bis(pyrazol-1-ylmethyl)-pyridine – Cu (I) derivatives (Fig. 2.4. (b)) used as a phosphorescent emitter.
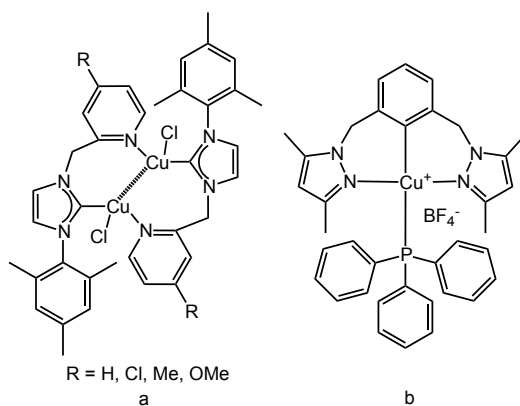
Fig. 2.4. Cu-containing organometallic complexes

The obtained yellow PhOLED turns on at 7 V and achieves the maximum brightness of 850 cd/m^2 and the maximum EQE of 1.0%. These results are hardly impressive, although, PhOLEDs based on Cu-containing complexes can be regarded as promising for further investigation and improvement, especially due to much lower production price as compared to PhOLEDs based on complexes containing very expensive platinoids.

The development of emitter materials is very important for creating high-efficiency PhOLEDs, however the implementation of a suitable host material is very important. The host materials have to meet a lot of requirements, for example: possess higher triplet energy value compared to the guest emitter, demonstrate high thermal and electrochemical stability and exhibit balanced charge-transporting properties. In addition, the ionization potential and electron affinity of the host material should have a small difference with the neighboring layers for reducing the injection barrier for holes and electrons. Morphological properties of host materials are also very important. The host-emitter system in a light-emitting device technically is a solid solution, so an appropriately selected host also reduces aggregation and intramolecular interactions between emitter molecules[30]. As a result, the design and synthesis of new organic materials which could be used as promising multifunctional host materials have attracted a lot of attention over the last years.

Triarylboron derivatives can be selected as suitable host materials due to their capability to show electron-transporting properties caused by sufficient electron-withdrawing abilities[31]. The group of Zhang *et. al.*[32] have synthesized a material constructed from triarylboron moiety core with three oligofluorene arms (DBF1). The triplet energy of this host material is high enough (2.76 eV) to perform efficient energy transfer to phosphorescent emitters for green PhOLEDs. DBF1 (Fig. 2.5.) was used as a host for green emitter Ir(ppy)$_3$ in the construction of solution-processed PhOLED achieving maximum external quantum efficiency (EQE), power efficiency (PE) and current efficiency (CE) of 7.38%, 13.14 lm/W and 25.10 cd/A.

Aromatic silane derivatives are well known for their great thermal and morphological stability and ability of glass-formation. In addition, silicon atoms in such structures are usually bonded to four carbon atoms with sp^3 orbital hybridizations

which "break" the π-conjugation and, thus, increases the total triplet energy value of the molecule. Therefore, silicon-based organic materials are capable of high performance as host materials for PhOLEDs.
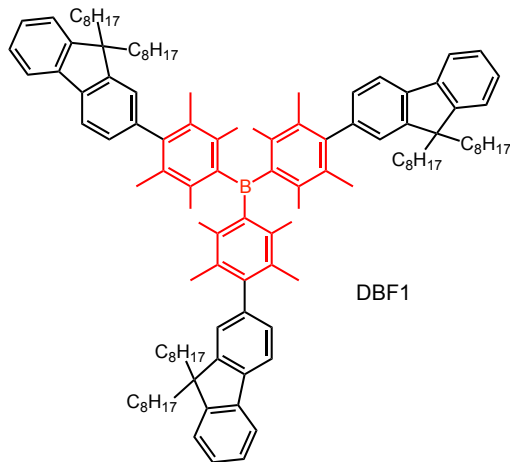
Fig. 2.5. The structure of trialrylboron-containing host material DBF1 for green PhOLEDs

Highly efficient blue PhOLEDs were constructed with polyarylsilane materials UGH1, UGH2 and UGH3 as hosts (Fig. 2.6.), reported by Thompson *et. al.*[33,34] as achieving 7.0%, 9.1% and 8.8% of maximum external quantum efficiencies, respectively, when utilizing FIr6 as a guest emitter.
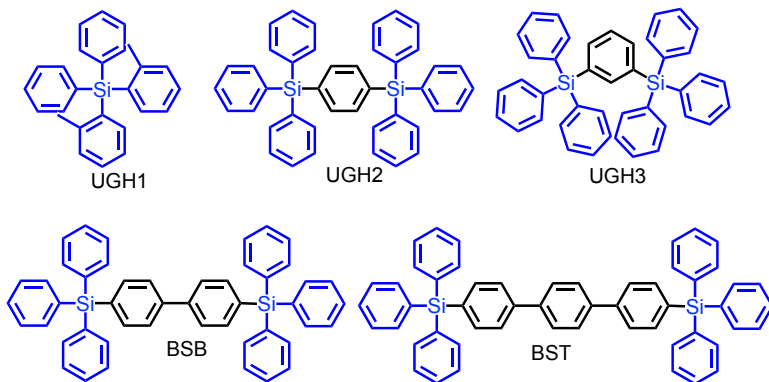
Fig. 2.6. Polyarylsilane host materials for phosphorescent emitters

These materials demonstrate an impressive high triplet energy level value of 3.5 eV, which makes them very convenient materials for constructing blue-emitting PhOLEDs. Another work by Cheng *et. al.*[35] investigated polyarylsilane materials with a prolonged π-conjugation chain obtained by including biphenyl and terphenyl linkers between silicon atoms (Fig. 2.6.). Increased molecular weight and improved conjugation of BSB and BST materials reduces E_T values to 2.76 eV and 2.58 eV, although the morphological properties of these materials improve dramatically. Glass-transition temperatures increase to 100°C and 113°C for BSB and BST compounds,

respectively, comparing to UGH1 and UGH3, which have T_g value lower than 50°C. While BST-based blue PhOLED doped by FIrpic exhibited moderate effectiveness: 2.9% EQE with CE 6.0 cd/A and PE 2.0 lm/W, BSB-based blue PhOLED with the same FIrpic dopant achieved an impressive 14.7% of maximum external quantum efficiency, followed by CE value of 30.4 cd/A and PE value of 7.4 lm/W. These results, can be explained by a much higher and more suitable triplet energy value of BSB material as compared to BST and better morphological properties as compared to UGH1, UGH2 and UGH3.

Carbazole-based compounds are well-known host materials, due to their impressive characteristics such as high triplet energy value, thermal and electrochemical stability and promising hole-injection and hole transporting properties provided by a lone electron pair based on sp^3-hybridized nitrogen atom. Well-known carbazole hosts CBP (4,4'-bis(9-carbazolyl)-biphenyl), CDBP (4,4'-bis(9-carbazolyl)-2,2'-dimethyl-biphenyl) and mCP (3,5-bis(9-carbazolyl)benzene) are recognized as one of the most advanced hosts utilized for the development of PhOLEDs[36,37]. However, despite massive advantages of CBP, such as good hole-injection and hole-transporting properties, CBP demonstrates some shortcomings, such as low T_g of 62°C, and a low E_T of 2.56 eV, which makes it impossible to utilize for the construction of blue PhOLEDs. As a result, multiple attempts have been made to improve the CBP properties by adjusting its chemical structure. Yang *et. al.*[38] performed structure modification and synthesized two CBP isomers – m-CBP and o-CBP (Fig. 2.7.). The twisted structure of obtained isomers strongly affected the triplet energy value, and as a result, m-CBP and o-CBP demonstrated impressive 2.84 eV and 3.00 eV, respectively. In addition, thermal properties were also improved, glass-transition temperatures increased to the value of 97°C and 82°C for m-CBP and o-CBP, respectively. This modification made it possible to use these materials in blue PhOLEDs with a FIrpic emitter achieving the maximum current efficiency of 18.6 cd/A, the maximum power efficiency of 11.3 lm/W, and the maximum external quantum efficiency of 8.7% for m-CBP:FIrpic system and the maximum CE of 29.9 cd/A, maximum PE of 25.3 lm/W, and maximum EQE of 14.2% for o-CBP:FIrpic system. Comparing to aCBP-based PhOLED authors achieved an improvement of nearly two times of the light-emitting device characteristics.
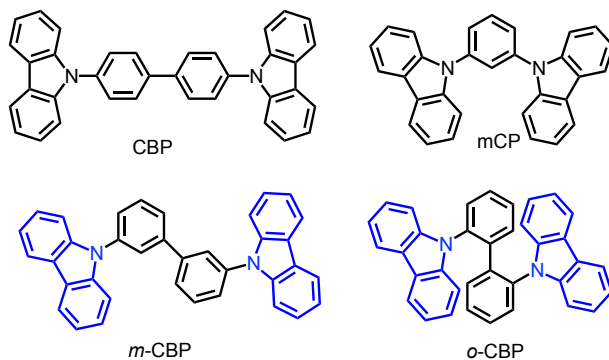
Fig. 2.7. Carbazole-based hosts for phosphorescent emitters

Aromatic phosphoryl derivatives have been widely used as host materials in OLEDs due to excellent electron-transporting properties caused by the presence of strongly-polarized P=O group. Arylphosphoryl-based compounds usually demonstrate high triplet energy values and decent thermal stability, due to their bulky size and weak π-conjugation. These properties make them suitable candidates for utilization in all types of PhOLED and especially in blue-emitting devices.

One of the most noteworthy arylphosphoryl hosts were synthesized and investigated by Lee and colleagues[39]. Diphenylphosphine oxide moiety was attached to spirobifluorene core at different positions, obtaining four materials SPPO1, SPPO2, SPPO11 and SPPO13 (Fig. 2.8.).
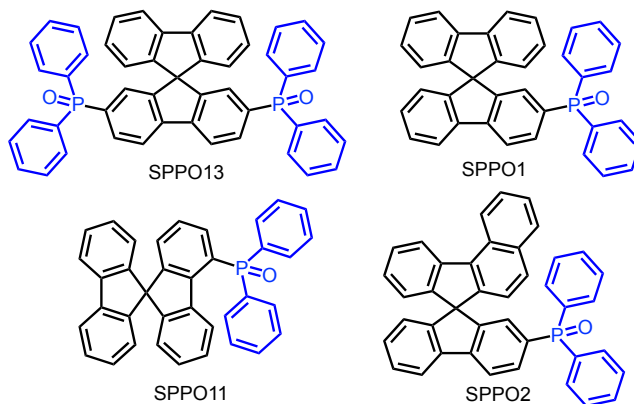
Fig. 2.8. Arylphosphoryl-based hosts for red and blue phosphorescent emitters

These materials exhibited impressive thermal stability and glass-forming ability with T_g in the range of 96–127°C, and SPPO1, SPPO11, SPPO13 demonstrated relatively high triplet energy level values of 2.77 eV, 2.78 eV and 2.73 eV, respectively. Highly efficient blue PhOLEDs were created with FIrpic dopant with these host materials, achieving impressive characteristics: 15.6% EQE for SPPO1, 17.2% EQE with SPPO11 and 19.6% EQE with SPPO13. Regardless the fact that SPPO2 demonstrated a relatively low E_T value of 2.4 eV, it was possible to utilize the material with a red phosphorescence emitter (pq)$_2$Ir(acac) creating a high-performance red PhOLED with the maximum EQE of 14.3%. These results clearly show great potential of diphenylphosphoryl-based materials in the construction of efficient phosphorescent devices.

The most effective approach to design a bipolar host material for PhOLEDs is to design and investigate the superior combination of donor and acceptor moieties for achieving high E_T, decent charge-carrier properties, thermal stability and morphological characteristics. The main advantage of bipolar host materials is the arrangement of good hole-injection/hole-transporting properties and good electron-injection/electron-transporting properties at the same time. However, in order to achieve high electroluminescence effectiveness in a PhOLED, the intramolecular donor-acceptor charge transfer in the host material should be minimized. Hence, the design of bipolar hosts should be performed very thoughtfully and carefully.

Carbazole is admittedly one of the most effective donor fragments due to its thermal stability, high triplet energy value, sufficient hole transporting ability and a variety of modification possibilities. On the other hand, there is a huge variety of electron-withdrawing fragments which can be connected to carbazole, such as sp^2-hybridized nitrogen heterocycles, arylnitriles, arylphosphoryl units, etc. Therefore, a huge variety of host materials can be developed for implementation in PhOLEDs.

Hudson et al.[40] replaced of one of the phenyl rings in the abovementioned CBP host to a pyridine or a pyrimidine ring to obtain effective bipolar hosts CPPY and CPHP (Fig. 2.9.).
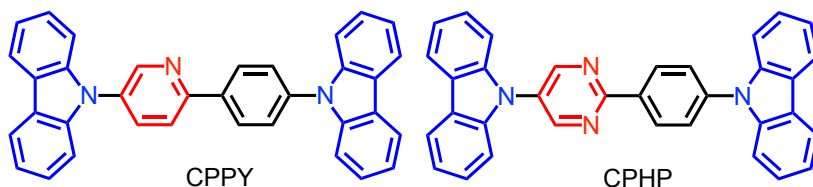
Fig. 2.9. N-heterocycle-based bipolar host materials for PhOLEDs

The synthesized materials were found to have a slightly lower E_T (2.62 eV for CPPY and 2.61 for CPHP) as compared to CBP (2.67 eV), although the electron-injection ability was greatly improved, which resulted in the construction of highly effective green PhOLEDs using (ppy)$_2$Ir(acac) as a guest emitter. CPPY-based device demonstrated EQE value of 21.5%, CE value of 74.9 cd/A and PE value of 56.3 lm/W, while CPHP-based PhOLED exhibited impressive 26.8% of EQE, 92.2 cd/A of CE and 106 lm/W of PE. In comparison, same-structured CBP-based device showed 13.3%, 54.3 cd/A and 36 lm/W EQE, CE and PE values, respectively.

Another successful attempt to modify well-known host materials mCP and CBP was made by introducing a cyano group into the molecular structure to obtain bipolar host materials mCPCN[41] and CBPCN[42] (Fig. 2.10.).
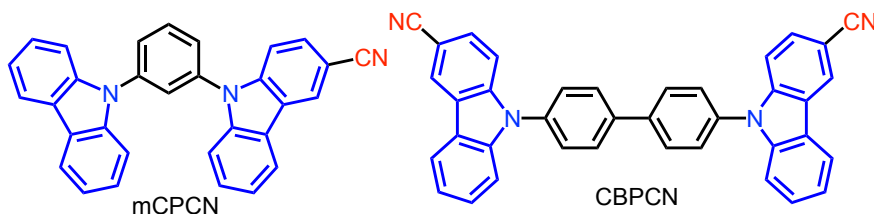
Fig. 2.10. Aryl-cyanide-based bipolar host materials for PhOLEDs

The synthesized materials exhibited improved glass-transition temperature (T_g value is 97°C and 162°C for mCPCN and CBPCN, respectively), as compared to their non-cyanated predecessors (60°C and 62°C for mCP and CBP, respectively) and, also, demonstrating high triplet energy values of 3.03 eV and 2.69 eV for mCPCN and CBPCN, respectively. Combining these host materials with different phosphorescent emitters, the authors managed to construct a full-color set of outstanding PhOLEDs, including blue (mCPCN:FIrpic, EQE 26.4%, CE 58.7 cd/A, PE 57.6 lm/W), green (CBPCN:Ir(ppy)$_3$, EQE 23.1%, CE 80.6 cd/A, PE 48.9 lm/W), red (CBPCN:Ir(piq)$_3$,

EQE 15.5%, CE 10.7 cd/A, PE 5.58 lm/W) and white (mCPCN:FIrpic and Os(bpftz)$_2$(PPh$_2$Me)$_2$, EQE 23.3%, PE 49.7 lm/W). The advantages of introducing a CN-group is definitely proven by these results.

The modification of a well-known mCP host also was performed for the construction of diphenylphosphoryl bipolar hosts in a series of publications presented by Lee and coworkers (Fig 2.11.). The diphenylphosphoryl unit is well-known for having a remarkably high E$_T$ with a rather strong electron-withdrawing ability, which can guarantee the improvement of electron-transporting properties of the final host material.
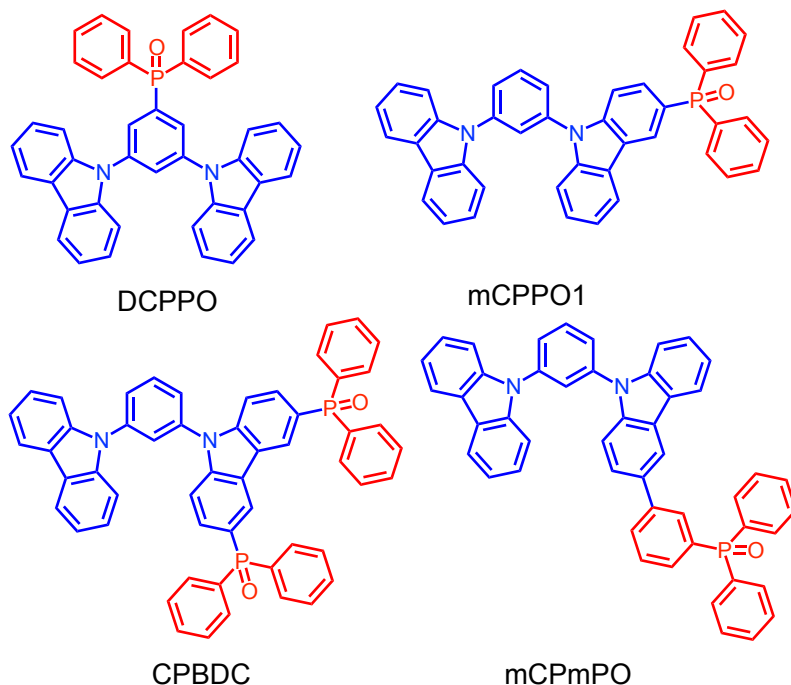
Fig. 2.11. Diphenylphosphoryl-based bipolar host materials for PhOLEDs

The obtained materials DCPPO[43], mCPPO1[44], CBPDC[45] exhibited high triplet energy value of *ca.* 3.0 eV, while mCPmPO[46] showed slightly lower 2.75 eV, which is most likely related to prolonged π-conjugation caused by the introduced phenyl linker between the diphenylphosphoryl unit and carbazole. However, utilizing these materials as hosts allowed to obtain a very efficient blue and white PhOLEDs. The application of blue phosphorescent emitter FCNIrpic with DCPPO, mCPPO1 and CBPDC resulted in a series of effective PhOLEDs, achieving the maximum external quantum efficiency of 22.4%, 25.1% and 24.5%, respectively. mCPPO1 was used for constructing a blue-emitting device with FIrpic dopant achieving 20.3% of maximum external quantum efficiency, 40.0 cd/A of maximum current efficiency and 39.7 lm/W of maximum power efficiency. The same host material was applied in white PhOLED with two dopants: blue-emitting FIrpic and yellow-emitting (fbi)$_2$Ir(acac) to obtain a device demonstrating 17.6% of maximum external quantum efficiency and 39.7 lm/W

of maximum power efficiency. These results prove the efficiency of simple mCP modification by introducing diphenylphosphoryl units.

To conclude, the development of PhOLED technology has a crucial role in the progress of organic microelectronics. PhOLEDs provide a very efficient source of light and achieve a wide range of color emission. However, phosphorescent light-emitting devices suffer from a bundle of shortcomings. Emitters based on rare-metal complexes usually are affected by efficiency roll-off at high current density and due to the nature of phosphorescent emitters, it is almost impossible to achieve deep-blue color emission according to the standards of International Commission on Illumination (CIE). In addition, the production cost of PhOLEDs is very high due to the extreme rarity and high price of platinoids. Phosphorescent OLEDs also require a very careful selection of host materials and supporting layers, which makes their production even more complicated and expensive. The application of phosphorescent light-emitting devices in the industry requires inexpensive materials, thus, researchers are highly motivated to investigate acceptable alternatives for PhOLEDs.

2.2.2 Enhancing OLED efficiency by exploiting delayed fluorescence

The most effective and cutting-edge method used for creating effective light-emitting devices is the implementation of organic materials exhibiting delayed fluorescence. The core idea of exploiting the delayed fluorescence mechanism is harvesting and utilizing triplet excitons in addition to singlet excitons *via* upconversion of nonradiative triplet states to radiative singlet states by using specially designed structures of organic emitting materials[47]. There are two main types of delayed fluorescence mechanism realization: triplet-triplet annihilation (TTA), also called P-type (first observed in pyrene) and thermally activated delayed fluorescence (TADF), also called E-type (first observed in eosin).

In the bimolecular TTA process[48], two excited triplet states combine their energy to produce one excited high-lying singlet state with double energy value comparing to the original triplet state. The generated additional singlet excitons increase the internal quantum efficiency by 37.5% (75% of triplet excitons divided by 2) and by adding the prompt fluorescence emission component (25%), the total internal quantum efficiency can reach 62.5%, if the upconversion ratio of triplet excitons is close to 100%[49].

The TADF mechanism (Fig. 2.12.) is the most promising and efficient approach to use triplet excitons and it is performed by realizing the reverse intersystem crossing process (RISC)[50]. TADF process is monomolecular, so all triplet excitons are harvested from a locally excited triplet state and transferred to a locally excited singlet state, which results in fluorescence in the same spectral wavelength, although, with longer decay time comparing to prompt fluorescence[51]. The RISC process is possible if two following criteria are met: singlet energy level should be energetically close to the locally excited triplet energy level and the endothermic RISC process should have compensation fulfilled by thermal energy[52].
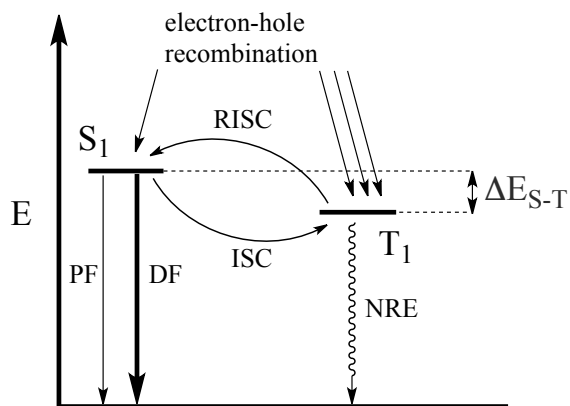
**Fig. 2.12.** A schematic depiction of TADF mechanism

The implementation of TADF allows to achieve 100% of internal quantum efficiency, if the triplet harvesting ratio is maximum. As a result, EQE of OLEDs constructed with the application of TADF is considerably higher than EQE of fluorescent light-emitting devices, and can compete with the state-of-the-art PhOLEDs, although TADF organic materials have some undisputable advantages over PhOLEDs. The first and probably the most crucial advantage is the possibility of refusing expensive noble-metal complexes, thus lowering the cost of the production process. The second solid advantage is high flexibility in the design and synthesis of TADF emitters, supported by the capabilities of organic chemistry. Technically, all required energy parameters can be carefully tuned by using simple structure modification.

On the other hand, molecules which can be recognized as TADF emitter candidates have to meet strict requirements[53]. The first, and the most important, is small singlet-triplet energy gap (ΔE_{S-T}) which can be caused by separating the HOMO and LUMO inside of the molecule. The second is effective intramolecular charge-transfer, which is required for successful exciton formation. And the third requirement is related to general physical properties of materials for their application in OLEDs: thermal and electrochemical stability, satisfactory morphological properties. While the last requirement is rather common and easily soluble, the first two are challenging, thus, careful structural design should be performed. While adequate ICT can be achieved with accurate combination of donating and accepting fragments of bipolar emitter, a small ΔE_{S-T} is achievable with the strict regulation of torsion angle between electron-rich (donor) and electron-deficient (acceptor) fragments, or rather between HOMO and LUMO. Difficult structural design and the correct prediction of physical properties of prospective TADF candidates remains the most important and complicated target for the scientific research.

Designing efficient TADF candidates requires the application of electron donating fragment with satisfactory physical properties such as thermal and electrochemical stability and electron-rich structure, thus, strong electron-donating ability[54]. Heterocycles containing sp^3-hybridized Nitrogen atom recommend themselves as best-in-class solution for these purposes not by only meeting these

requirements, but also because of the low cost of their production. Carbazole, dimethylacridane, phenothiazine and phenoxazine and their derivatives show the best physical properties which is necessary for synthesis TADF candidates. As for acceptor selection, many electron-deficient moieties which usually show a mesomeric withdrawing effect are suitable for the application in TADF candidates, and the most popular are: benzophenone, diphenylsulfone, arylnitrile, pyridine, pyrimidine, triazine and diphenylphosphine oxide. A large quantity of possible donor-acceptor combination with various methods of their linkage provides high flexibility and a wide range of obtainable materials for using in TADF OLEDs[55].

One of the first works about the investigation of TADF phenomenon was published by Adachi and colleagues in 2012[47]. The authors designed and synthesized a series of highly efficient delayed fluorescent emitters utilizing carbazole as an electron donating unit and various phthalonitriles as acceptor units (Fig 2.13.).
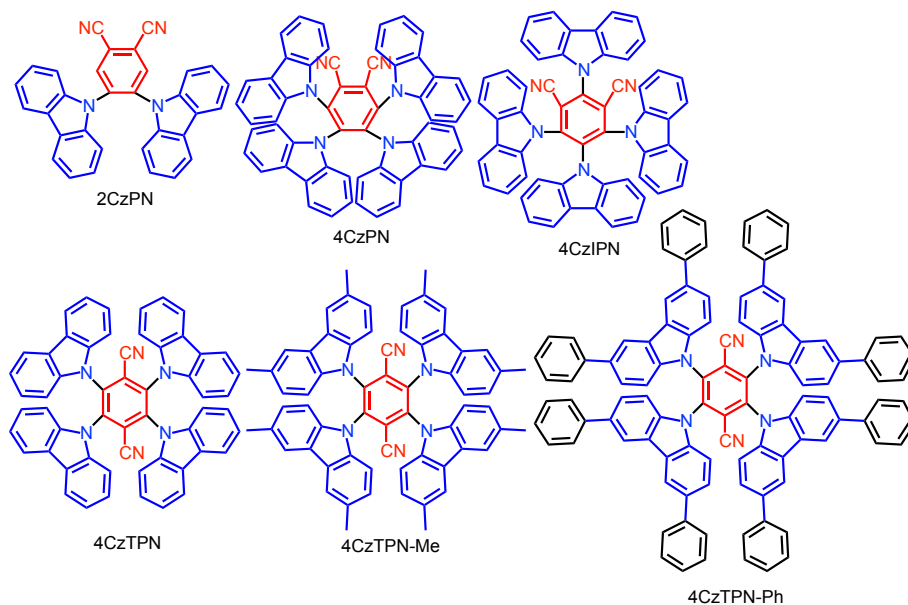
Fig. 2.13. Carbazole-phthalonitrile derivatives as efficient TADF emitters

A low value of ΔE_{S-T} was achieved by successfully separating HOMO and LUMO, which was performed by creating dimensional hindrances caused by attaching a carbazole unit to adjacent positions in phthalonitrile isomers. By the changing the quantity and positioning of the carbazole unit a wide range of emission wavelengths was achieved from sky-blue emission (473 nm) of 2CzPN shifting to orange emission (577 nm) of 4CzTPN-Ph. CBP was selected as the host material for the construction of OLED and the following results were obtained: green OLED with structure (ITO/4,4-bis[N-(1-naphthyl)-N-phenylamino]- biphenyl, a-NPD(35 nm)/5 wt % 4CzIPN:CBP (15 nm)/1,3,5-tris-(N-phenylbenzimidazol-2-yl)benzene, TPBi(65 nm)/LiF(0.8 nm)/Al(70 nm)) demonstrated impressive 19.3% EQE, while the orange and sky-blue OLEDs (ITO/a-NPD(35 nm)/5 wt % 4CzTPN-Ph:CBP(15 nm)/TPBi(65 nm)/LiF(0.8 nm)/Al(70 nm) and ITO/ α-NPD(40 nm)/1,3-bis(9-

carbazolyl)benzene, mCP (10 nm)/ 5 wt % 2CzPN:PPT(20 nm)/PPT(40 nm)/LiF(0.8 nm)/Al(70 nm)) showed EQE values of 11.2% and 8.0%, respectively. These results clearly indicate a significant progress as compared to the effectiveness of fluorescent OLEDs with the maximum EQE of 5%.

The usage of pyrimidine unit as a possible acceptor in TADF molecules was investigated by Kido *et. al.*[56] A series of emitters was synthesized using dimethylacridane as the donor unit which is linked with a phenyl ring to the substituted pyrimidine acceptor (Fig. 2.14.). Hosted in the DPEPO matrix, Ac-MPM exhibited a high photoluminescence quantum yield of 80%. Furthermore, the OLED based on Ac-MPM demonstrated an impressive 25% EQE with high PE of 62 lm/W, followed by a promising turn-on voltage value of 2.8 V.
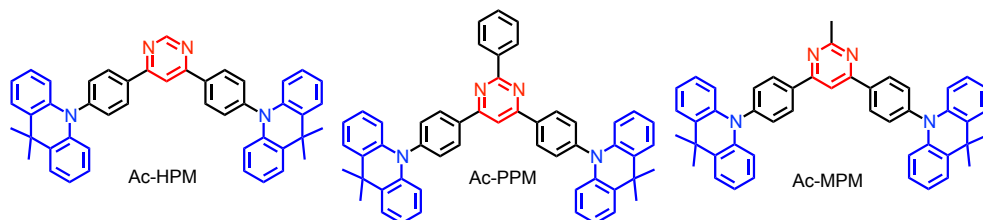
Fig. 2.14. Acridane-pyrimidine TADF emitter materials for OLEDs

Lee *et. al.*[57] reported an effective design strategy using dual emitting core molecules with a bicarbazole unit as a donor and a triazine unit as an acceptor (Fig. 2.15.).
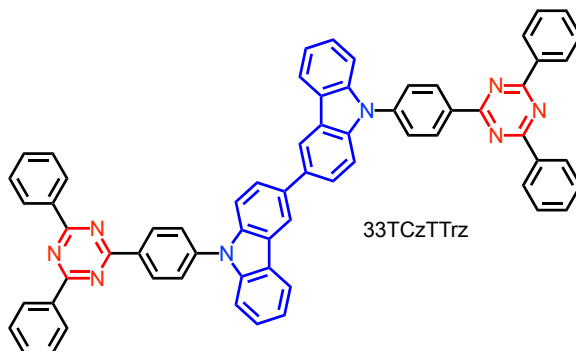
Fig. 2.15. Bicarbazole-triazine TADF emitter for OLEDs

The 33TCzTTrz material showed the best photophysical properties alongside with a small singlet-triplet gap within the series and was used as an emitter in OLED construction. The obtained greenish-blue OLED exhibited outstanding 25% of external quantum efficiency, which is one of the best results obtained so far.

A novel accepting unit, dibenzo-[a,j]phenazine was presented by Monkman *et al.*[58] as another illustration of possible sp²-hybridized N-heterocycles utilization in TADF emitters. Based on the D-A-D structure model, three materials were synthesized containing substituted carbazole, diphenylamine and phenoxazine units as donors (Fig. 2.16.). All obtained materials demonstrated low ΔE_{S-T} value ranging

from 0.02 eV to 0.20 eV. The orange OLED obtained with POZ-DBPHZ as an emitter demonstrated 16% of maximum EQE, while the OLED based on t-BuCZ-DBPHZ and MeODP-DBPHZ exhibited more humble results with c.a. 8% of maximum EQE each. The turn-on voltage for all three devices is around 3.7 V, which is a relatively impressive result.
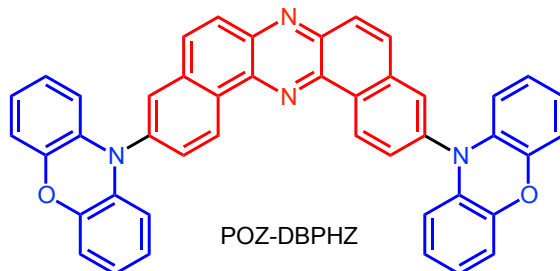
Fig. 2.16. Dibenzophenazine-based TADF emitter for OLED

The proof of high suitability of diphenylsulfone accepting unit for the construction of TADF OLEDs was reported by Adachi *et al.*[59], where three donor-acceptor materials were synthesized and investigated. A diphenylsulfone moiety was used as an acceptor unit, while dimethylacridane (DMAC), phenoxazine (PXZ) and phenyldihydrophenazine (PPZ) were selected to be donation fragments. The obtained materials (Fig. 2.17.) demonstrated a very low ΔE_{S-T} value of c.a. 0.08 eV for each compound, followed by short TADF lifetimes in the range of 1.0 to 3.1 μs in mCP films at room temperature. PLQYs of deaerated toluene solutions of PXZ-DPS and DMAC-DPS reached the value of 80% with the wavelengths of 507 nm and 460 nm, respectively. Doped light-emitting devices based on PXZ-DPS and DMAC-DPS achieved a relatively high EQEs of 17.5% and 19.5%, respectively, with the maximum brightness reaching 1000 cd/m^2. Unfortunately, the stability of DMAC-DPS-based OLED is its weak point. This device demonstrated only c.a. 1h of half-life with the brightness level of 500 cd/m^2. In later work[60], authors also achieved impressive 19.5% of EQE for DMAC-DPS non-doped OLED. Since non-doped OLEDs are much more attractive for researchers and more perspective for future implementation in the industry due to lowering cost and simplification of production, these results should be recognized as very important.
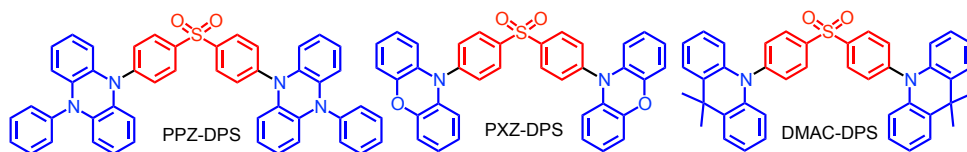
Fig. 2.17. Diphenylsulfone derivatives as emitters for TADF OLEDs

Benzophenone also can be used as an acceptor unit in the construction of luminescent TADF materials. Adachi *et al.*[61] report a series of donor-acceptor materials containing carbazole, phenoxazine and acridane with a benzophenone acceptor, which are suitable as emitters in OLED construction. The synthesized materials Cz2BP, CC2BP, Px2BP, m-Px2BBP and p-PxBBP (Fig. 2.18.)

demonstrated a low ΔE_{S-T} value situated in the range of 0.03–0.21 eV. A series of doped (mCP and DPEPO matrix have been used) OLEDs was prepared from these materials achieving a wide emission color range: the blue-emitting Cz2BP-based OLED achieved 8.1% of EQE, the sky-blue CC2BP-based OLED demonstrated 14.3% EQE, the green-emitting Px2BP-based OLED exhibited 10.7% of EQE, the yellow-emitting m-Px2BBP OLED showed 6.9% EQE and the red-emitting p-PxBBP OLED achieved only 4% of EQE. Based on these results, a two-color white-emitting OLED also was constructed utilizing CC2BP and Px2BBP materials as emitters, which resulted in a 6.7% maximum EQE device. In later work, another green emitter, DMAC-BP[60] (Fig. 2.18.) was reported, based on which the un-doped green OLED was developed. This device demonstrated excellent 18.9% of maximum external quantum efficiency with impressive 50 kcd/m² of maximum brightness. These valuable results were achieved due to a relatively small ΔE_{S-T} value of 0.07 eV of DMAC-BP.
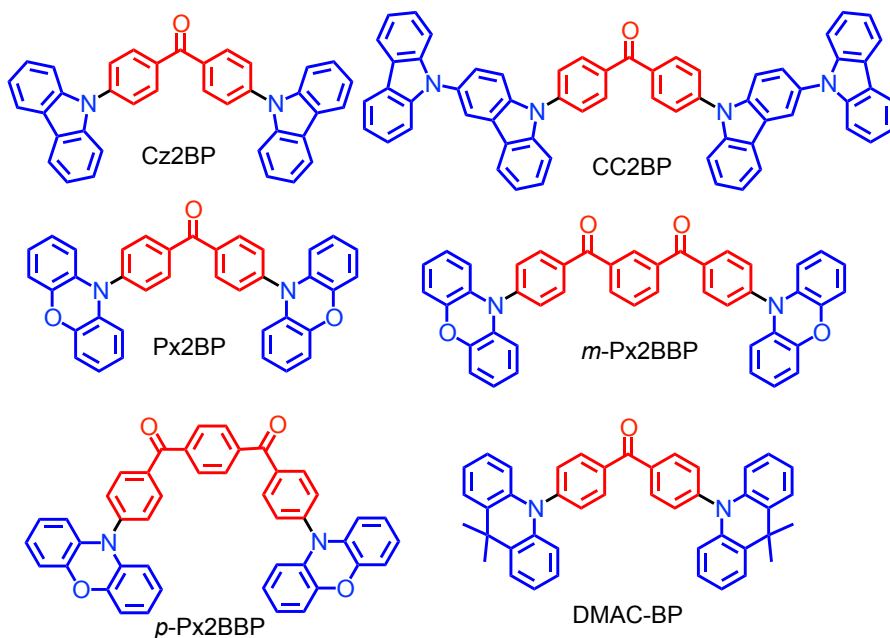
Fig. 2.18. Benzophenone-based TADF emitters for OLEDs

Further development of D-A-D architecture strategy using ketones as an acceptor group resulted in a series of works studying the utilization of benzoylpyridine moiety as an acceptor fragment in TADF-candidates. Firstly, Cheng *et al.* presented two carbazole-benzoylpyridine derivatives, DCBPy and DTCBPy[62] (Fig. 2.19), which exhibited an extremely low ΔE_{S-T} value of 0.03 eV and 0.04 eV, respectively. OLEDs based on DCBPy and DTCBPy demonstrated outstanding results achieving 24% of max. EQE, 54.7 cd/A of max. CE, 57.2 lm/W of max. PE for sky-blue-emitting (DCBPy-based) device and 27.2% of max. EQE, 94.6 cd/A of max. CE, 84.5 lm/W of max. PE for green-emitting (DTCBPy-based) device. The green-emitting OLED was compared to the same-structured PhOLED, where Ir(ppy)₃

was used as an emitter and outperformed it in all parameters. Both devices showed close to the best performance achieved by TADF OLEDs so far.

In their second work, the authors investigated benzoylpyridine-based materials in greater detail and synthesized a modified compound mDCBP[63] (Fig. 2.19.) discovering mechanochromism properties of this material. Four OLEDs were prepared by using various concentrations of mDCBP in the emitting layer. Depending on the concentration change of mDCBP from lower to higher OLEDs exhibited a change in the emission color from sky-blue (474 nm) region to green (500 nm). The best performance characteristics were achieved for the sky-blue OLED (18.4% of max. EQE, 34 cd/A of max. CE and 26.5 lm/W of max. PE), however other constructed OLEDs also showed great performance with EQEs situated in the range from 14.7% to 17.9%.

DCBPy   DTCBPy   mDCBP
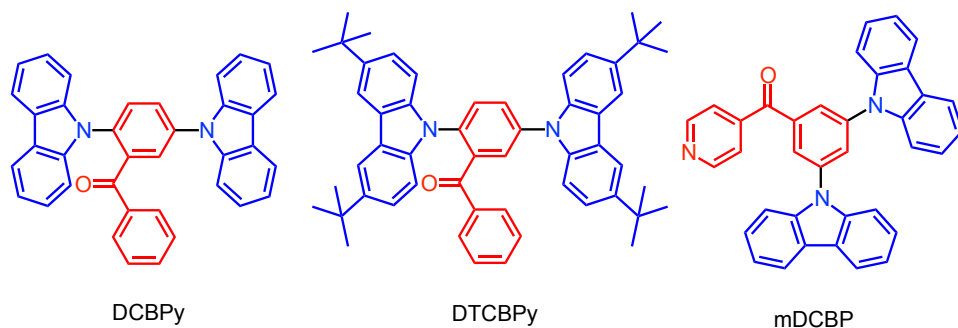
Fig. 2.19. Benzoylpyridine-based TADF emitters for OLEDs

Recently, triarylboron derivatives attracted a lot of attention from researchers because of their promising electron-accepting abilities caused by an empty p-orbital of the boron atom. The donor-acceptor triarylboron-containing derivatives demonstrated strong ICT properties which resulted in wide application of these materials in non-linear optics and optoelectronics[64,65].

Their application in the creation of OLEDs was reported by Adachi *et al.*[66], where a series of donor-acceptor materials contained 10*H*-phenoxaborin as an electron-withdrawing moiety. The synthesized materials, TIPP-DMAC, TIPP-SAF, TIPP-SAX and TIPP-4MCz (Fig. 2.20.) exhibited promising photophysical properties: high photoluminescence quantum yields situated in the range from 56% to 100% with emission in blue region ranging from 443 nm to 475 nm. PLQY of these materials is concentration-independent, which is a valuable addition to the simplification of OLED fabrication; moreover, the ΔE_{S-T} value of these compounds is found to be very low (0.06–0.12 eV), which makes them perfect candidates for application in OLEDs. As a result, blue-emitting OLEDs fabricated with TIPP-SAF, TIPP-SAX and TIPP-4MCz demonstrated great performance reaching 19.0%, 20.1% and 13.3% of EQE, respectively.
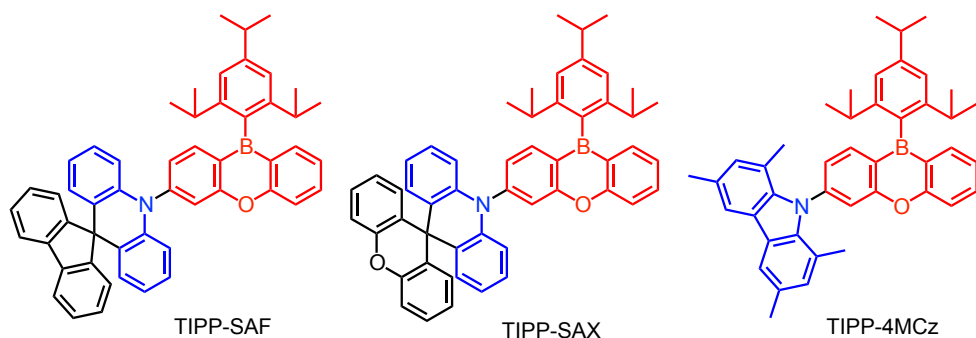
Fig. 2.20. Phenoxaborin-based TADF emitters for OLEDs

Another work on the synthesis and analysis of physical properties of triarylboron-based materials was published by Kitamoto *et al.* about donor-acceptor materials with the 10*H*-phenoxaboryl unit as an electron-acceptor connected to carbazole, dimethylacridane and phenoxazine units as electron-donating moieties *via* a phenyl linker (Fig. 2.21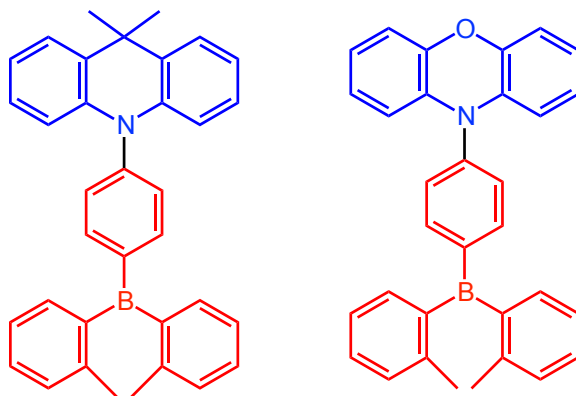.)[67]. TD-DFT calculations revealed an extremely low ΔE_{S-T} value of POB-DMAC (0.013 eV) and POB-PXZ (0.028 eV) materials in contrast to a relatively high ΔE_{S-T} value of POB-Cz (0.35 eV). As a result, POB-Cz demonstrates only prompt fluorescence emission, while POB-DMAC and POB-PXZ exhibit delayed fluorescence with PLQYs close to 100%. The sky-blue device (466 nm emission wavelength) fabricated with POB-DMAC as an emitter and DPEPO as a host exhibited 15.1% EQE, while the green-emitting OLED with a POB-PXZ emitter and an mCP host showed impressive 22.1% of EQE. In addition, the maximum brightness value of c.a. 8200 cd/m^2 and high 14.6% of EQE at the brightness value of 1000 cd/m^2 were achieved, which are rather valuable results.
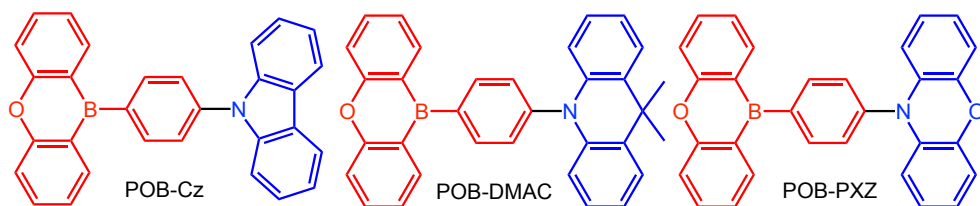
Fig. 2.21. Tryarylboron-based TADF emitters for OLEDs

Oi *et al.*[68] reported an investigation of using a dimesitylphenylborane fragment as an electron-acceptor in emitters for TADF OLEDs. An interesting design strategy was applied to create these materials. Bulky mesityl groups were attached to a boron atom to improve stability and avoid the hydrolysis process of attacking a boron atom by H$_2$O molecules. In addition, the authors expected that bulky mesityl groups would be rigid enough to prevent the non-radiative relaxation by free rotation of C-B bonds. Three compounds were synthesized containing the abovementioned acceptor fragment and carbazole, phenoxazine and dimethylacridane units as donors (Fig. 2.22.).

Fig. 2.22. Dimesitylphenylborane-based TADF emitters for OLEDs

TD-DFT calculations for the last two materials revealed extraordinarily low values of $\Delta E_{S\text{-}T}$ (0.0072 eV and 0.0057 eV, respectively). Moreover, the measurement of photophysical properties of acridane and phenoxazine derivatives revealed very high PLQY in toluene solutions: 0.89 and 0.87, respectively. Thus, the doped OLEDs were fabricated using these materials with mCP and CBP hosts. The sky-blue-emitting device with an acridane-dimesitylphenylborane emitter achieved 16% EQE, while the green-emitting OLED with a phenoxazine-dimesitylphenylborane emitter showed the maximum external quantum efficiency value of 17.3%.

Aromatic imides have recently drawn considerable amount of researchers' attention due to their excellent photoelectrical properties and strong electron-accepting ability, which is required for the construction of donor-acceptor materials for application in OLEDs[69].

Li *et al.* reported about the design, synthesis and application of twisted D-A-D structures containing carbazole and *tert*-butylcarbazole as donor moieties and N-phenyl-phthalimide as an electron-withdrawing unit[70]. The twisted structure of AI-Cz and AI-TBCz (Fig. 2.23.) resulted in an extremely low experimental value of $\Delta E_{S\text{-}T}$ (0.06 eV and 0.03 eV, respectively). Despite the fact that the PL emission wavelengths of the materials are located in the green-yellow region 530–545 nm and exhibited moderate quantum yields of 38% and 28%, respectively, the co-doped film of AI-Cz with an mCBP host demonstrated a significant blue shift of emission to 510 nm; moreover, PLQY of both doped films also increased by the factor of two to achieve the values of 72% and 67%, respectively. As a result, multilayer OLEDs were fabricated with the abovementioned doped film as an emissive layer. The device based on AI-Cz emitted green electroluminescence with the wavelength of 510 nm and achieved an outstanding maximum EQE of 23.2% with the maximum CE and PE of 66.2 cd/A and 56.2 lm/W, respectively. The AI-TBCz-based OLED exhibited yellow emission with $\lambda = 545$ nm, reaching the maximum EQE, CE and PE values of 21.1%, 66.8 cd/A and 51.2 lm/W, respectively. These results are comparable with the most effective reported OLEDs based on the TADF phenomena.
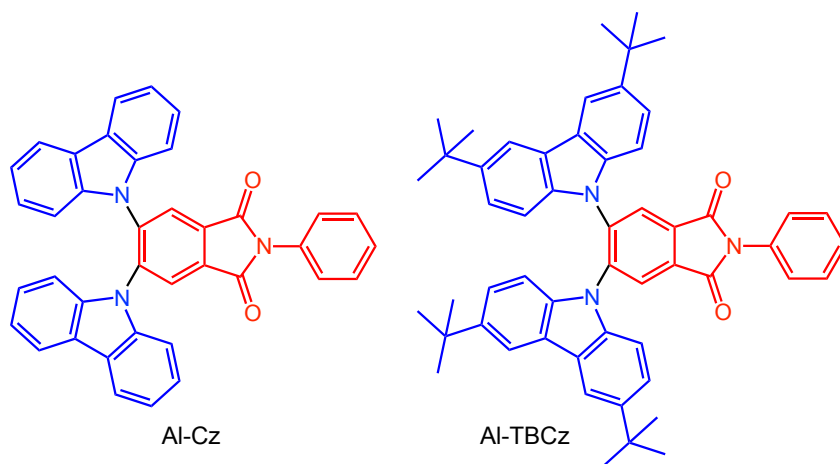
Fig. 2.23. N-Phenyl-phthalimide-based TADF emitters for OLEDs

Another work published by Adachi *et al.* is dedicated to the synthesis and investigation of properties of acridane-imide D-A-D emitting materials for OLEDs[71]. N-methyl-phthalimide (Fig. 2.24.) and N-methyl-diphenylmaleimide were selected as acceptor fragments, however, only phthalimide derivatives are capable of showing TADF properties. TD-DFT calculations revealed that AcMI have a relatively high value of ΔE_{S-T} (0.24 eV) compared to AcPI (0.01 eV). As a result, AcPI demonstrated much efficient electroluminescence performed by effective upconversion through rapid RISC. Prompt fluorescence quantum yields were found to be almost identical: 0.50 for AcPI and 0.42 for AcMI, with peak wavelengths of emission of 517 and 559, respectively. However, the fabricated devices clearly described the efficiency difference between these two emitters. An AcPI-based green-yellow emitting device (λ_{em} = 530 nm) demonstrated 11.5% of maximum EQE, while the non-TADF AcMI-based orange emitting device (λ_{em} = 581 nm) exhibited only 1.4% of maximum EQE.
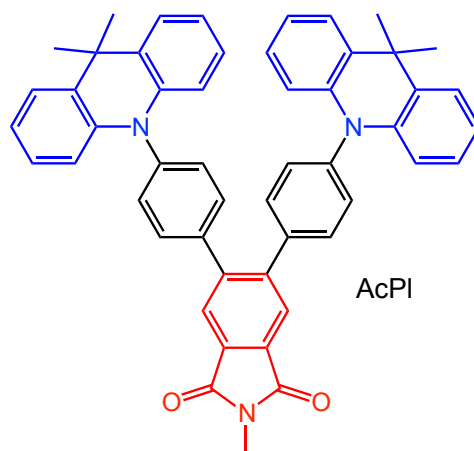
Fig. 2.24. Acridane-phthalimide TADF emitter for OLEDs

To conclude, various categories of donor-acceptor TADF materials with a wide range of emission color were reviewed. The main requirements for efficient upconversion for TADF achievement are: a low value of ΔE_{S-T}, a high PLQY in doped film and high thermal and electrochemical stability. Utilizing the TADF phenomenon reveals promising horizons in the fabrication of high-performance OLEDs with a wide color range of emission. However, the necessity of carefully designing the emitter structure to obtain required properties and lowering the production price led to incessant search of improved design and synthesis strategies to find the best available materials for emitter application.

2.2.3. Application of aggregation-induced emission enhancement for the improvement of OLEDs efficiency

Commonly, emissive layers in OLEDs consists from an emitter which is doped into the host matrix to form a solid solution, moreover, the concentration of the emitter in the matrix is usually in the range from 5% to 10%. This kind of approach appeared to reduce the emission intensity and increase the emitter concentration caused by intermolecular interaction in highly concentrated solutions. This phenomenon, aggregation-caused quenching (ACQ), was firstly reported by Förster in 1954[72]. Conventional luminophores usually present strong emission when their molecules are isolated, but in the case of highly concentrated solutions, different aggregates and clusters form. The aromatic rings and systems of adjacent luminophores in the aggregate assemble into intermediate structures with an intensive interaction between π-orbitals. This π−π stacking leads to the advantage of the non-radiative relaxation over the photon emission in luminophores causing emission quenching.

In contrast, aggregation-induced emission (AIE) is another photophysical phenomenon, described firstly by Tang *et al.* in 2001[73]. The concept of AIE lays in the enhancement of the emission intensity caused by the aggregation of chromophores into clusters. Typically, AIE luminogens are non-emittive in the solution when molecules are isolated. The twisted structure of such kind of luminophores generates non-radiative relaxation realized *via* intramolecular rotations, vibrations and motions. Although in aggregated state, steric hindrance produced by adjacent molecules of luminophores is restricting intramolecular rotations, and a highly twisted structure is blocking the π−π interaction between the molecules. All these facts result in quenching of all non-radiative relaxations and led to strong emission enhancement.

There are three types of working mechanisms of AIE molecules: the restriction of intramolecular rotation (RIR), the restriction of intramolecular vibrations (RIV) and the restriction of intramolecular motions (RIM). The brightest example of AIEgen with RIR is hexaphenylsilole (HPS)[74] (Fig 2.25.). In an isolated state, e.g. in a solution, HPS molecules after exciting perform non-radiative relaxation by rotating the phenyl rings rotors against the heterocycle stator around the single bond axes. After aggregation, the rotation of phenyl rings is sterically hindered, thus the energy from excitation is relaxed *via* photon emission[75]. The RIV mechanism can be clearly described by the behavior of THBA[76] (Fig 2.25.) molecule. It has no rotatable units because its phenyl rings are locked by an ethylene linker. However, it exhibits AIE properties, THBA is highly luminescent in a solid state and non-luminescent in a

solution. These properties can be explained by intermolecular vibration motions of phenyl rings which consume the energy of excitation and convert it to non-radiative relaxation. In contrast, vibrations decrease in aggregates and a highly twisted THBA structure avoids π−π stacking, which results in emission enhancement[77].

The restriction of intermolecular motions is usually achieved by combining RIR and RIV mechanisms by creating a structure of vibratable core and rotatable peripheries.

HPS   THBA
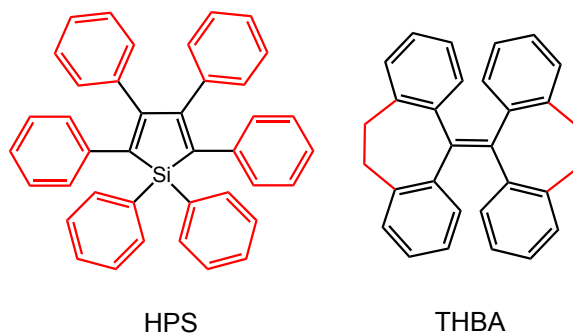
Fig. 2.25. AIE luminogens with RIR and RIV emission mechanisms

Recently, the AIE phenomenon has drawn great research attention due to possible applications in OLEDs fabrication[78]. The implementation of AIE materials has very significant advantages when compared to traditional luminophores, and the most important is simplification of the OLED fabrication process. With an AIE emitter, there is no need to control the use a host material and, thus precisely control emitter concentration. Also, without using a host matrix, the production cost is decreased, which is a positive feature. On the other hand, creating AIEgens requires specific design strategies to create highly twisted structures.

Moreover, most of conventional AIE luminogens exhibit only prompt fluorescence, which has a negative impact on the efficiency of OLEDs. As a result, nowadays, strategies of creating materials exhibiting both AIE and DF became very important. A combination of TADF and AIE phenomena can create the ultimate light-emitting device without any shortcomings. The effectiveness of the TADF OLEDs would combine with simple and low-cost production which would be possible due to the use of AIE-active materials. These factors motivate strong research interest in the creation of AIE-DF materials and their implementation in OLEDs.

One of the first studies dedicated to the implementation of TADF AIEgens into non-doped OLEDs was reported by Wang *et al.* in 2014[79]. Two novel thioxanthone (TXO)-based emitters TXOD-TPA and TXOD-PhCz (Fig. 2.26) were synthesized by introducing triphenylamine and N-phenylcarbazole donation units into the structure. The selection of thioxanthone unit was motivated by the expectation of high electron-transporting properties, which, in combination with the well-known hole-transporting properties of TPA and N-PhCz would conclude in an excellent bipolar nature of the final materials. AIE properties of the obtained materials were examined and confirmed, while a small value of ΔE_{S-T} (0.052 eV and 0.073 eV, respectively) were estimated experimentally. PLQY of the neat films of the materials were established

to be 0.93 and 0.36. Two non-doped OLEDs were constructed with these materials. TXOD-TPA-based yellow electroluminescent device with $\lambda_{em} = 552$ nm exhibited the maximum EQE of 18.5% with the maximum CE of 43.3 cd/A, the maximum PE of 47.4 lm/W and the turn-on voltage of 5.3 V and reached the maximum brightness of 16.3 kcd/m^2. TXOD-PhCz-based green-emitting non-doped OLED achieved 21.5% of maximum EQE with the maximum CE of 76.0 cd/A and the maximum PE of 70.0 lm/W with the turn-on voltage 4.7 V and the maximum brightness 21 kcd/m^2. Moreover, these outstanding results can be supported by excellent electroluminescence stability.
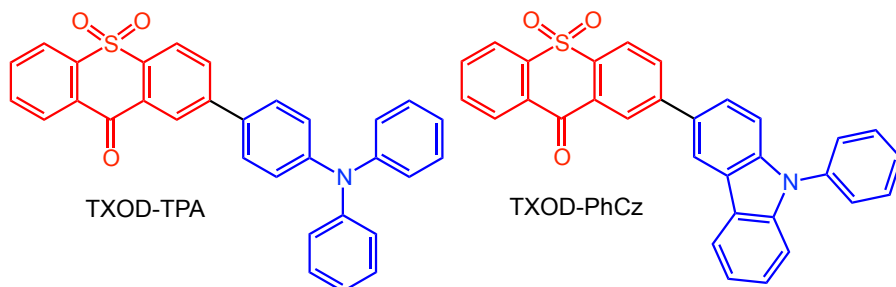
Fig. 2.26. Thioxanthone AIE-TADF emitters for OLEDs

Another AIE-TADF material was reported by Lee *et al.*, containing diphenyl sulfone as an electron acceptor[80]. An interesting design strategy was selected for this material: an asymmetric structure obtained by attaching two different donor moieties, phenoxazine and phenothiazine, to the core acceptor. PTSOPO (Fig. 2.27) demonstrated a low experimental ΔE_{S-T} value of 0.09 eV with intensive aggregation-induced emission enhancement and high PLQY of neat film of 0.80. Using PTSOPO as an emitting material, two green-emitting electroluminescent devices were constructed. The non-doped device exhibited a high EQE value of 17.0%, while the DPEPO-doped PTSOPO-based OLED demonstrated an almost similar maximum external quantum efficiency of 17.7%. Nearly identical efficiencies are probably related to that fact that in doped OLED, the TADF phenomenon mainly influenced high EQE, while in the non-doped OLED, the AIE effect played the main role in high efficiency.
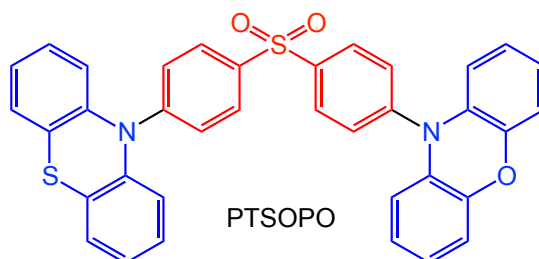
Fig. 2.27. Asymmetric diphenylsulfone-based AIE-TADF emitter for OLED

A similar strategy design based on creating asymmetric D-A-D materials by attaching different donors was published by Tang *et al.*[81] The synthesized materials

CP-BP-PXZ, CP-BP-PTZ and CP-BP-DMAC (Fig. 2.28.) were constructed by Friedel-Crafts acylation of N-phenylcarbazole with 4-fluorobenzoyl chloride, followed by aromatic nucleophilic substitution of a fluorine atom to a phenoxazine, phenothiazine and dimethylacridane.
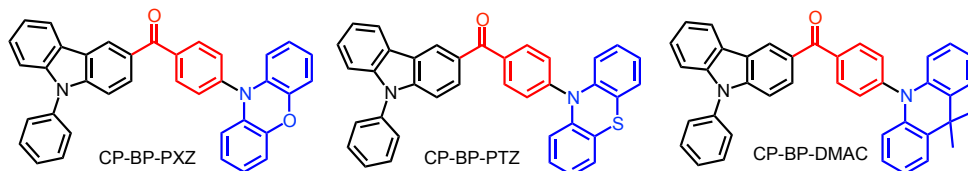
**Fig. 2.28.** Benzoylcarbazole-based AIE-TADF emitters for OLEDs

The obtained materials demonstrated a strong AIE effect, achieving PLQY in neat film values of 0.58, 0.45 and 0.67 for CP-BP-PXZ, CP-BP-PTZ and CP-BP-DMAC, respectively. Interestingly, in the CBP matrix PLQYs of the materials also remain high, which can be explained by the suppression of intermolecular dipole-dipole interaction. ΔE_{S-T} values of the materials in the neat films were revealed to be very small and situated in the range from 0.016 to 0.033 eV. For each of these materials, a non-doped and CBP-doped electroluminescence device was fabricated. Non-doped devices showed the following characteristics: 18.4% of max. EQE, 59.1 cd/A of max CE, 65.7 lm/W of max. PE with 100 kcd/m^2 and 2.5 V of turn-on voltage for the CP-BP-PXZ-based green-emitting device; 15.3% of max. EQE, 46.1 cd/A of max. CE, 55.7 lm/W of max. PE with 46 kcd/m^2 of max. brightness and 2.5 V of turn-on voltage for the CP-BP-PTZ green-emitting device; 15.0% of max. EQE, 41.6 cd/A of max CE, 37.9 lm/W of max PE, with 37.7 kcd/m^2 of maximum brightness and 2.7 V of turn-on voltage for the CP-BP-DMAC sky-blue emitting device. Compared to CBP-doped devices which also demonstrated good characteristics, the non-doped OLED outperformed the doped OLEDs in all electroluminescent parameters. Considering the excellent stability of non-doped OLEDs and its simplified fabrication, these results can be considered as state-of-the-art electroluminescence devices produced so far.

Phenothiazine derivatives demonstrating the AIE-TADF properties were recently reported by Aizawa et al.[82] Two novel materials, PTZ-XT and PTZ-BP (Fig. 2.29.), which use benzophenone and xanthone acceptors were synthesized and investigated.
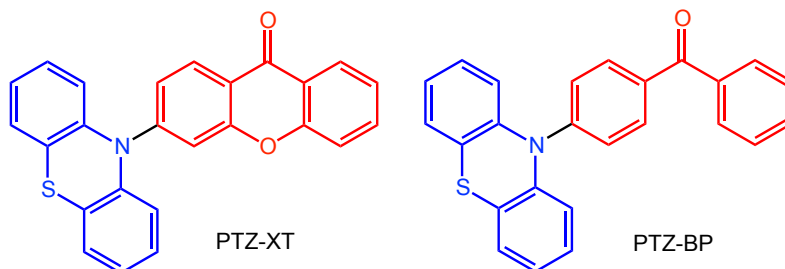
Fig. 2.29. Benzophenone/xanthone derivatives as AIE-TADF emitters for OLEDs

Both compounds exhibited emission in the yellow region with emission peaks of 545 nm for PTZ-XT and 565 nm for PTZ-BP with PLQYs of 0.53 and 0.31, respectively. Strong AIE properties of these two materials were revealed with a combination of the TADF effect provided by the low values of ΔE_{S-T} in the range of 65–71 meV. Non-doped OLEDs fabricated from both compounds used as emitter layers achieved 11.1% and 7.6% of maximum EQEs for PTZ-XT and PTZ-BP, respectively. These results can be acknowledged as a valuable contribution to AIE-TADF technology utilization mostly due to very simple and low-cost synthesis of the emitters.

Red AIE-TADF emitters based on antraquinone derivatives for solution-processed OLEDs were reported by Huang *et al.*[83] While using carbazole and triphenylamine donor moieties the authors performed simple and low-cost synthesis of donor-acceptor materials with both AIE and TADF features (Fig. 2.30.).
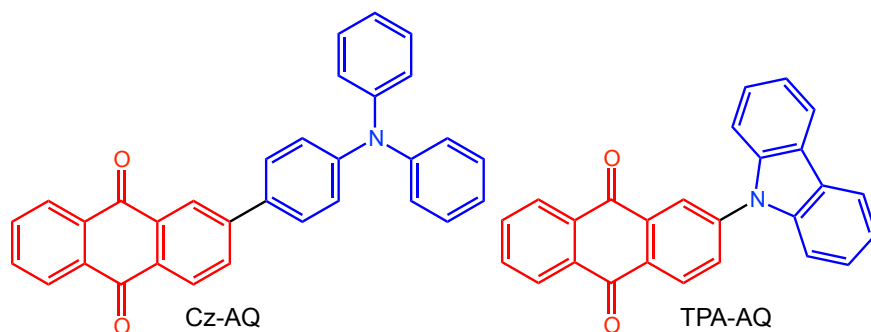
Fig. 2.30. Antraquinone-based AIE-TADF emitters for OLEDs

ΔE_{S-T} values were experimentally measured to be 0.11 eV and 0.05 eV for Cz-AQ and TPA-AQ materials and with an approved strong AIE effect of both materials, which raises the expectation of using these materials in non-doped OLEDs. The orange-emitting device with Cz-AQ as an emitter achieved 5.8% of maximum EQE with 10.8 cd/A of maximum CE, the turn-on voltage of 3.5 eV and the maximum luminance of 3200 cd/m^2. The TPA-AQ-based red-emitting device turned on at 3.8 V and demonstrated 7.8% of maximum EQE and 10.6 cd/A of maximum CE with the maximum luminance of 2200 cd/m^2. The performance of the OLEDs is comparable to the results achieved with red solution-processed PhOLEDs based on iridium(III) complexes[84] and europium(III) complexes[85]; however, the main advantage of using these materials for the fabrication of OLEDs is significant reduction of the production cost and simplification.

Utilizing a combination of AIE and TADF phenomena can be established as an important breakthrough in the production of most advanced and efficient organic light-emitting devices. This approach merges all advantages of known OLED efficiency-boost techniques: high effectiveness compared to PhOLEDs and TADF OLEDs, inexpensive production in contrast to PhOLEDs and simplified production compared to TADF OLEDs. Therefore, AIE-TADF OLEDs can be accepted as the most cutting-edge devices fabricated so far, as well as AIE-TADF emitters can be

recognized as the most promising and noteworthy for the next few years of research in the field of OLED construction.

2.3. Conclusions of the literature review

Several approaches to OLED efficiency enhancement were examined and analyzed in this review. Using the phosphorescence emitters in combination with different hosts, adopting TADF emitters or AIE-TADF emitters significantly improves the performance of OLEDs. The main requirements for the organic materials intended for OLED application are high thermal, chemical and electrochemical stability, suitable morphological, photophysical and energetic properties and convenient and inexpensive synthesis. For each of the abovementioned points, additional requirements can be established. PhOLEDs require hosts with high electron/hole transport abilities and high triplet energy values, TADF OLEDs need emitters with low ΔE_{S-T} values and high PLQYs, AIE-TADF materials, in addition to TADF requirements, must have the AIE feature provided by a highly-twisted structure. High flexibility of the organic materials realized by simple chemical modification of structure and, in turn, thermal, photophysical, electrochemical and morphological properties, can fulfill all these requirements to achieve the best available performance of the light-emitting devices.

However, considering all shortcomings of the abovementioned approaches of OLED efficiency enhancement, such as high fabrication cost and high roll-off of PhOLEDs and TADF OLEDs, low working lifetime of TADF/AIE-based OLEDs, especially with blue emission, research activity in this field is still very important and relevant. The development of novel materials for implementation in OLEDs as components of ETL, HTL, hosts or emitters, with improved characteristics remains an urgent topic.

There are still very few reports considering materials exhibiting the symbiosis of AIE and TADF phenomena. Thus, this work implements alternative design strategies based on inexpensive and simplified synthesis to obtain novel organic materials exhibiting improved physical properties and AIEE or a combination of AIEE and TADF phenomena. The structure-properties relationships are carefully examined to understand the nature of energy processes occurring in the molecules and the physical properties of the materials and their application in OLEDs are investigated. Eventually, the advantages of utilizing materials with AIE and AIE/TADF properties in optoelectronics applications were established and discussed.

3. EXPERIMENTAL SECTION

3.1. Instrumentation and measurements

^{1}H and ^{13}C NMR spectra were recorded on a Varian Unity Inova 300 NMR spectrometer operating at 300 MHz frequency for ^{1}H and at 75 MHz frequency for ^{13}C analysis, respectively, or Varian Mercury 400 MHz at 400 MHz, 100 MHz, and 375 MHz for ^{1}H, ^{13}C, and ^{19}F NMR spectra, respectively. The samples were prepared by dissolving 15 mg of the material in 600 µl of deuterated chloroform (CDCl$_3$) or dimethyl sulfoxide (DMSO-d^6) with an inner standard, tetramethylsilane (TMS). Chemical shifts (δ) are reported in parts per million (ppm) and referenced to tetramethylsilane or internal solvent signal.

IR spectra in the range of 400–4000 inverse centimeters (cm–1) were recorded from neat materials on a Perkin Elmer Spectrum BX II FT-IR System. FT-IR spectra are analyzed as a function of transparency (T) expressed in percent against wavenumber (ν) expressed in cm^{-1}.

Mass spectra were obtained by the electrospray ionization mass spectrometry (ESI- MS) method on an Esquire-LC 00084 mass spectrometer, or a Synapt G2-S HDMS (*Waters Inc.*) mass spectrometer equipped with an electrospray ion source and q-TOF type mass analyzer. The samples were prepared as diluted solutions (of ppm order) of the materials.

Elemental analysis data were obtained on a EuroEA Elemental Analyser. A weighed sample of a material (1–3 mg) is combusted at *ca.* 1100°C in pure oxygen. The combustion products are carried through the analytical system using inert argon gas. Components of the sample gas are separated by absorption traps. Concentrations of the components are detected using thermal conductivity cells by comparing the output signal to a reference cell through which pure argon flows. Acetanilide (C$_8$H$_9$NO) is used as a standard for calibration.

UV/Vis spectra of 10^{-5} M solutions of the compounds were recorded in quartz cells using a Perkin Elmer Lambda 35 spectrometer. The obtained results are presented as normalized spectra in which the intensities of bands are equalized at certain wavelengths. Photoluminescence (PL) spectra of 10^{-5} M solutions and of solid films of the compounds were recorded using the Edinburgh Instruments' FLS980 Fluorescence Spectrometer. For recording the UV/VIS and PL spectra, thin solid films were prepared by employing the spin-coating technique and an SPS-Europe Spin150 Spin processor using 2.5 mg/mL solutions of the compounds in THF or by drop casting 2 mg/ml solutions of the compounds in toluene on the pre-cleaned quartz substrates. Solid solutions of the molecularly dispersed compounds in Zeonex polymer matrices were obtained with the concentrations of 1 wt%, respectively, by mixing the dissolved compounds and polymer in toluene solutions at an appropriate ratio and casting the solutions on quartz substrates in ambient air. Each PL measurement was repeated 3 times and the error value was estimated to be ±2 nm.

Fluorescence quantum yields of the solutions and of the solid films were estimated using an integrated sphere. An integrating sphere (Edinburgh Instruments) coupled to the FLS980 spectrometer was calibrated with two standards: quinine

sulfate in 0.1 M H_2SO_4 and rhodamine 6G in ethanol[86]. Each quantum yield measurement was repeated 5 times and the error value was estimated to be ±0.02.

Fluorescence decay curves of the samples were recorded using a time-correlated single photon counting technique utilizing the PicoQuant PDL 820 ps diode laser as an excitation source (wavelength 374 nm). Variable temperature liquid nitrogen cryostat (Optistat DN2) was used to characterize the photophysical properties of the samples at different temperatures in an inert nitrogen atmosphere.

Cyclic voltammetry (CV) measurements were performed in a three-electrode cell connected to a μAutolab Type III potentiostat-galvanostat. A silver wire (Ag) was applied as a potential reference electrode (RE), glassy carbon as a working electrode (WE), and platinum wire (Pt) as a counter electrode (CE). The samples were dilute solutions (10^{-4} M) of the materials in dry dimethylformamide containing 0.1 M of the supporting electrolyte, tetra-n-butylammonium hexafluorophosphate ($TBAPF_6$). The solutions were bubbled with inert gas for several minutes before measurements. Ferrocene (Fc) was used as an external standard for calibration[87]. Electrochemical ionization potentials (IP_{CV}) were estimated according to the procedure reported[88]. IP_{CV} value for Fc with respect to zero vacuum level was determined as 4.8 eV[88]. The voltammograms are plotted as WE current (i) against RE potential (E). CV measurements were conducted at 50 mV/s potential rate. Each experiment was repeated three times, and the error value was estimated to be ±0.04 eV.

Ionization potentials of the studied materials in solid-state were measured by photoelectron emission spectrometry in air[89] using a deep UV deuterium light source ASBN-D130-CM, a CM110 1/8 m monochromator, and an electrometer 6517B Keithley[90]. Fluorine doped tin oxide (FTO) coated glass slides were used as substrates for the preparation of samples. The layers of the compounds were fabricated by using thermal vacuum evaporation onto the substrates.

Hole- and electron-transporting properties of the layers of the compounds were studied by the time-of-flight (TOF) and charge extraction by linearly increasing voltage (CELIV) techniques[91,92]. The studied compounds were thermally sublimated onto pre-cleaned ITO coated glass substrates in a vacuum chamber with a base pressure below $3 \cdot 10^{-6}$ mbar. The samples with the area of 6 mm^2 were obtained by depositing an Al electrode on the top of organic layers. Positive/ negative voltage was applied for detecting hole- and electron-transport of compounds exploiting Keithley 6517B electrometer. Free charges in the organic layer were photogenerated by a light pulse of third-harmonic Nd:YAG laser EKSPLA NL300. DET10A/M Si based detector was used for synchronization of the laser pulse with a digital storage oscilloscope Tektronix TDS 3032C. The TOF and photo-CELIV photocurrent transients for the studied compounds were recorded with an oscilloscope at different electric fields at the moment of photogeneration. In TOF experiment, the transit time (t_{tr}) was determined at a kind of photocurrent transients in the log–log scale for the calculation of drift mobility (μ(TOF)) using the formula μ(TOF) = $d^2/U \cdot t_{tr}$, where d is the thickness of a sample and U is voltage. In photo-CELIV experiment using the extraction maximum (t_{max}) which was seen as the maximum on CELIV transients, the charge carrier mobilities (μ) were estimated by using the formula μ(photoCELIV) =

$2d^2/(A \times t^2max)$, where $A = U/t_{pulse}$ is the slope of a linearly increasing voltage pulse which was applied to the sample to extract the equilibrium charge carriers[93].

TGA was performed on a Metter TGA/SDTA851e/LF/1100 apparatus at a heating rate of 20°C/min under a nitrogen atmosphere. The samples were open alumina (Al_2O_3) crucibles loaded with a few milligrams of the investigated material. The equipment was calibrated with indium and aluminum standards.

DSC measurements were taken on a DSC Q100 (TA Instruments) at a heating rate of 10°C/min under a nitrogen atmosphere. The samples were closed aluminum pans loaded with a few milligrams of the investigated material. An empty pan was used for reference. Baseline calibration was performed with sapphire disks and the temperature was calibrated with an indium standard.

The melting points of the synthesized compounds were checked by using an Electrothermal Melt-Temp apparatus. Each measurement was repeated twice and the error value were estimated to be ±1°C.

The X-ray diffraction patterns of the monocrystal were recorded using the Rigaku XtaLAB mini, or the SuperNova Agilent diffractometer with Mo $K\alpha$ (λ = 0.71073 Å) and Cu Kα (λ = 1.54184 Å) radiation. Crystals of compounds were obtained by slowly evaporating their dimethylformamide solution.

The theoretical calculations were carried out using the Gaussian 09[94] and Spartan 14[95] quantum chemical packages. Full geometry optimizations of the compounds in their electronic ground state were performed with DFT using the B3LYP functional consisting of Becke's three parameter hybrid exchange functional combined with the Lee-Yang-Parr correlation functional with the 6-31G(d) basis set in vacuum. The energies of the highest occupied (HOMO) and the lowest unoccupied (LUMO) molecular orbitals and triplet energy values E_T were obtained from single point calculations in the framework of DFT B3LYP/6-311G(d,p) approach for the CH_2Cl_2 solution.

Electroluminescence devices were fabricated by using vacuum deposition onto a pre-cleaned ITO-coated glass substrate under vacuum higher than 2×10^{-6} mBar. The density-voltage and luminance-voltage characteristics were recorded utilizing a Keithley 6517B electrometer, a certificated photodiode PH100-Si-HA-D0 together with the PC-Based Power and Energy Monitor 11S-LINK (from STANDA) and a Keithley 2400C sourcemeter assuming the lambertian distribution of OLED emission. Electroluminescence (EL) spectra were taken using an Avantes AvaSpec-2048XL spectrometer. Device efficiencies were calculated from the luminance, current density, and EL spectrum.

3.2. Reagents

The starting compounds i.e. 9*H*-carbazole (97%), pentachloropyridine (98%), potassium hydroxide (98%), potassium *tert*-butyloxide (98%), 2-fluoronitrobenzene (99%), nickel (II) bromide hydrate (98%), cesium carbonate (99%), sodium borohydride (96%), acetic acid (99%), acetic anhydride (98%), phthalic anhydride (99%) and 1,8-naphthalic anhydride (98%) were purchased from Sigma-Aldrich or TCI Chemicals and used as received without further purification. The Zeonex cyclo-olefin polymer was purchased from ZEON Corporation. The starting materials used

to synthesize the compounds described in Chapter 4.3. are reported in corresponding work[98].

The solvents, i.e. toluene, o-xylene, chloroform, ethyl acetate, *n*-hexane, n-heptane, diethyl ether, methanol, ethanol, acetone, acetonitrile, tetrahydrofuran, dichloromethane, *o*-dichlorobenzene, pyridine, dimethylsulfoxide and *N,N*-dimethylformamide (Sigma-Aldrich) were dried and distilled according the conventional procedures[96].
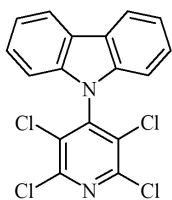
3.3. Procedures

Procedure I. Nucleophilic aromatic substitution. A mixture of aromatic amine (e. g. carbazole) (0.665 g, 3.98 mmol) and a finely grounded strong base (e. g KOH or *t*BuOK) (0.223 g, 3.98 mmol) was dissolved in dimethyl sulfoxide (DMSO) (10 mL) in a 100 ml two-necked round-bottom flask equipped with a magnetic stirrer and a water condenser and placed into an oil bath. A blanket of inert gas (nitrogen or argon) is maintained above the reaction mixture during the whole heating process. After stirring the mixture for 1 h at room temperature, the solution of activated arylhalide-nucleophile (e. g. pentachloropyridine) (1.000 g, 3.98 mmol) in DMSO (20 mL) was slowly added to the reaction mixture. Then, the reaction mixture was heated to *c. a.* 100°C and stirred for 12 h while monitoring the formation of a product by employing thin layer chromatography (TLC). Then, the reaction was cooled to room temperature, poured into water, filtered, and the crude product was purified by using column chromatography over silica gel. After column chromatography, the product was recrystallized from the mixture of appropriate solvents to afford pure crystals of product.

Procedure II. Imide condensation. A mixture of appropriate primary amine (e. g. 2-(9H-carbazol-9-yl)aniline) (1 eq.) and respective anhydride (1 eq.) was dissolved in acetic acid in a 100 ml single-necked round-bottom flask equipped with a magnetic stirrer and an air condenser furnished with a water absorber tube filled with calcium (II) chloride. The solution was stirred for 24h at 110°C. Then 1 eq. of acetic anhydride was added to the solution and the mixture was stirred for another 24h. After cooling, the mixture was poured into cold water, the precipitate was filtered and recrystallized from the mixture of *i*-PrOH and DMF to afford off-white crystals.

3.4. Materials

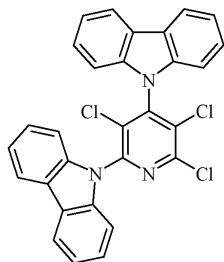**9-(Perchloropyridin-4-yl)-9H-carbazole (4-CzPyCl₄)**

4-CzPyCl₄

Obtained according to procedure I. Eluent for column chromatography is 1:1 mixture of CH_2Cl_2 and n-hexane. After column chromatography the product was recrystallized from the mixture of i-PrOH and DMF to afford yellowish crystals (fw = 380 g/ mol) (1.171 g, yield=77%), m.p. = 189°C. ^{1}H NMR (300 MHz, CDCl₃), δ ppm: 8.18(d, 2H, J=7.7Hz), 7.48(td,2H,J=7.60Hz,J=0.9Hz), 7.40 (td, 2H, J=7.60Hz, J=0.9Hz), 6.99 (d, 2H, J=7.7Hz) ^{13}C NMR (75 MHz, CDCl₃), δ ppm: 147.52, 144.69, 138.39, 131.23, 126.57, 124.09, 121.48, 120.84, 109.85. IR (neat): vmax = 2924, 1739, 1524, 1452, 1326, 1308, 1223, 743 cm^{-1}; MS (ES+, 60

V), m/z (%) = 381 ([M + H]$^+$, 70). Elemental analysis. Calcd. for $C_{17}H_8Cl_4N_2$ (%): C 53.44, H 2.11, Cl 37.12, N 7.33; found (%): C 53.41, H 2.10, N 7.36, Cl 37.13.

9,9'-(3,5,6-Trichloropyridine-2,4-diyl)bis(9*H*-carbazole) (2,4-CzPyCl₃)


2,4-CzPyCl₃

Obtained according to procedure I. Eluent for column chromatography is 1:30 mixture of ethyl acetate and n-hexane. After column chromatography the product was recrystallized from a mixture of *i*-PrOH and DMF to afford yellowish amorphous powder (fw=511 g/mol) (0.502 g, yield=49 %), m.p. = 231°C. ^{1}H NMR (300 MHz, CDCl₃), δ ppm: 8.22 (d, 2H, J=7.7 Hz), 8.16 (d, 2H, J=7.7 Hz), 7.61–7.49 (m, 4H), 7.45–7.37 (m, 6H), 7.19 (d, 2H, J=8.1 Hz); ^{13}C NMR (75 MHz, CDCl₃), δ ppm: 148.2, 147.03, 145.59, 139.29, 138.64, 130.9, 128.83, 126.66, 126.37, 124.47, 124.17, 121.62, 121.49, 120.94, 120.55, 111.09, 109.79. IR (neat): ν_{max} = 2967, 1738, 1444, 1218, 745 cm^{-1}; MS (ES+, 60 V), m/z (%) = 511 ([M]$^+$, 10) Elemental analysis. Calcd. for $C_{29}H_{16}Cl_3N_3$ (%): C 67.92; H 3.14; Cl 20.74; N 8.19; found (%): C 67.88; H 3.13; N 8.21, Cl 20.78;

9,9',9''-(3,5-Dichloropyridine-2,4,6-triyl)tris(9*H*-carbazole) (2,4,6-CzPyCl₂)
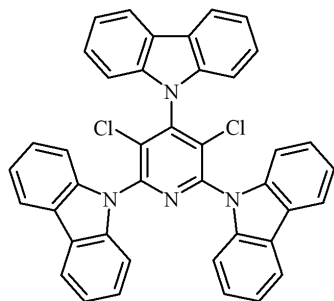

2,4,6-CzPyCl₂

Obtained according to procedure I. Eluent for column chromatography is 1:10 mixture of CH_2Cl_2 and n-hexane. After column chromatography the product was recrystallized from a mixture of *i*-PrOH and DMF to afford white amorphous powder (fw=642 g/mol) (0.445 g, yield=65 %), m.p. = 311°C. ^{1}H NMR (300 MHz, CDCl₃), δ ppm: 8.25 (d, 2H, J=7.7 Hz), 8.15 (d, 4H, J=7.7 Hz), 7.64 (t, 2H, J=7.7 Hz), 7.54–7.43 (m, 10H), 7.42–7.33 (m, 6H); ^{13}C NMR (75 MHz, CDCl₃), δ ppm: 147.58, 146.33, 139.4, 138.83, 128.4, 126.75, 126.34, 124.4, 124.26, 121.51, 121.03, 120.52, 111.17, 109.7. IR (neat): ν_{max} = 3049, 1738, 1536, 1442, 1413, 1332, 1308, 1221, 747, 722 cm^{-1}; MS (ES+, 100 V), m/z (%) = 643 ([M + H]$^+$, 70) Elemental analysis. Calcd. for $C_{41}H_{24}Cl_2N_4$ (%): C 76.52; H 3.76; Cl 11.02; N 8.71; found (%): C 76.51; H 3.75; N 8.73, Cl 11.01;
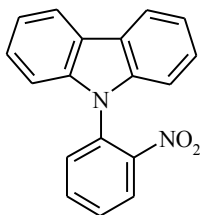
9-(2-nitrophenyl)-9H-carbazole

Prepared according to the method described in literature[97]. Orange crystalline solid (fw=288 g/mol, 9.2 g, yield=89%).

2-(9H-carbazol-9-yl)aniline
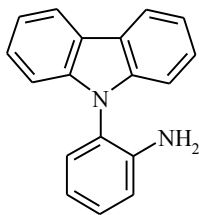
A mixture of 9-(2-nitrophenyl)-9H-carbazole (2.00 g, 6.95 mmol) and nickel (II) bromide trihydrate (3.04g, 13.9 mmol) were dissolved in a methanol/DMF solvent mixture (40/10 ml) by stirring for 30 min at room temperature. Solid sodium borohydride (1.06 g, 27.8 mmol) was added slowly to the solution over 30 min. After addition, the mixture was stirred for additional 2h at room temperature and then the mixture was filtered through celite three times, using ethylacetate as a washing solvent. The resulting mixture was washed with water (30 ml) three times and distilled obtaining brownish crystals (fw=258 g/mol) (1.29 g, 72%). ^{1}H NMR (400 MHz, CDCl$_3$) δ 3.54 (s, 2H), 6.91 (td, J = 7.4, 1.3 Hz, 1H), 6.96 (dd, J = 8.1, 1.2 Hz, 1H), 7.18 (td, J = 8.1, 0.8 Hz, 2H), 7.24–7.31 (m, 3H), 7.32 (ddd, J = 8.1, 7.4, 1.5 Hz, 1H), 7.41 (ddd, J = 8.1, 7.2, 1.2 Hz, 2H), 8.15 (ddd, J = 7.8, 1.2, 0.8 Hz, 2H); ^{13}C NMR (100 MHz, CDCl$_3$) δ 110.1, 116.5, 118.9, 119.8, 120.3, 122.3, 123.3, 126.0, 129.60, 129.63, 140.6, 144.0; MS (ES+, 100 V), m/z (%) = 259 ([M + H]+, 70). Elemental analysis. Calcd. for C$_{18}$H$_{14}$N$_2$ (%): C 83.69, H 5.46, N 10.84; found (%): C 83.66, H 5.45, N 10.87;

2-(2-(9H-carbazol-9-yl)phenyl)isoindoline-1,3-dione (CzPhPI)
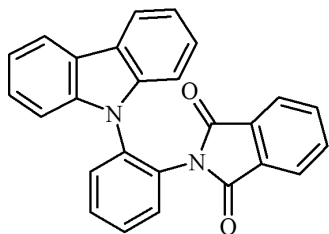
CzPhPI

Obtained according to procedure II. Yellowish crystals. FW = 388 g/mol. Yield = 1.04 g, 76%. ^{1}H NMR (300 MHz, CDCl$_3$), δ ppm: 8.01 (d, 2H, J=7.7 Hz), 7.73–7.67 (m, 2H), 7.66–7.60 (m, 4H), 7.59–7.54 (m, 2H), 7.35 (t, 2H, J=7.7 Hz), 7.29 (d, 2H, J=7.7 Hz), 7.19 (t, 2H, J=7.7 Hz); ^{13}C NMR (75 MHz, CDCl$_3$), δ ppm: 166.29, 140.72, 135.53, 134.04, 131.42, 130.45, 130.33, 130.01, 129.75, 128.90, 126.00, 123.52, 123.45, 120.07, 119.99, 110.12. MS (ES+, 60 V), m/z (%) = 389 ([M + H]+, 60). Elemental Analysis. Calcd for C$_{26}$H$_{16}$N$_2$O$_2$ (%): C 80.40, H 4.15, N 7.21, O 8.24; found (%): C 80.39, H 4.16, N 7.23, O 8.22;

2-(2-(9H-carbazol-9-yl)phenyl)-1H-benzo[de]isoquinoline-1,3(2H)-dione (CzPhNI)
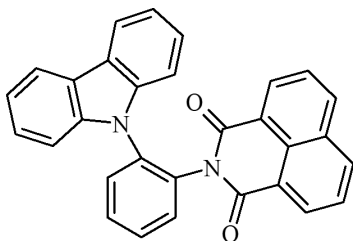
CzPhNI

Obtained according to procedure II. Yellow crystals. FW = 438 g/mol. Yield = 0.27 g, 39%. ^{1}H NMR (300 MHz, DMSO-d^6), δ ppm: 8.35 (d, 2H, J=8.3 Hz), 8.27 (d, 2H, J=7.3 Hz), 7.98 (d, 2H, J=7.7 Hz), 7.87 (dd, 1H, J=7.6, 1.8 Hz), 7.83–7.69 (m, 4H), 7.57 (dd, 1H, J=7.6, 1.6 Hz), 7.27 (t, 2H, J=7.7 Hz), 7.19 (d, 2H, J=8.1 Hz), 7.09 (t, 2H, J=7.4 Hz); ^{13}C NMR (75 MHz, DMSO-d^6) δ ppm: 163.59, 141.48, 136.72, 136.07, 135.05, 134.67, 132.53, 131.19, 130.85, 130.31, 129.87, 127.78, 127.61,

126.21, 123.00, 122.30, 120.49, 120.20, 110.98. MS (ES+, 60 V), *m/z* (%) = 439 ([M + H]+, 50). Elemental Analysis. Calcd. for $C_{30}H_{18}N_2O_2$ (%): C 82.18, H 4.14, N 6.39, O 7.30; found (%): C 82.15, H 4.15, N 6.40, O 7.31;

4-(1,1-Difluoro-1*H*-1λ^4,8λ^4-thiazolo[3,2-*c*][1,3,5,2]oxadiazaborinin-3-yl)-*N,N*-dimethylaniline (5a)
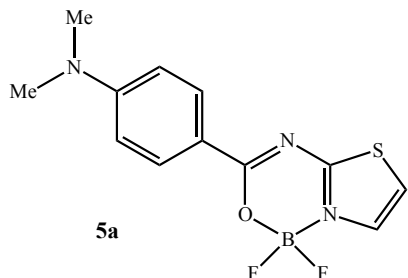
Obtained according synthetic pathway reported by M. Potopnyk *et al.*[98]

¹H NMR (400 MHz, CDCl₃): δ = 8.18 (2H, d, *J* = 9.2 Hz, Ar-H), 7.46 (1H, d, *J* = 4.4 Hz, thiazole-H), 6.95 (1H, d, *J* = 4.4 Hz, thiazole-H), 6.67 (2H, d, *J* = 9.2 Hz, Ar-H), 3.09 (6H, s, 2 × CH₃); ¹³C NMR (100 MHz, CDCl₃): δ = 173.9, 167.0, 154.2, 132.3 (2C), 129.6, 117.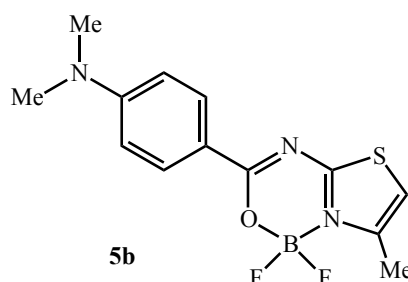4, 112.3, 110.9 (2C), 40.0 (2C); ¹⁹F NMR (375 MHz, CDCl₃): δ = −136.63 (d, *J* = 11.4 Hz), −136.69 (d, *J* = 11.4 Hz). HRMS (ESI-TOF) calcd for $C_{12}H_{12}BN_3OF_2SNa$ [M + Na]⁺: 318.0660, found: 318.0654.

5a

4-(1,1-Difluoro-7-methyl-1*H*-1λ^4,8λ^4-thiazolo[3,2-*c*][1,3,5,2]oxadiaza-borinin-3-yl)-*N,N*-dimethylaniline (5b)
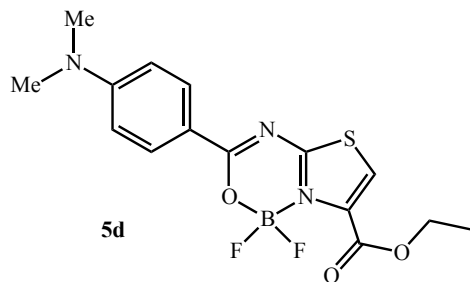
Obtained according synthetic pathway reported by M. Potopnyk *et al.*[98]

¹H NMR (400 MHz, CDCl₃): δ = 8.18 (2H, d, *J* = 9.2 Hz, Ar-H), 6.67 (2H, d, *J* = 9.2 Hz, Ar-H), 6.50 (1H, d, *J* = 0.7 Hz, thiazole-H), 3.08 (6H, s, 2 × CH₃), 2.49 (3H, d, *J* = 0.7 Hz, thiazole-CH₃); ¹³C NMR (100 MHz, CDCl₃): δ = 173.6, 166.2, 154.1, 141.9, 132.2 (2C), 117.5, 110.9 (2C), 106.9, 40.0 (2C), 14.9; ¹⁹F NMR (375 MHz, CDCl₃): δ = −133.77 (d, *J* = 13.0 Hz), −133.84 (d, *J* = 13.0 Hz). HRMS (ESI-TOF) calcd for $C_{13}H_{15}BN_3OF_2S$ [M + H]⁺: 310.0997, found: 310.0991.

5b

Ethyl 3-(4-(dimethylamino)phenyl)-1,1-difluoro-1*H*-1λ^4,8λ^4-thiazolo[3,2-*c*][1,3,5,2]oxadiazaborinine-7-carboxylate (5c)

Obtained according to a synthetic pathway reported by M. Potopnyk *et al.*[98]

¹H NMR (500 MHz, CDCl₃): δ = 8.19 (2H, d, *J* = 9.2 Hz, Ar-H), 7.75 (1H, s, thiazole-H), 6.67 (2H, d, *J* = 9.2 Hz, Ar-H), 4.43 (2H, q, *J* = 7.5 Hz, CH₂), 3.10 (6H, s, 2 × CH₃), 1.42 (3H, t, *J* = 7.2 Hz, CH₃); ¹³C NMR (125 MHz, CDCl₃): δ = 174.8, 167.1, 157.3, 154.4, 136.2, 132.7 (2C), 120.5, 116.7, 110.9 (2C), 62.3, 40.0 (2C), 14.0; ¹⁹F NMR (470 MHz, CDCl₃): δ

5d

= –131.57 (d, J = 6.6 Hz), –131.63 (d, J = 10.8 Hz). HRMS (ESI-TOF) calcd for C$_{15}$H$_{17}$BN$_3$O$_3$F$_2$S [M + H]$^+$: 368.1052, found: 368.1043.

4-(1,1-Difluoro-7-phenyl-1*H*-1λ^4,8λ^4-thiazolo[3,2-*c*][1,3,5,2]oxadiaza-borinin-3-yl)-*N*,*N*-dimethylaniline (5d)
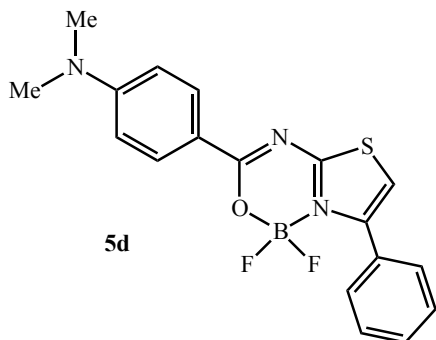
5d

Obtained according to a synthetic pathway reported by M. Potopnyk et al.[98]

^{1}H NMR (400 MHz, CDCl$_3$): δ = 8.18 (2H, d, J = 9.2 Hz, Ar-H), 7.68 (2H, dd, J = 8.4 Hz, J = 2.0 Hz, Ar-H), 7.43–7.48 (3H, m, Ar-H), 6.76 (1H, s, thiazole-H), 6.67 (2H, d, J = 9.2 Hz, Ar-H), 3.07 (6H, s, 2 × CH$_3$); ^{13}C NMR (100 MHz, CDCl$_3$): δ = 174.2, 166.3, 154.2, 146.1, 132.3 (2C), 131.0, 126.2 (2C, t, J_{C-F} = 5.6 Hz), 129.1, 128.3 (2C), 117.3, 110.9 (2C), 109.1, 40.0 (2C); ^{19}F NMR (375 MHz, CDCl$_3$): δ = –130.47 (d, J = 10.0 Hz), –130.53 (d, J = 10.0 Hz). HRMS (ESI-TOF) calcd for C$_{18}$H$_{16}$BN$_3$OF$_2$SK [M + K]$^+$: 410.0712, found: 410.0704.

4,4'-(1,1-Difluoro-1*H*-1λ^4,8λ^4-thiazolo[3,2-*c*][1,3,5,2]oxadiazaborinine-3,7-diyl)bis(*N*,*N*-dimethylaniline) (5e)

Obtained according to a synthetic pathway reported by M. Potopnyk et al.[98]

5e

^{1}H NMR (500 MHz, CDCl$_3$): δ = 8.19 (2H, d, J = 9.2 Hz, Ar-H), 7.58 (2H, d, J = 8.9 Hz, Ar-H), 6.75 (2H, d, J = 8.9 Hz, Ar-H), 6.67 (2H, d, J = 9.2 Hz, Ar-H), 6.65 (1H, s, thiazole-H), 3.08 (6H, s, 2 × CH$_3$), 3.01 (6H, s, 2 × CH$_3$); ^{13}C NMR (125 MHz, CDCl$_3$): δ = 173.9, 165.9, 154.0, 151.0, 147.0, 132.2 (2C), 130.0 (2C), 118.5, 117.5, 111.5 (2C), 110.9 (2C), 107.2, 40.2 (2C), 40.1 (2C); ^{19}F NMR (470 MHz, CDCl$_3$): δ = –130.50 (d, J = 10.1 Hz), –130.55 (d, J = 8.8 Hz). HRMS (ESI-TOF) calcd for C$_{20}$H$_{22}$BN$_4$OF$_2$S [M + H]$^+$: 415.1575, found: 415.1576.

4-(3-(4-(Dimethylamino)phenyl)-1,1-difluoro-1*H*-1λ^4,8λ^4-thiazolo[3,2-*c*][1,3,5,2]oxadiazaborinin-7-yl)benzonitrile (5f)
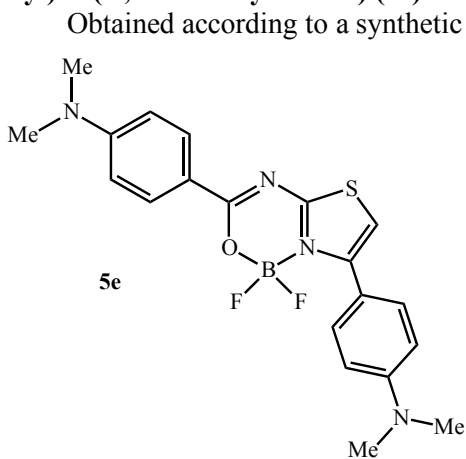
5f

Obtained according to a synthetic pathway reported by M. Potopnyk *et al.*[98]

^{1}H NMR (500 MHz, CDCl$_3$): δ = 8.19 (2H, d, *J* = 9.0 Hz, Ar-H), 7.82 (2H, d, *J* = 8.0 Hz, Ar-H), 7.75 (2H, d, *J* = 8.0 Hz, Ar-H), 6.87 (1H, s, thiazole-H), 6.68 (2H, d, *J* = 9.0 Hz, Ar-H), 3.10 (6H, s, 2 × CH$_3$); ^{13}C NMR (125 MHz, CDCl$_3$): δ = 174.6, 166.6, 154.4, 143.8, 135.3, 132.6 (2C), 132.2 (2C), 129.8 (2C), 118.3, 116.8, 113.4, 110.9 (2C), 110.6, 40.1 (2C); ^{19}F NMR (470 MHz, CDCl$_3$): δ = −129.97 (d, *J* = 10.3 Hz), −130.02. HRMS (ESI-TOF) calcd for C$_{19}$H$_{15}$BN$_4$OF$_2$SNa [M + Na]$^+$: 419.0925, found: 419.0916.

4-(1,1-Difluoro-7-(4-nitrophenyl)-1*H*-1λ^4,8λ^4-thiazolo[3,2-*c*][1,3,5,2]-oxadiazaborinin-3-yl)-*N,N*-dimethylaniline (5g)
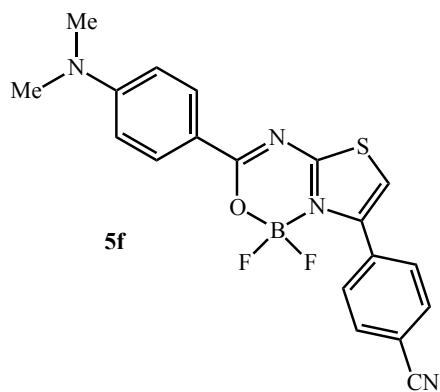
Obtained according to a synthetic pathway reported by M. Potopnyk *et al.*[98]

^{1}H NMR (400 MHz, CDCl$_3$): δ = 8.31 (2H, d, *J* = 8.8 Hz, Ar-H), 8.19 (2H, d, *J* = 9.2 Hz, Ar-H), 7.89 (2H, d, *J* = 8.8 Hz, Ar-H), 6.91 (1H, s, thiazole-H), 6.68 (2H, d, *J* = 9.2 Hz, Ar-H), 3.11 (6H, s, 2 × CH$_3$); ^{13}C NMR (150 MHz, CDCl$_3$): δ = 174.7, 166.7, 154.4, 148.4, 143.4, 137.0, 132.6 (2C), 130.2 (2C), 123.6 (2C), 116.8, 111.0 (2C), 110.9, 40.1 (2C); ^{19}F NMR (375 MHz, CDCl$_3$): δ = −129.89 (d, *J* = 9.8 Hz), −129.96 (d, *J* = 9.8 Hz). HRMS (ESI-TOF) calcd for C$_{18}$H$_{16}$BN$_4$O$_3$F$_2$S [M + H]$^+$: 417.1004, found: 417.0996.

5g
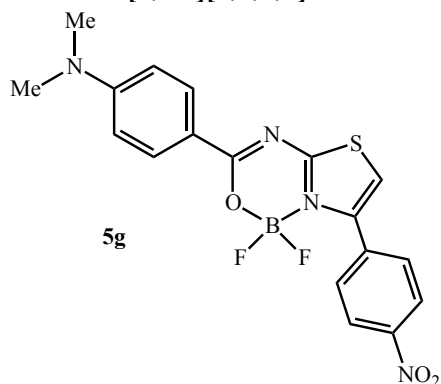
4. RESULTS AND DISCUSSIONS

4.1. Carbazole-chloropyridine derivatives

Over the past few decades, the synthesis and investigation of π-conjugated organic materials has drawn considerable amount of research attention owing to their possible applications in the field of organic optoelectronics. One of the important advantages of low-molar-mass organic semiconductors is that the energy of levels of their peripheral orbitals and subsequent energy gaps of the organic molecules can be modified easily by molecular design and, as a result, the photoelectronic and electrochemical properties can be finely adjusted. Presently, conjugated compounds with electron-donating (D) and electron-accepting (A) units receive the special attention because of their applicability in optoelectronic and electronic devices, such as organic light emitting diodes (OLEDs)[99,100], solar cells[101] and chemical sensors[102]. Compounds which have donor and acceptor moieties often exhibit narrow energy gaps resulting from intramolecular charge transfer (ICT)[103]. The nature, strength and type of the donor and acceptor fragments affect the energy levels of the frontier orbitals and thus influence light-absorbing, light-emitting, and charge-transporting properties of organic electroactive materials. Many studies concerning the synthesis and relationship between the structure and properties of organic semiconductors were reported[104,105]. Nevertheless, the necessity of designing and synthesizing new donor-acceptor low-molar-mass molecular materials with improved optical, photophysical and thermal properties is still an urgent topic. Further improvement of characteristics and stability of optoelectronic devices are the key points of research work in field of materials science. The newly appearing variations of the devices generate new requirements to such materials.

Emissive donor-acceptor organic semiconductors exhibiting either thermally activated delayed fluorescence or aggregation induced emission enhancement effects have great potential for their use as luminophores in different areas including bioimaging, chemosensing and optoelectronics[106,78]. This potential is supported by emission enhancement of luminescent materials due to, 1) harvesting of triplet exitons, and 2) restriction of intramolecular rotation and twisting of molecular moieties in case of TADF and AIEE molecules, respectively. Both TADF and AIE effects allow high photoluminescence quantum yields (PLQY) of organic electroactive materials in a solid state to be obtained thus expanding their applicability. To realize TADF, light-emitting materials with a small energy difference between S_1 and T_1 states (ΔE_{S-T}) are required[47]; however, free intramolecular motions of donor and/or acceptor units in a molecule are required to observe AIEE[107]. Recently, just few donor-acceptor molecular materials showing both TADF and AIEE emitting in mainly green-yellow region were reported[78,108]. Thus, studies about compounds exhibiting aggregation-induced emission enhancement and thermally activated delayed fluorescence with emission in deep-blue region remains important topic, due to its rarity.

This chapter describes the synthesis and characterization of new donor-acceptor molecular materials exhibiting TADF and AIEE. To design these compounds, carbazole was selected as a donor moiety. It is one of the most popular building blocks

for organic optoelectronic materials due to high triplet energy, good hole transporting properties and thermal stability of carbazole derivatives[109,110,111]. Chlorinated pyridine was selected as an acceptor moiety. The pyridine moiety is a well-known component of electron transporting materials. Its derivatives exhibit high triplet levels[112,113]. Pentachloropyridine is a useful and inexpensive starting compound to obtain donor-acceptor compounds with a high triplet energy by a one-step simple aromatic nucleophilic substitution reaction.

4.1.1. Theoretical calculations, synthesis and structural characterization

To study the impact of substitution of carbazole-chloropyridine conjugates on their properties, derivatives of chloropyridine containing one, two and three carbazole moieties were designed (Scheme 4.1.). Pre-synthetic time-dependent density functional theory (TD-DFT) calculations were performed for compounds **4-CzPyCl$_4$, 2,4-CzPyCl$_3$** and **2,4,6-CzPyCl$_2$**. The calculations were carried out with the use of Spartan 14` software package[95]. Both equilibrium geometries and energies of triplet levels (E_T) of the compounds were calculated in a vacuum using the basis B3LYP/6-31+G*. The calculated values of E_T, ΔE_{S-T}, HOMO and LUMO are presented in Table 4.1., while its distribution is depicted in Fig. 4.1. All three synthesized materials demonstrate relatively high E_T estimated to be in the range from 2.85 eV to 3.01 eV. Low theoretical values of ΔE_{S-T} for **4-CzPyCl$_4$** signal about a possible presence of TADF phenomena, moreover, high theoretical values of E_T of all three materials are positive characterizing them for the application in construction of blue-emitting OLEDs as hosts or emitters.



HOMO	HOMO	HOMO
LUMO	LUMO	LUMO
4-CzPyCl$_4$	2,4-CzPyCl$_3$	2,4,6-CzPyCl$_2$
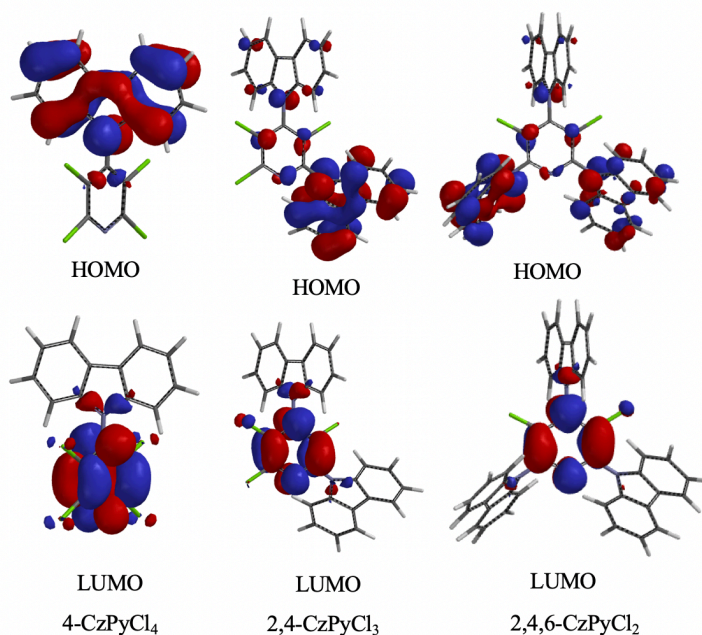
Fig. 4.1. Frontier orbitals distribution for the compounds **4-CzPyCl$_4$, 2,4-CzPyCl$_3$** and **2,4,6-CzPyCl$_2$**

HOMOs of the compounds are mainly located on the electron-donating carbazole moieties while LUMOs are located on the electron-deficient pyridine ring. Such delocalization of electron orbitals allows to predict whether the compounds will exhibit both electron and hole transporting properties. It is also evident that molecules are twisted with a torsion angle close to 75° in the ground state, which leads to the expectation of a small experimental ΔE_{S-T}. Small values of ΔE_{S-T} for carbazole-containing D-A materials are achievable only in the case of implementing strong acceptor moieties such as dicyanobenzene[114,115]. When using weaker acceptors, the values of ΔE_{S-T} of carbazole containing D-A compounds usually range from 0.2 to 0.5 eV[105].

Table 4.1. TD-DFT calculation data for the compounds **4-CzPyCl₄, 2,4-CzPyCl₃** and **2,4,6-CzPyCl₂**

Sample	**4-CzPyCl₄**	**2,4-CzPyCl₃**	**2,4,6-CzPyCl₂**
HOMO (DFT)	-5.9	-5.8	-5.6
LUMO (DFT)	-2.1	-2.0	-2.0
E_T (theor.)	3.01	2.93	2.85
ΔE_{S-T} (theor.)	0.077	0.230	0.124

The synthesis of the derivatives of pyridine and carbazole were performed *via* a one-step catalyst-free aromatic nucleophilic substitution reaction. Depending on the molar ratio of the starting compounds mono-, di- and tri-substituted pyridines (**4-CzPyCl₄**, **2,4-CzPyCl₃** and **2,4,6-CzPyCl₂**) were obtained in fair to good yields. The synthesis and chemical structures of the obtained derivatives are presented in Scheme 4.1.


a = KOH/DMSO, 80°C, 12h
b = KOH/DMSO, 100°C, 12h
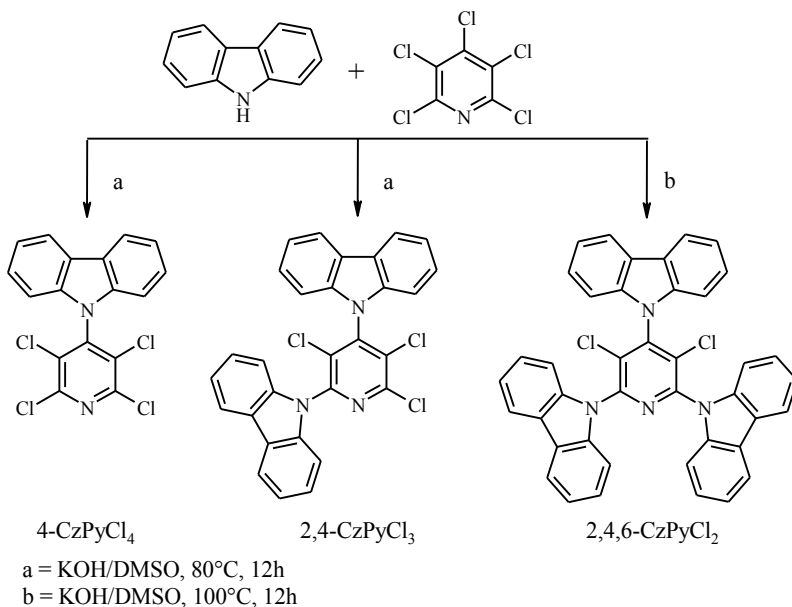
Scheme 4.1. The synthesis of **4-CzPyCl₄**, **2,4-CzPyCl₃** and **2,4,6-CzPyCl₂**.

The target compounds were isolated as either white or off-white crystalline solids after column chromatography and recrystallization. The chemical structures of the compounds were characterized by ^{1}H and ^{13}C NMR and IR spectroscopy and mass spectrometry. The compounds were found to be well soluble in polar organic solvents, such as chloroform, DMF, acetonitrile and methylene chloride. However, solubility decreased with decreasing polarity of a solvent, e.g., the solubility in toluene was considerably lower. The compounds were insoluble in non-polar organic solvents such as *n*-hexane.

In addition, **4-CzPyCl$_4$** was analysed by single crystal X-ray analysis. The data were found to be in good agreement with the proposed structures. The molecules can be characterized by well-ordered packing, despite a highly twisted structure of **4-CzPyCl$_4$**. For a single crystal of **4-CzPyCl$_4$** the dihedral angle between carbazole and pyridine planes was found to be of 71° (Fig. 4.2.). As it seen from the molecular packing diagram, there are no additional intermolecular interactions in the crystal which can have influence on the physical properties of the studied molecule due to perpendicular packing and relatively high (more than 4 Å) distances between molecules.
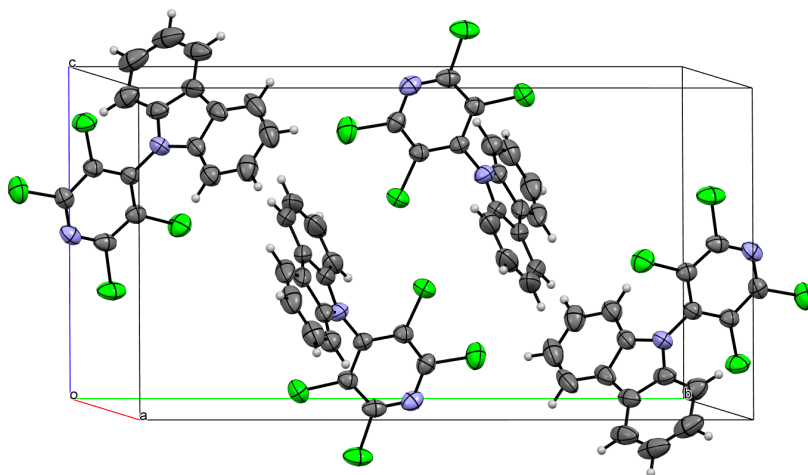
Fig 4.2. Molecular packing ORTEP diagram of **4-CzPyCl$_4$**.

4.1.2. Investigation of thermal properties

The behaviour of **4-CzPyCl$_4$**, **2,4-CzPyCl$_3$**, and **2,4,6-CzPyCl$_2$** under heating was studied by using differential scanning calorimetry (DSC) and thermogravimetric analysis (TGA). Melting points (T_m), glass-transition (T_g), crystallization (T_c), and initial thermal degradation temperatures (T_d) were estimated during analysis and are summarized in Table 4.2. Compounds **4-CzPyCl$_4$**, **2,4-CzPyCl$_3$**, and **2,4,6-CzPyCl$_2$** were obtained as polycrystalline materials after recrystallization from the *i*PrOH/DMF solvent mixture. T_m values are well-defined from the DSC measurement. The positions of single endothermic DSC peaks correspond precisely to the T_m values obtained by measuring melting points in capillary.

Table 4.2. Thermal characteristics of **4-CzPyCl$_4$**, **2,4-CzPyCl$_3$**, and **2,4,6-CzPyCl$_2$**

Compound	T$_g$ (°C)[a]	T$_m$ (°C)[b]	T$_c$ (°C)[c]	T$_d$ (°C)[d]
4-CzPyCl$_4$	n/a	189	98	233
2,4-CzPyCl$_3$	93	231	n/a	307
2,4,6-CzPyCl$_2$	134	311	n/a	380

[a] Glass transition temperature determined by DSC from the 2nd heating scan (scan rate 10°C/min, N$_2$ atmosphere). [b] Melting temperature. [c] Crystallization temperature determined by DSC from the cooling scan (scan rate 10°C/min, N$_2$ atmosphere). [d] Decomposition temperature (5% weight loss temperature) estimated by TGA (scan rate 20°C/min, N$_2$ atmosphere).

DSC scans of **4-CzPyCl$_4$**, **2,4-CzPyCl$_3$** and **2,4,6-CzPyCl$_2$** are shown in Fig. 4.3. and Fig. 4.4. Endothermic melting peaks were estimated at 189°C, 231°C and 311°C for mono-, di- (1st heating scan) and tri- (2nd heating scan) carbazole-substituted chloropyridines, respectively. The value of T$_m$ notably increases correspondingly to the quantity of carbazole substituents in the structure. Crystallization for **4-CzPyCl$_4$** was observed at 98°C in the cooling scan, while glass transition temperature cannot be estimated for this material, due to its low molar mass. The repeated heating scans revealed glass transition temperatures at 93°C for **2,4-CzPyCl$_3$** and at 134°C for **2,4,6-CzPyCl$_2$**.

(a) (b)
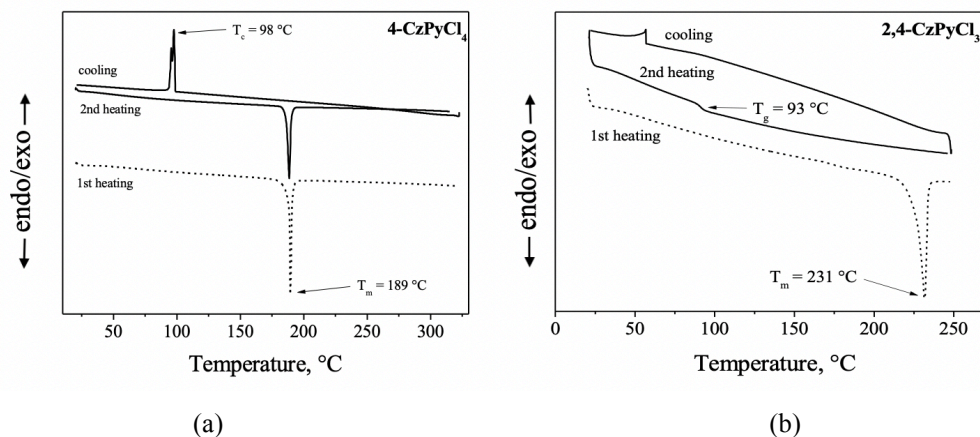
Fig. 4.3. DSC thermograms of compounds **4-CzPyCl$_4$ (a)** and **2,4-CzPyCl$_3$ (b)**

Fig. 4.4. shows TGA curves of the studied compounds. The analysis revealed moderate thermal stability for all three materials with the temperatures of 5% weight loss in the range from 233°C to 380°C. The shapes of TGA curves show that materials are not decomposed but sublimed during the analysis. The difference of thermal stabilities of the compounds were evidently predetermined by different quantities of chlorine atoms present in the molecules and difference in molecular weight. **4-CzPyCl$_4$** has the lowest molecular weight, containing four atoms of chlorine, two of which (at C-2 and C-6 positions) are highly reactive especially at high temperatures, exhibited the lowest 5% weight loss. On the other hand, **2,4-CzPyCl$_3$** and, moreover,

2,4,6-CzPyCl₂ containing fewer active chlorine atoms and much higher molecular weight which in higher temperature results in 5% weight loss.

(a)   (b)
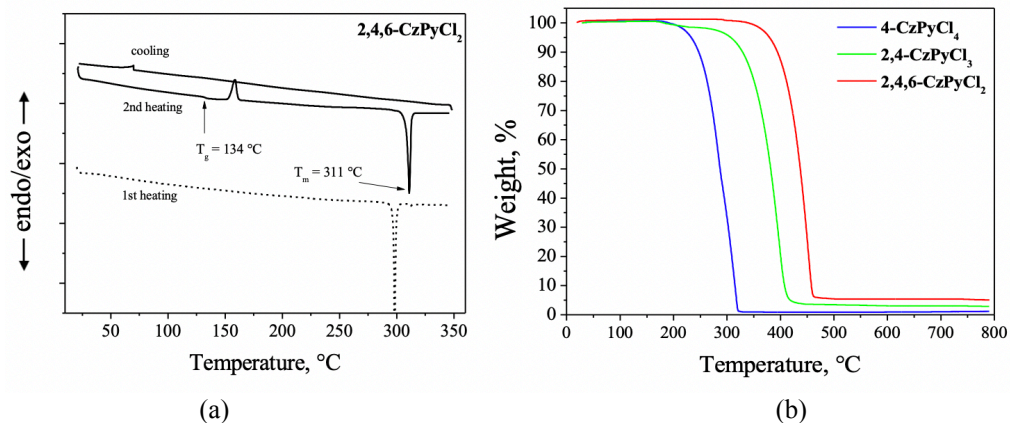
Fig. 4.4. A DSC thermogram of **2,4,6-CzPyCl₂ (a)** and TGA curves of **4-CzPyCl₄**, **2,4-CzPyCl₃** and **2,4,6-CzPyCl₂ (b)**

4.1.3. Studying the electrochemical and photoelectrical properties

To experimentally examine the energy levels of the studied molecules, electrochemical properties of DMF solutions of the compounds were studied by using cyclic voltammetry (CV). The electrochemical oxidation and reduction onset potentials were used to estimate the ionization potentials and electron affinities of the materials. Fig. 4.5. shows the CV curves of compounds **4-CzPyCl₄**, **2,4-CzPyCl₃** and **2,4,6-CzPyCl₂**.
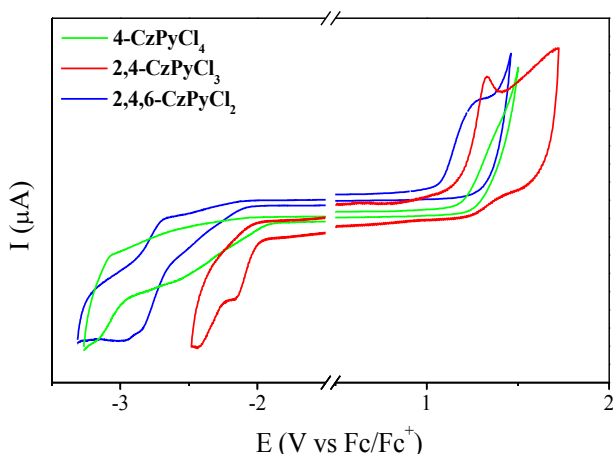
Fig. 4.5. CV voltammograms of **4-CzPyCl₄**, **2,4-CzPyCl₃** and **2,4,6-CzPyCl₂**.

Irreversible oxidation processes were observed at 1.14 V for **4-CzPyCl₄**, at 1.10 V for **2,4-CzPyCl₃** and at 1.03 V for **2,4,6-CzPyCl₂**, respectively. Unsubstituted active C-3 and C-6 positions of carbazole moieties are evidently responsible for the

irreversibility of oxidation processes. Similar observations were reported earlier[116]. In addition, **4-CzPyCl$_4$, 2,4-CzPyCl$_3$** and **2,4,6-CzPyCl$_2$** demonstrated irreversible reduction at -1.83 V, -1.94 V and -2.02 V, respectively (Table 4.3.**)**.

The ionization potential (IP$_{CV}$) and electron affinity (EA$_{CV}$) values of the synthesized compounds were estimated using ferrocene/ferrocenium as the standard redox system. IP$_{CV}$ and EA$_{CV}$ values are summarized in Table 4.3. **4-CzPyCl$_4$** was found to show the highest IP$_{CV}$ value of 6.20 eV, while **2,4,6-CzPyCl$_2$** exhibited the lowest IP$_{CV}$ value of 6.04 eV and, thus, the highest electron donating ability. Relatively high values of the electrochemical band gap were estimated for the **4-CzPyCl$_4$, 2,4-CzPyCl$_3$** and **2,4,6-CzPyCl$_2$** situated in the range from 2.97 eV to 3.05 eV. In comparison, optical energy band gaps (E$_g$) obtained from the UV spectra were found to be slightly larger (3.27–3.30) which apparently can be explained by different solvation effects which can have influence during the CV and UV spectra measurements (Table 4.3.).

Potential application of these materials in solid-state electronic devices requires to precisely estimate the ionization potentials (IP$_{PE}$) of the solid layers of **4-CzPyCl$_4$, 2,4-CzPyCl$_3$** and **2,4,6-CzPyCl$_2$** which were measured by recording their electron photoemission spectra (Fig. 4.6.). The solid-state IP$_{PE}$ values were found to be in the range from 5.74 to 5.88 eV (Table 4.3.). The relatively notable variances between the values of IP obtained by using electron photoemission spectrometry and electrochemical analysis are caused by the difference in molecular interactions and the presence of molecular arrangements in the solid layers compared to dilute solutions of the derivatives. However, the IP values of photoelectron emission spectrometry are close and comparable to the respective values of E$_{HOMO}$ obtained by the theoretical TD-DFT calculations.
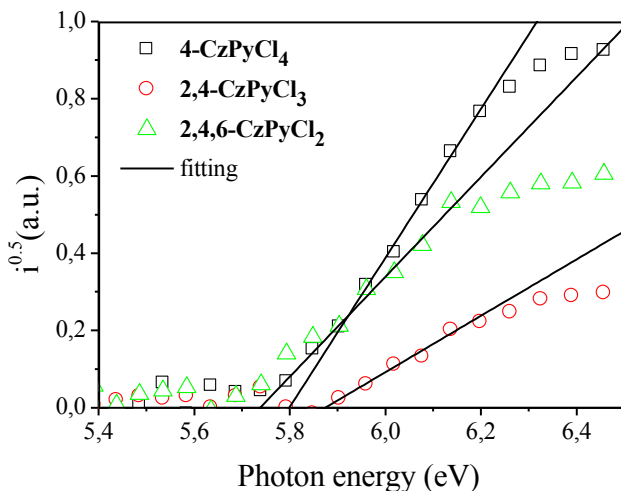
**Fig. 4.6.** Photoelectron emission spectra of **4-CzPyCl$_4$, 2,4-CzPyCl$_3$** and **2,4,6-CzPyCl$_2$**.

Table 4.3. Electrochemical and photoelectrical characteristics of compounds

Param. /Comp.	E_{ox}, eV,[a]	E_{red}, eV,[a]	IP_{CV}, eV,[b]	IP_{PE}, eV,[c]	EA_{CV}, eV,[b]	E_g^{opt}, eV,[d]	E_g^{CV}, eV[e]
4-CzPyCl$_4$	1.14	-1.83	6.20	5.88	2.60	3.30	2.97
2,4-CzPyCl$_3$	1.10	-1.94	6.14	5.74	2.47	3.28	3.04
2,4,6-CzPyCl$_2$	1.03	-2.02	6.04	5.80	2.38	3.27	3.05

[a] Onset E_{red} and onset E_{ox} are measured vs. ferrocene/ferrocenium. [b] Ionization potentials and electron affinities are estimated according to $IP_{CV} = (-1.4*E_{ox} - 4.60)$. $EA_{CV} = (-1.19*E_{red} - 4.78)$. [c] Ionization potentials are measured by electron photoemission spectrometry. [d] E_g^{opt} is calculated using equation $E_g^{opt} = 1239.75/\lambda$ ($\lambda_{4-CzPyCl4} = 376$ nm, $\lambda_{2,4-CzPyCl3} = 378$ nm, $\lambda_{2,4,6-CzPyCl2} = 379$ nm (from UV spectra)); [e] was calculated using equation $E_g^{CV} = E_{ox} - E_{red}$.

4.1.4. Charge-transporting properties

Charge-transporting properties of the studied derivatives were characterized by applying the CELIV technique. Noting that the maxima on photocurrent transient curves were seen, the charge mobility can be calculated using the extraction time taken at the time of maxima (Fig. 4.7. (a)). The dependencies of the hole drift mobility on the square root of electric field for the layers of **4-CzPyCl$_4$,** and **2,4,6-CzPyCl$_2$** are shown in Fig. 4.7. (b). The CELIV samples for **2,4-CzPyCl$_3$** were not fabricated due to strong crystallinity of the **2,4-CzPyCl$_3$** non-doped layer hence hole mobility was not calculated for this compound. Similar hole mobility values for the layer of compound **4-CzPyCl$_4$** and **2,4,6-CzPyCl$_2$** were obtained exceeding 1×10^{-5} cm^2/Vs at an electric field higher than 2×10^5 V/cm. These hole mobility values are also comparable to many other carbazole-based organic semiconductors[117,118].

(a)   (b)
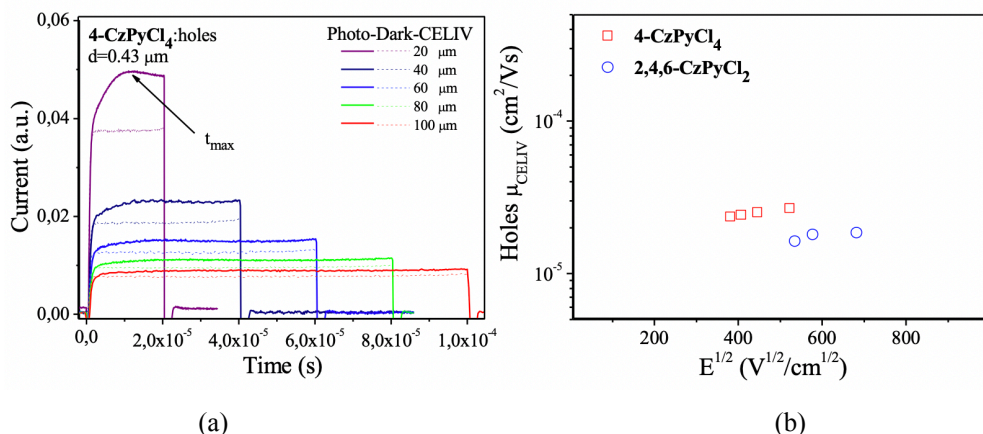
Fig. 4.7. CELIV transient curves **(a)** for the layer of **4-CzPyCl$_4$** representing holes, and hole drift mobility as a function of electric field ($E^{1/2}$) for the layers of **4-CzPyCl$_4$,** and **2,4,6-CzPyCl$_2$ (b)**.

4.1.5. Photophysical properties

The photophysical properties of chloropyridine-carbazole conjugates were investigated in tetrahydrofuran (concentration 1×10^{-5} mol/L) solutions and in solid films deposited on glass substrates by using vapour deposition. All the studied compounds absorbed in the ultraviolet range and emitted in the visible region. The photophysical data are summarised in Table 4.4., while the absorption and fluorescence spectra of the dilute solutions and of the solid films are depicted in Fig. 4.8.

Low-energy band of absorption spectrum of **4-CzPyCl₄** with a maximum at 248 nm is attributed to the PL of a locally excited carbazole unit[119]; while a shoulder band at 387 nm originates from the CT emission. All materials exhibited sky-blue emission in THF solutions, however, in a solid state **4-CzPyCl₄** and **2,4-CzPyCl₃** present a slight hypsochromic shift. This can be explained by a higher dielectric constant of THF solution compared to the neat films of materials. PL of the solid sample of **4-CzPyCl₄** with the intensity maximum at 435 nm is characterized by a deep-blue colour with the chromaticity coordinates of (0.17, 0.13). The solutions of **4-CzPyCl₄**, **2,4-CzPyCl₃**, and **2,4,6-CzPyCl₂** in THF exhibited low PLQYs which do not exceed 4%; moreover the PLQY of the solid-state samples of **2,4-CzPyCl₃**, and **2,4,6-CzPyCl₂** remains low, although PLQY of **4-CzPyCl₄** achieves a value of 16% demonstrating emission enhancement which can be explain by exhibiting AIEE caused by the restriction of intramolecular rotations without the planarization of the molecular structure[120].
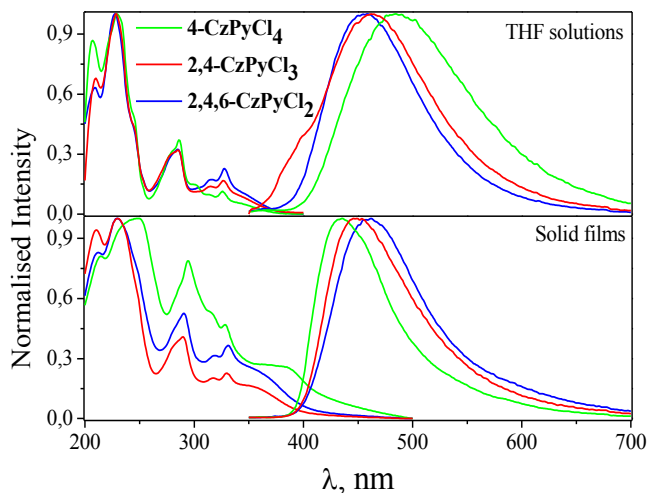
Fig. 4.8. UV and PL spectra of THF solutions and solid films of **4-CzPyCl₄**, **2,4-CzPyCl₃**, and **2,4,6-CzPyCl₂**

The solvatochromic solvent effect on the photoluminescence spectra of **4-CzPyCl₄**, **2,4-CzPyCl₃**, and **2,4,6-CzPyCl₂** was studied (Fig. 4.9.). The wavelengths of maximum intensities exhibited bathochromic shifts with the increase of the solvent polarity. The monosubstituted chloropyridine derivative **4-CzPyCl₄** exhibited larger

bathochromic shifts with respect to those of the di- and tri- substituted derivatives. These observations demonstrate that the photoluminescence of the studied compounds originates from a photoinduced intramolecular charge transfer (ICT) state and **4-CzPyCl₄** demonstrates the highest ICT energy in comparison to the **2,4-CzPyCl₃**, and **2,4,6-CzPyCl₂** (Table 4.4.).
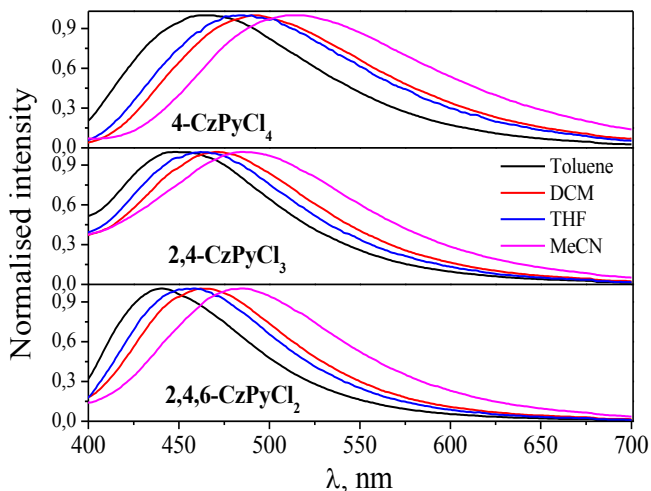
Fig. 4.9. Solvent effect on PL spectra of **4-CzPyCl₄**, **2,4-CzPyCl₃**, and **2,4,6-CzPyCl₂**

Table 4.4. Photoluminescence wavelengths of emission maxima for compounds **4-CzPyCl₄**, **2,4-CzPyCl₃**, and **2,4,6-CzPyCl₂** in various solvents

Compound	Wavelength of emission in solvent, nm			
	Toluene	Tetrahydrofuran	Dichloromethane	Acetonitrile
4-CzPyCl₄	467	485	492	512
2,4-CzPyCl₃	448	462	471	485
2,4,6-CzPyCl₂	441	459	462	485

To estimate the experimental values of E_T and $\Delta E_{S\text{-}T}$, photoluminescence and phosphorescence spectra were recorded at 77K without and with a >50 ms delay (Fig. 4.10. and Fig. 4.11.).
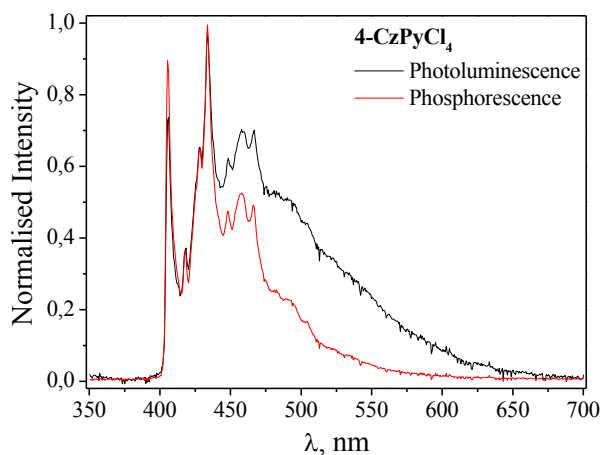
Fig. 4.10. Normalized low-temperature photoluminescence and phosphorescence spectra at 77K of THF solution of **4-CzPyCl₄**

(a)   (b)
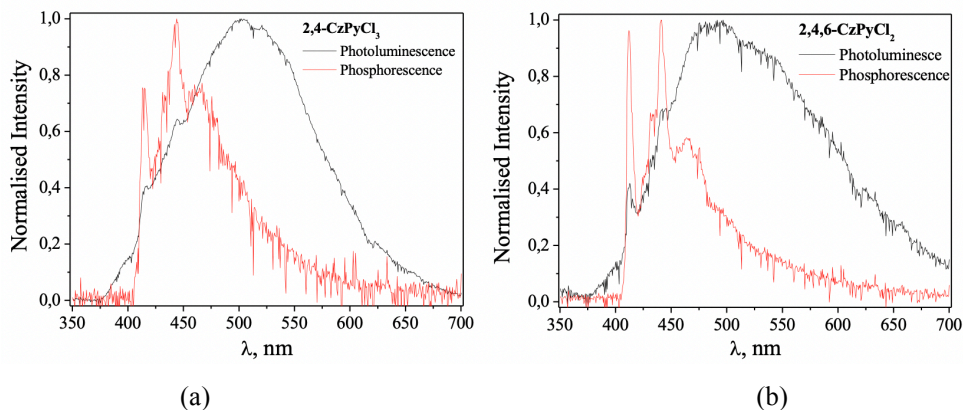
Fig. 4.11. Normalized low-temperature photoluminescence and phosphorescence spectra at 77K of THF solutions of **2,4-CzPyCl₃ (a)**, and **2,4,6-CzPyCl₂ (b)**

Triplet energy values of the compounds **4-CzPyCl₄, 2,4-CzPyCl₃** and **2,4,6-CzPyCl₂** were established to be 3.08 eV, 3.07 eV and 3.05 eV, respectively. The values of $\Delta E_{S\text{-}T}$ for the studied compounds are 0.06 eV, 0.31 eV and 0.22 eV, respectively, depending on the number of attached carbazolyl moieties: **4-CzPyCl₄** demonstrated the lowest $\Delta E_{S\text{-}T}$ while increasing the quantity of carbazole substituents resulted in an increment of $\Delta E_{S\text{-}T}$ value. This can be explained by that fact that the ICT is originated from less twisted carbazole units in **2,4-CzPyCl₃** and **2,4,6-CzPyCl₂**. The triplet energy value and singlet-triplet gap energy values were estimated from equations: $E_T = 1239.75/\lambda_{\text{phosphorescence}}$ and $\Delta E_{S\text{-}T} = 1239.75/\lambda_{\text{low-temp PL}}$ – $1239.75/\lambda_{\text{phosphorescence}}$, where $\lambda_{\text{low-temp PL}}$ and $\lambda_{\text{phosphorescence}}$ were taken by onset. These results are in good correlation with the theoretical values obtained by the TD-DFT measurements (Table 4.1.).

56

Table 4.4. The photophysical properties of chloropyridine-carbazole conjugates

Compound	$\lambda_{abs}{}^{a}$ (nm)	$\lambda_{em}{}^{a}$ (nm)	Φ^{a}	Stokes shift^{a} (cm^{-1})	$\lambda_{abs}{}^{b}$ (nm)	$\lambda_{em}{}^{b}$ (nm)	Φ^{b}	Stokes shift^{b} (cm^{-1})	τ^{b} (ns)	χ
4-CzPyCl₄	326	485	0.03	10056	329, 387*	435	0.16	7407	5.52; 48.53; 292.54	1.188
2,4-CzPyCl₃	326	462	0.04	9030	330	446	0.02	7882	10.36; 321.13	1.247
2,4,6-CzPyCl₂	328	459	0.02	8701	331	462	0.02	8566	20.68; 369.66	1.129

^{a} In a THF solution. ^{b} In a solid state. λ_{abs} – the wavelength of absorption maximum, λ_{em} – the wavelength of fluorescence emission maximum, Φ – fluorescence quantum yield, τ – excited-state lifetime. * – shoulder.

4.1.6. Investigating aggregation-enhanced and thermally-activated deep-blue emission of 4-CzPyCl₄

Since solid samples of **4-CzPyCl₄** were characterized by higher PLQY than its dilute solutions, the fluorescent properties of **4-CzPyCl₄** were examined in more detail. THF-water mixtures of various ratios with the same quantity of **4-CzPyCl₄** were prepared for estimation of the aggregation effect on emission properties. **4-CzPyCl₄** is well soluble in THF but not soluble in water which leads to the formation of solid-state particles of **4-CzPyCl₄** with increasing water fraction in the THF solution. The PL intensity of the dispersions of **4-CzPyCl₄** in THF-water mixtures decreased with increasing the water fraction up to 70% (Fig. 4.12.).
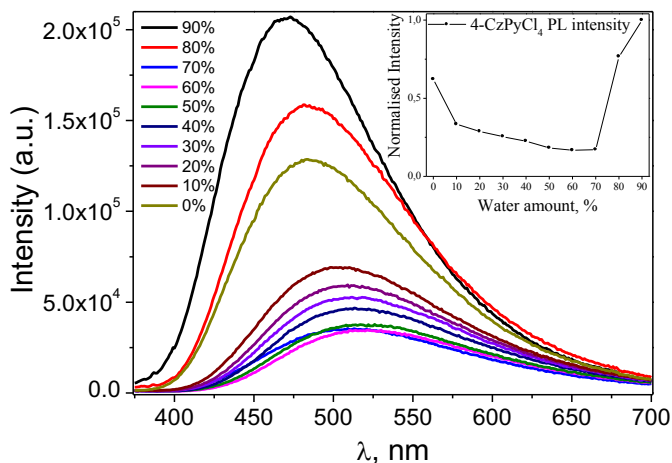
Fig. 4.12. Emission spectra of **4-CzPyCl₄** dispersed in THF/water mixture with different concentrations of water. Inset: dependence of emission intensity of **4-CzPyCl₄** on the concentration of water

In addition, the wavelength of emission maximum steadily red-shifted from 484 nm to 522 nm with an increase of water fraction from 0 to 70%. Both the decreasing intensity and the bathochromic shift of emission of **4-CzPyCl₄** dispersed in the THF-water mixtures observed with the increase of the fraction of water up to 70% can be explained mainly by increasing the polarity of mixtures. In addition, the dynamic quenching of the excited states caused by thr enhancement of H-bonding can be one reason for the decreased PLQY in THF-water mixtures[121]. A significant increase of the fluorescence intensity and high-energy shift of PL maximum were detected with further increase of water fraction in the mixtures. When the concentration of water approached the critical point of 70%, the aggregation of **4-CzPyCl₄** started increasing the PL intensity and high-energy shift of PL maximum. This observation indicates the effect of aggregation-induced emission enhancement for **4-CzPyCl₄**.

To further ascertain the nature of emission of **4-CzPyCl₄**, **2,4-CzPyCl₃**, and **2,4,6-CzPyCl₂** in the solid-state, PL decay transients of the solid layers of the synthesized compounds were recorded. Short-lived and long-lived components can be recognized. The PL decay transients were fitted at both short- and long-lived time ranges (Fig. 4.13, Table 4.4., Table 4.5.).

(a)   (b)
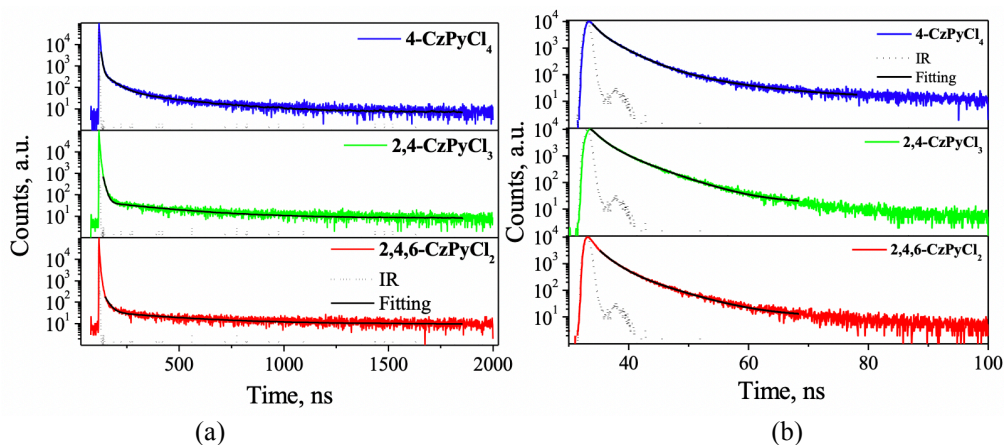
Fig. 4.13. PL decay transients of long-lived **(a)** and short-lived **(b)** time ranges for the solid layers of **4-CzPyCl₄**, **2,4-CzPyCl₃**, and **2,4,6-CzPyCl₂**

Table 4.5. Short-lived PL decay data of **4-CzPyCl₄**, **2,4-CzPyCl₃**, and **2,4,6-CzPyCl₂**

Comp./Parameter	4-CzPyCl₄	2,4-CzPyCl₃	2,4,6-CzPyCl₂
τ, ns	1.06;3.26;10.17	1.63;5.26	1.81;5.90
χ^2	1.043	1.278	1.001

The short-lived component is definitely related to prompt fluorescence, while the long-lived component can be attributed to TADF. The shapes of PL decay curves are similar to those of TADF molecules[122]. To confirm the presence of TADF, PL

decay transients of the layer of **4-CzPyCl4**, which was characterized by the highest PLQY, were recorded at different temperatures ranging from 77 to 300 K (Fig. 4.14.).
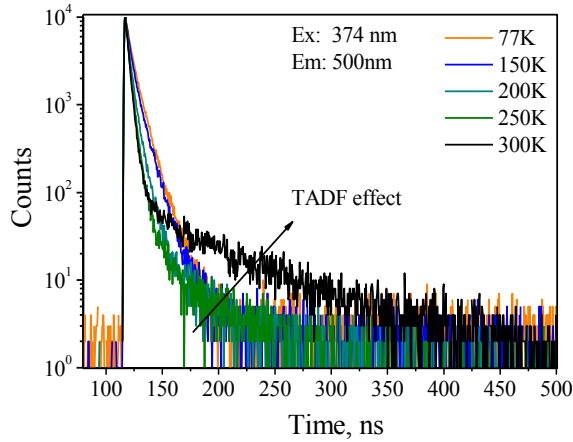
Fig. 4.14. PL decay curves of the solid film of **4-CzPyCl4** recorded at different temperatures

The long-lived time component is clearly seen at 300 K while at 77 K it is absent. This observation confirms the presence of TADF in the emission of the layer of **4-CzPyCl4**. TADF occurs despite a relatively high ΔE_{S-T} of 0.15 eV in the solid-state (Fig. 4.15. (a)). The layer of **4-CzPyCl4** showed a similar PL spectra at different temperatures, perhaps due to the similarity of the spectra of phosphorescence, prompt and delay fluorescence (Fig. 4.15. (b)).

a)   b)
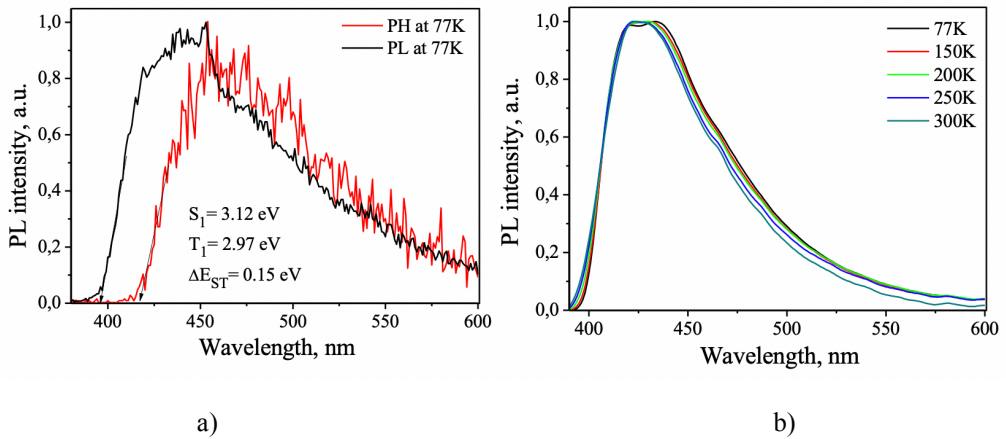
Fig. 4.15. PL and PH spectra **(a, b)**, of the solid film of **4-CzPyCl4** recorded at different temperatures

Thus, the data, discussed above show that both AIEE and TADF effects are characteristic of the solid samples of deep blue emitting **4-CzPyCl4**. According to the X-ray single crystal analysis, a combination of TADF and AIEE effects for the monocarbazolyl-substituted chloropyridine is possible due to the relatively large dihedral angle between carbazole and pyridine planes (71°). Apparently, the angle

59

between carbazole and pyridine planes is high enough due to the presence chlorine atoms which reinforce HOMO and LUMO orbitals of **4-CzPyCl₄** resulting in small ΔE_{ST} and TADF. At the same time, relatively free intramolecular motions of carbazole and pyridine units are possible in **4-CzPyCl₄** which make it possible for the AIEE to result in its higher PLQY of solid-state samples relative to those of the solutions.

To conclude, mono-, di- and tri- carbazolyl-substituted low-molar-mass derivatives of chloropyridine were synthesized by using aromatic nucleophilic substitution. The monocarbazolyl-substituted chloropyridine showed aggregation-induced emission enhancement of the deep-blue emission with thermally activated delayed fluorescence. The combination of TADF and AIEE effects for the monocarbazolyl-substituted chloropyridine was observed due to both the relatively large dihedral angle between carbazole and pyridine planes and the relatively free intramolecular motions. The compounds were characterized as thermally stable and triplet energy levels of the compounds were estimated to be higher than 3 eV. In addition, materials were found to have good semiconductor properties with decent charge-carrier mobilities.

These results form a good background for the design and synthesis of highly-effective deep-blue luminophores. Monocarbazolyl-substituted chloropyridine exhibiting both deep-blue TADF and AIEE effects may have great use potential in different areas including bioimaging, chemosensing and optoelectronics.

4.2. Carbazole-imide conjugates

The employment of novel design strategies and synthetic approaches for the development of materials for organic optoelectronics is very important to achieve high efficiency results in the fabrication of OLEDs. Suitable donor-acceptor materials for DF OLEDs application must fit a lot of requirements: thermal and electrochemical stability, decent morphological properties, low ΔE_{S-T} values and high charge-transporting abilities; moreover, high PLQY is desirable for the construction of an effective OLED. The presence of AIEE effect can be an additional advantage for the application of materials in optoelectronics.

Novelty in design also can be implemented through an alternative way of ICT in donor-acceptor materials, e. g. intermolecular exciplexes or compounds with charge transfer through space[123]. Such materials can be successfully applied in the fabrication of OLEDs[124] and OFETs[125].

Usually charge-transfer through space in any type of exciplex are provided by donor-acceptor bonds between electron pairs of electron-rich donor moiety and electron-deficient acceptor moiety[126]. The most difficult is the selection of a suitable and appropriate donor to the corresponding acceptor as well as achieving efficient light emission from their cooperation.

This chapter describes the synthesis and characterization of physical properties of new donor-acceptor molecular materials exhibiting TADF and AIEE with charge transfer occurring through space. To design these compounds, carbazole was selected as a donor moiety and aromatic imides were selected as acceptor moieties. Aromatic imides recently became a popular acceptor in the synthesis of materials for electronic applications and the construction of OLEDs[69-71]. Aromatic imides are convenient and inexpensive starting materials to obtain donor-acceptor compounds demonstrating the TADF phenomenon. Donor-acceptor materials based on aromatic imides can be obtained with simple and inexpensive synthesis with low quantity of synthetic steps.

4.2.1. Theoretical calculations, synthesis and structural characterization

Computational studies applying the time dependent density functional theory (TD-DFT) were carried out to predict electrochemical and photophysical properties of **CzPhPI** and **CzPhNI**. Spartan 14` software package[95] was used for the implementation of the calculations. Basis set B3LYP/6-31+G* was used for the calculation of triplet level energy values (E_T) and equilibrium geometries. The computed values of parameters (E_S, E_T, ΔE_{S-T}, HOMO, LUMO) are presented in Table 4.6, while the delocalization of HOMOs and LUMOs is depicted in Fig. 4.16. LUMOs are strictly located on the electron-deficient aromatic imide fragments while HOMOs are mostly located on the electron-rich carbazole fragments.

Theoretically obtained delocalization of electron orbitals indicates the compounds' potential ability of transporting both electrons and holes. Electron-donating and electron-withdrawing fragments are twisted with respect to phenyl linker with a torsion angle of ca. 75° in the ground state, which significantly reduces conjugation and leads to the expectation of a low singlet-triplet energy splitting (ΔE_{S-T}). The position of nitrogen atom with respect to the carbon atom of a carbonyl group of an imide moiety allows to predict the possible interactions between the free electron

pair of a nitrogen atom with the double bond of a carbonyl group. Such n→π*
interactions were previously reported[127,128,129], however, charge transfer between
particularly carbazole and phthalimide units through this interaction has not been
reported earlier.

| CzPhPI HOMO | CzPhPI LUMO | CzPhNI HOMO | CzPhNI LUMO |
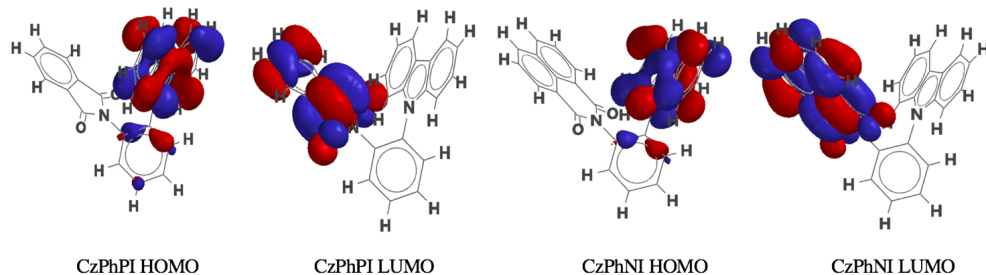
Fig. 4.16. Delocalization of HOMOs and LUMOs for compounds **CzPhPI** and **CzPhNI**

Tab. 4.6. TD-DFT theoretical calculation data for compounds **CzPhPI** and **CzPhNI**

Compound	HOMO, eV	LUMO, eV	E_S, eV	E_T, eV	ΔE_{S-T}, eV
CzPhPI	-5.3	-2.2	2.4465	2.4323	0.0142
CzPhNI	-5.2	-2.4	2.2861	2.2786	0.0075

The synthetic pathways for **CzPhPI** and **CzPhNI** contained three steps (Scheme
4.2.). The first step was aromatic nucleophilic substitution, the second step was a
reduction of the nitro group to an amino group using nickel bromide hydrate as a
catalyst and the last stage was the formation of cyclic imides.
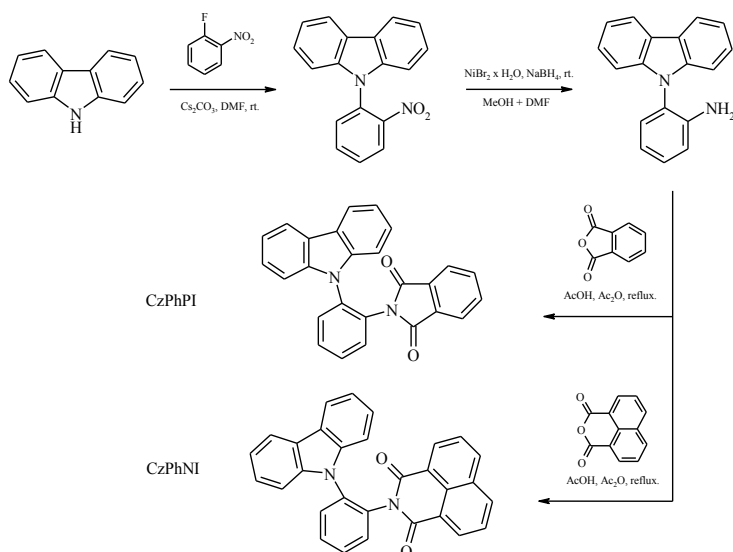
Scheme 4.2. The synthetic pathway for synthesis of **CzPhPI** and **CzPhNI**

After recrystallization, the target compounds were obtained as crystalline substances. Mass spectrometry, ^{1}H and ^{13}C NMR spectroscopy and single crystal X-ray analysis were utilized to confirm the chemical structures of the materials. **CzPhPI** demonstrated moderate solubility in polar organic solvents such as chloroform, dichloromethane, dimethylformamide (DMF), acetonitrile and acetone while solubility in toluene was very low. **CzPhNI** was found to be considerably less soluble than **CzPhPI**. It could be dissolved only in DMF and DMSO.

Single crystal X-Ray analysis of compounds **CzPhPI** and **CzPhNI** (Fig. 4.17.) was performed.

CzPhPI   CzPhNI

Fig. 4.17. ORTEP structures of compounds **CzPhPI** and **CzPhNI**

It revealed that torsion angles for **CzPhPI** were 69° between the carbazole and benzene ring planes and 64° between the phthalimide plane and the benzene ring plane. For **CzPhNI** these angles were 86° between the carbazole plane and the benzene ring plane and 78° between the napththalic imide plane and the benzene ring plane. Interatomic distances between the nitrogen atom of carbazole and the ca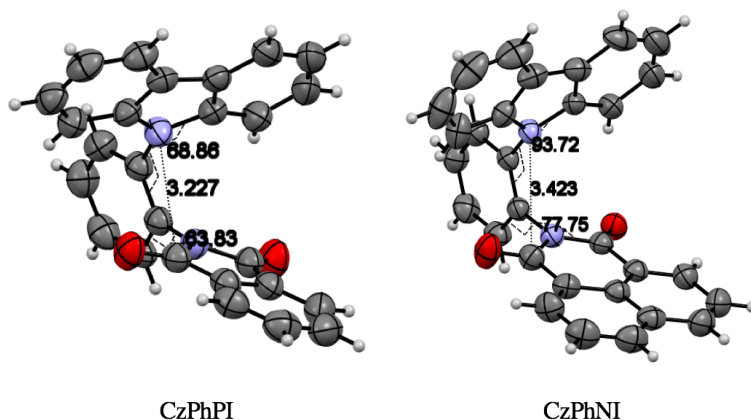rbon atom of carbonyl group of respective imide were also measured. For **CzPhPI** this distance was estimated to be 3.227 Å, and for **CzPhNI** it was 3.423 Å. The value of N-C interatomic distance for **CzPhPI** was slightly less than the sum of the van der Waals radii of carbon and nitrogen atoms (3.25 Å) which makes possible n→π* interaction between the free electron pair of a nitrogen atom of carbazole with the unoccupied orbital of a carbon atom of a carbonyl group[128,129].

Additionally, molecular packings of **CzPhPI** and **CzPhNI** were analysed (Fig. 4.18.). As it seen from the molecular packing diagrams, there are no additional intermolecular interactions in the crystals of **CzPhPI** which can have influence on the charge transfer process due to perpendicular packing and relatively high (more than 4 Å) distances between carbazole and imide moieties of adjacent molecules. In contrast, **CzPhNI** have sandwich-like packing, although, the stacking of naphthylamide planes can not cause any intermolecular charge transfer.
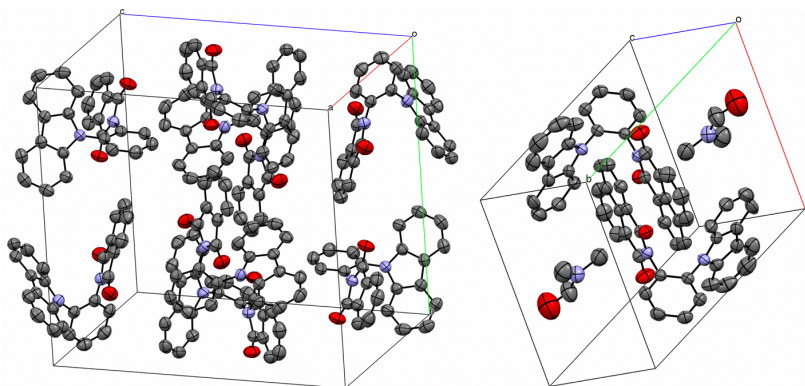
Fig. 4.18. Molecular packing diagrams of the **CzPhPI** (left) and **CzPhNI** (right)

4.2.2. Thermal characterization

Thermal gravimetric analysis (TGA) and differential scanning calorimetry (DSC) were used to investigate thermal stability and determine the temperatures of morphological transitions. After the synthesis, both compounds were isolated as crystalline substances. DSC scans of **CzPhPI** and **CzPhNI** are depicted in Fig. 4.19. Endothermic peaks at 232°C and 249°C for **CzPhPI** and **CzPhNI**, respectively, can be characterized as melting temperatures. The exothermic peak which is observed at 154°C for **CzPhPI** on a cooling scan can be characterized as crystallization temperature, while the cooling scan of **CzPhNI** revealed two close peaks of crystallization at 158°C and 162°C. In addition, the 2nd heating scan for **CzPhNI** revealed an exothermic peak at 180°C. This behavior, can be explained as two crystalline forms of **CzPhNI**. On the cooling scan two crystallization peaks are responsible for the formation of two types of different crystals, and the following heating scan presents a solid-solid phase transition between crystalline forms. Melting points (T_m), crystallization temperatures (T_c), solid-solid phase transition temperature (T_{s-s}) and 5% weight loss temperatures (T_d) are summarized in Table 4.7.

| (a) | (b) |
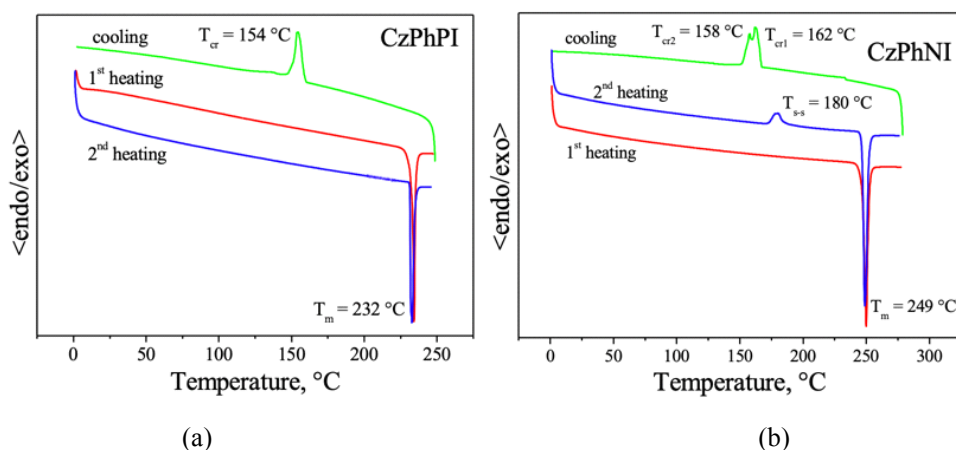
Fig. 4.19. DSC thermograms of compounds **CzPhPI (a)** and **CzPhNI (b)**

TGA curves of the studied materials are shown in Fig. 4.20. The results of the measurements revealed 5% weight loss temperatures of 280°C and 310°C for **CzPhPI** and **CzPhNI**, respectively, which can be characterized as relatively high. Practically full loss of weight of the sample in the temperature range between 360°C and 380°C shows that the process of sublimation was recorded by TGA but not thermal decomposition.
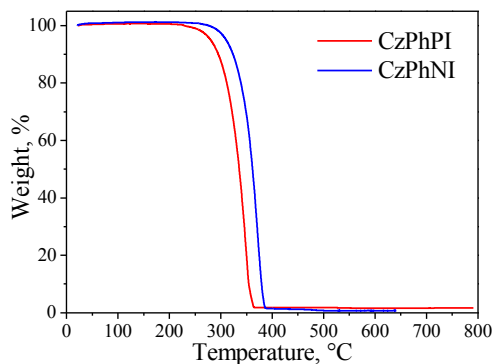
Fig. 4.20. TGA curves of the compounds **CzPhPI** and **CzPhNI**

Table 4.7. Thermal characteristics of **CzPhPI** and **CzPhNI**

Compound	T_m, °C[a]	T_c, °C[b]	T_{s-s}, °C[c]	T_d, °C[d]
CzPhPI	232	154	n/a	280
CzPhNI	249	158, 162	180	310

[a] Melting temperature. [b] Crystallization temperature determined by DSC from the cooling scan (scan rate 10°C/min, N_2 atmosphere). [c] Solid-solid phase transition [d] Decomposition temperature (5% weight loss temperature) estimated by TGA (scan rate 20°C/min, N_2 atmosphere).

4.2.3. Electrochemical and photoelectrical properties

Cyclic voltammetry (CV) was used to study the electrochemical properties of DMF solutions of the compounds for an experimental estimation of the ionization potentials (IP_{CV}) and electron affinities (EA_{CV}). IP_{CV} and EA_{CV} of the solutions of the compounds were calculated with equations $IP_{CV} = (E_{ox} + 4.8)$ and $EA_{CV} = (E_{red} + 4.8)$ using electrochemical oxidation and reduction onset potentials of the solutions and ferrocene/ferrocenium as a standard. The CV curves of **CzPhPI** and **CzPhNI** are depicted in Fig. 4.21. (a). Irreversible oxidation processes were observed at 0.99 eV for **CzPhPI** and at 0.94 eV for **CzPhNI**. The irreversibility of oxidation processes can be explained by an absence of substituent in active 3rd and 6th positions of carbazole units[108]. CV curves of **CzPhPI** and **CzPhNI** revealed reversible reduction at -1.77 eV and -1.57 eV, respectively (Tab. 4.8.).

The compounds demonstrated comparable IP_{CV} values of 5.74–5.79 eV. EA_{CV} values were estimated to be 3.03 eV and 3.23 eV for **CzPhPI** and **CzPhNI**, respectively. Electrochemical band gaps were estimated to be 2.76 eV for **CzPhPI** and 2.51 eV for **CzPhNI** (Tab. 4.8.).
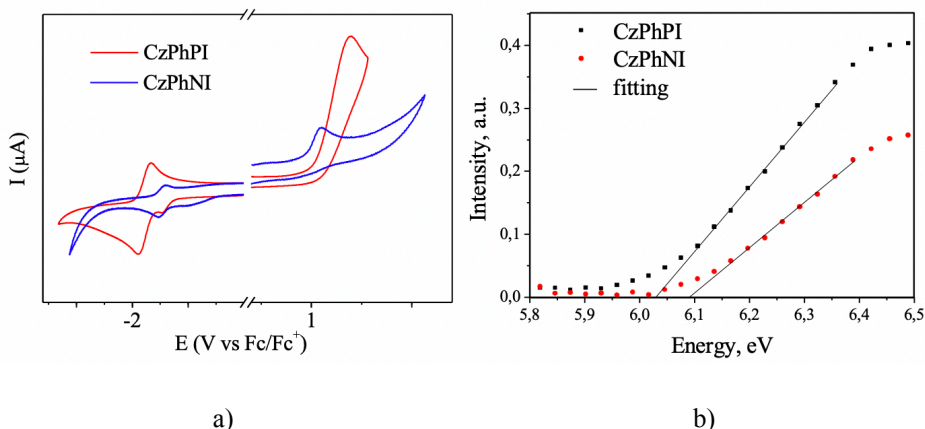
Fig. 4.21. Cyclic voltammograms of **CzPhPI** and **CzPhNI (a)** and photoelectron emission spectra **(b)** for solid films

Since electron affinities and ionization potentials evaluated for the solutions of compounds by using CV measurements are different than transport energy levels (HOMO and LUMO) for solid-state samples[130], the ionization potentials (IP$_{PE}$) of the layers of **CzPhPI** and **CzPhNI** were measured recording their electron photoemission spectra. The square root of photoelectron spectra versus photon energy are plotted in Fig. 4.21. (b). The IP$_{PE}$ values for compounds **CzPhPI** and **CzPhNI** were taken from the photoelectron spectra extrapolating their linear parts to Y=0. The solid-state IP$_{PE}$ values were found to be 6.03 eV and 6.09 eV for **CzPhPI** and **CzPhNI**, respectively (Table 4.8.). A relatively high difference between the values of IP obtained by electron photoemission spectrometry and electrochemical analysis is caused by the existence of intermolecular interactions in the solid layers compared to dilute solutions of the investigated materials. Electron affinities (EA$_{PE}$) of 2.03 and 2.44 eV for the studied materials **CzPhPI** and **CzPhNI** in solid-state were calculated using the formula EA$_{PE}$ = IP$_{PE}$ − 1.37×E_g where the optical band-gap energies (E_g) of 2.95 and 2.67 eV taken from absorption spectra of the layers of **CzPhPI** and **CzPhNI** and the constant of 1.37 was used due to the reasons described[130] earlier, respectively (Fig. 4.22., Table 4.8.).

Table 4.8. Electrochemical characteristics of **CzPhPI** and **CzPhNI**

Compound	E_{ox}, eV,[a]	E_{red}, eV,[a]	IP$_{CV}$, eV,[b]	EA$_{CV}$, eV,[b]	E_g^{CV}, eV[c]	IP$_{PE}$, eV[d]	EA$_{PE}$, eV[e]
CzPhPI	0.99	-1.77	5.79	3.03	2.76	6.03	2.03
CzPhNI	0.94	-1.57	5.74	3.23	2.51	6.09	2.44

[a] Onset E$_{red}$ and onset E$_{ox}$ are measured vs. ferrocene/ferrocenium. [b] Ionization potentials and electron affinities estimated according to IP$_{CV}$ = (E$_{ox}$ + 4.8). EA$_{CV}$ = (E$_{red}$ + 4.8). [c] Calculated using equation E$_g^{CV}$= E$_{ox}$ − E$_{red}$. [d] Ionization potentials measured using electron photoemission spectrometry. [e] Electron affinities for solid-state samples were calculated according to the formula $EA^{PE} = IP^{PE}-1.37 \times Eg$.

The trends of IP$_{PE}$ and EA$_{PE}$ values for solid-state samples of **CzPhPI** and **CzPhNI** are in good agreement with the trend of IP$_{CV}$ and EA$_{CV}$ values estimated for solutions of **CzPhPI** and **CzPhNI** and with the trends of their theoretically calculated HOMO and LUMO energy values (Table 4.6. and Table 4.8.).

4.2.4. Photophysical properties

Photophysical properties of the solutions of **CzPhPI** and **CzPhNI** in tetrahydrofuran (THF) and toluene (concentration 1×10^{-5} mol/L) and of vacuum deposited neat films were studied. Photoluminescence (PL) and absorption spectra of the solutions and of the neat films are plotted in Fig. 4.22. The corresponding values are provided in Table 4.9.
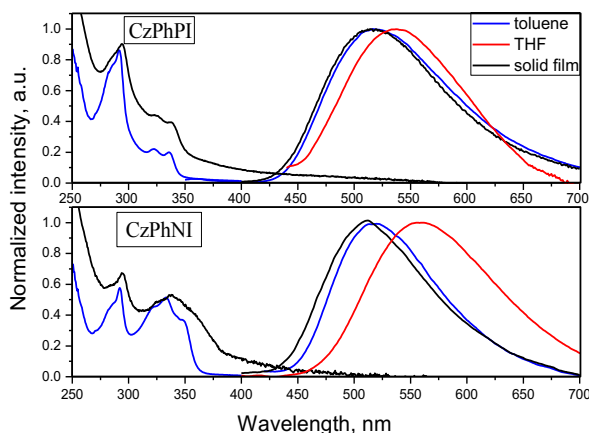
Fig. 4.22. PL and absorption spectra of toluene/THF solutions and neat films for **CzPhPI** and **CzPhNI**

High-energy bands of absorption spectra of **CzPhPI** and **CzPhNI** with maxima in the range of 232–245 nm are responsible for the excitation of the carbazole unit[119], while the shoulder bands in the range of 333–337 nm are associated with charge transfer (CT). In contrast to absorption spectra of the toluene solutions of **CzPhPI** and **CzPhNI**, low-energy tails were well observed in the absorption spectra of the solid samples (Fig. 4.22.). This observation can be explained by enhanced CT in the solid-state. Both solid samples and toluene solutions of **CzPhPI** and **CzPhNI** demonstrated PL with the intensity maxima in the range of 512–520 nm. However, the photoluminescence spectra of the **CzPhPI** and **CzPhNI** solutions in the more polar tetrahydrofuran were shifted to the low-energy region proving positive solvatochromism (Fig. 4.22.).

Toluene solutions of **CzPhPI** and **CzPhNI** showed very low PL quantum yields (QY), which were lower than 1%. Weak overlapping of HOMO and LUMO orbitals observed for **CzPhPI** and **CzPhNI** was likely the reason of low PLQYs. (Fig. 4.16).

Similarly, the solid sample of **CzPhNI** demonstrated weak photoluminescence with a negligible value of PLQY. A considerably higher PLQY value of 20% was observed for the solid sample of **CzPhPI**. A higher PLQY value observed for the solid sample, was most likely caused by the existence of n→π* interaction between the

unoccupied orbital of a carbon atom of the carbonyl group and the free electron pair of a nitrogen atom of the carbazole moiety in **CzPhPI** which makes charge-transfer through space possible. This was not the case with **CzPhNI**, in which the corresponding interatomic distances are considerably higher (Fig. 4.17.). Low values of PLQY of the solutions of **CzPhPI** can be explained by intramolecular rotations and motions, which lead to an unstable distance between the nitrogen atom and the carbonyl group in the **CzPhPI** structure and results in blocking of charge-transfer. Summarizing, the different interatomic distances of respective atoms in **CzPhPI** and **CzPhNI** lead to different overlapping of HOMO and LUMO orbitals through space, and as a result, their PLQY values are notably different.

The emission enhancement of **CzPhPI** in a solid state comparing to that of a solution also can be explained by the restriction of intramolecular rotations without the planarization of the molecular structure as it demonstrated for emitters exhibiting aggregation-induced emission enhancement (AIEE)[74]. To study the AIEE phenomenon for **CzPhPI**, PL spectra of the dispersions in THF/H_2O systems with different amounts of H_2O with the same concentration of **CzPhPI** were recorded (Fig. 4.23.).
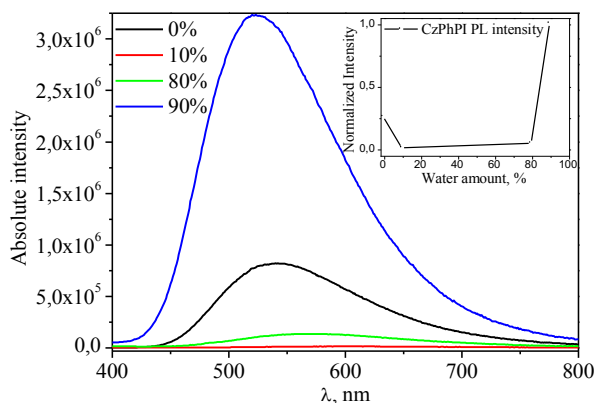
Fig. 4.23. Emission spectra of **CzPhPI** dispersed in THF/water mixture with the different concentration of water. Inset: dependence of emission intensity of **CzPhPI** on the concentration of water.

CzPhPI formed solid aggregates with an increasing amount of H_2O in the THF/H_2O system due to much lower solubility in water as compared to that in tetrahydrofuran. With the increase of H_2O fraction, the intensity of PL considerably decreased and the emission maximum bathochromically shifted from 542 nm to 618 nm. Hence, increased polarity of the THF/H_2O system was responsible for the change of photophysical properties. One more reason of decreasing PL intensity could be the enhancement of H-bonding which leads to the dynamic quenching of the excited states, as it was reported earlier[131]. However, further increase of H_2O fraction to 90% leads to a considerable increase of PL intensity accompanied by a hypsochromic shift of PL maximum to 523 nm, which can be explained by a rapid formation of insoluble aggregates with higher PL intensity. These observations clearly indicate the effect of AIEE.

Table 4.9. Photophysical characteristics of **CzPhPI** and **CzPhNI**

Compound	λ_{abs}^{Tol} / λ_{abs}^{film} (nm)	λ_{em}^{Tol} / λ_{em}^{THF} / λ_{em}^{film} (nm)	Φ^{Tol} / Φ^{film}
CzPhPI	245, 291, 336 / 236, 295, 335	517 / 538 / 514	<0.01 / 0.20
CzPhNI	245, 292, 333 / 232, 294, 337	520 / 561 / 512	<0.01 / 0.01

λ_{abs} – the wavelength of absorption maximum, λ_{em} – the wavelength of fluorescence emission maximum, Φ – fluorescence quantum yield.

Theoretical (TD-DFT) calculations revealed a very low theoretical value of ΔE_{S-T} for both materials (Tab 4.6.). To estimate experimental ΔE_{S-T} values and examine the availability of a possible upconversion of triplet excitons, photoluminescence (PL) and phosphorescence (Ph) spectra were measured for THF solutions at 77 K (Fig. 4.24.).
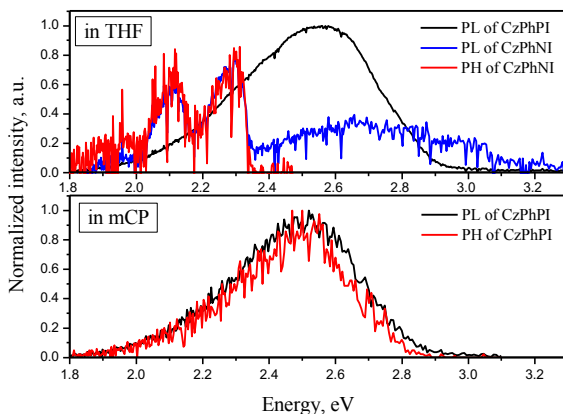
Fig. 4.24. PL and PH spectra at 77 K of **CzPhPI** and **CzPhNI** in THF solutions and in solid mCP matrices

In contrast to the expectations, a relatively large ΔE_{S-T} of 0.8 eV was observed for **CzPhNI** (Fig. 4.24.). Analysis indicates that the recorded PL and Ph spectra for **CzPhNI** in THF solution at 77 K were related to the recombination of local exciton singlet and triplet of napththalic imide unit. Unfortunately, the Ph spectrum of **CzPhPI** in THF solution at 77 K was not recorded due to a weak Ph emission. However, PL and Ph spectra were taken for the doped **CzPhPI**:mCP film allowing to calculate ΔE_{S-T} of 0.03 eV for **CzPhPI** (Fig. 4.24.). Such small ΔE_{S-T} value can induce reverse intersystem crossing (RISC) resulting in an effective TADF. Indeed, delayed fluorescence the intensity of which increased with increasing temperature was detected for the **CzPhPI**:mCP film (Fig. 4.25.). PL spectra of **CzPhPI**:mCP film at different temperatures were analogous indicating the similarity of fluorescence and phosphorescence of **CzPhNI**. The shape of PL decay for **CzPhNI**:mCP at 300 K was similar to many published TADF emitters with intramolecular CT[56-60].
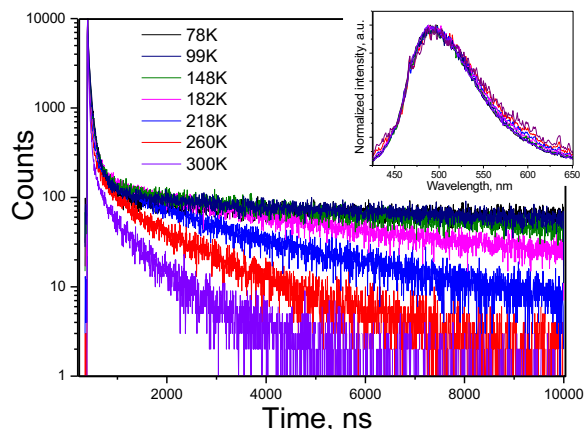
Fig. 4.25. PL decays and PL spectra (insets) of doped film **CzPhPI**:mCP at different temperatures

To prove that TADF of **CzPhNI** is related to intramolecular CT but not to intermolecular CT, the photophysical behavior of **CzPhNI** in a ZEONEX matrix has been studied considering the nature of charge transfer in a **CzPhPI** film. The photoluminescence of the neat film was compared with the photoluminescence of the 1% wt **CzPhPI**/ZEONEX film with equal concentrations (Fig. 4.26.). The comparison revealed a considerably higher PL intensity and a hypsochromic shift of emission peak (from 512 nm to 486 nm) of the spectrum of molecular mixture in comparison to those of the neat film. These results clearly indicate the intramolecular nature of the charge through-space charge transfer because low concentration of **CzPhPI** inside the matrix exclude any possible intermolecular interactions between two different molecules. Photoluminescence quantum yield of the solid solution (0.26) was found to be higher than that of the neat film (0.2) (Tab. 4.9.) and the intensity of emission of the doped film was enhanced by the factor of 2.24.
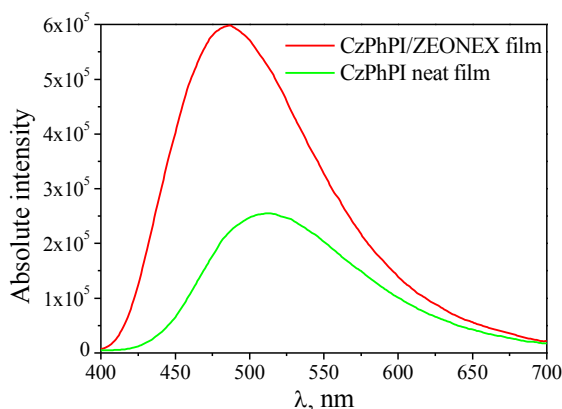
Fig. 4.26. PL emission intensity comparison of equal-concentrated **CzPhPI** neat film and 1% wt **CzPhPI**/ZEONEX film

The enhancement was estimated by dividing the integral square of emission spectrum of **CzPhPI**/ZEONEX film by the integral square of emission spectrum of the film of **CzPhPI**. Lower emission intensity of the neat film of **CzPhPI** can be explained by aggregation-caused quenching. A hypsochromic shift of emission peak of **CzPhPI**/ZEONEX film relative to that of the neat film of **CzPhPI** was caused by the decrease of dielectric constant.

PL decay curves of the neat film of **CzPhPI** and of the film of molecular mixture **CzPhPI**/ZEONEX are shown in Fig. 4.27. Short- and long-lived components, corresponding to prompt and delayed fluorescence, respectively, can be identified in PL decay curves. Excited-state lifetimes of both short-lived and long-lived parts are considerably longer in the case of the film of **CzPhPI** doped in ZEONEX compared to those of the neat film of **CzPhPI** (Tab. 4.9.). This difference is likely caused by the absence of intermolecular interactions in the film of molecular dispersion in ZEONEX which leads to the suppression of non-radiative decay in the polymer film[160].
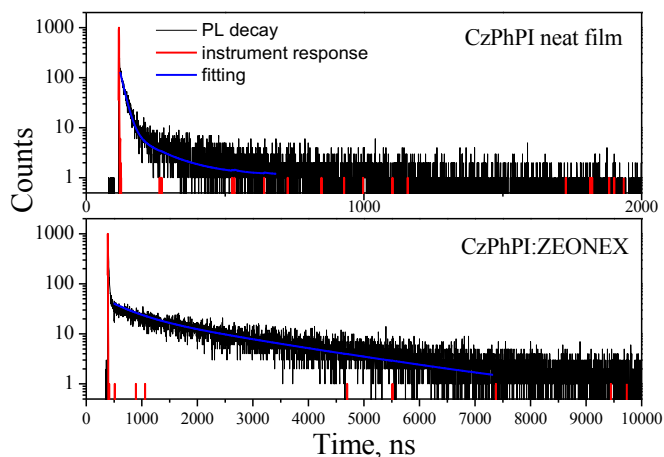
Fig. 4.27. PL decay transients of **CzPhPI** and **CzPhPI**:ZEONEX films

Tab. 4.9. PL decay data of the of **CzPhPI** and **CzPhPI**:ZEONEX films

Film	τ_1, ns / distrib., %	τ_2, ns / distrib., %	χ^2	Φ
CzPhPI neat	16.61 / 73.51	118.83 / 26.49	1.005	0.20
CzPhPI:ZEONEX	468.72 / 17.95	2349.38 / 82.05	1.259	0.26

4.2.5. Charge-transporting properties

The time-of-flight (ToF) technique was used to estimate the charge-transporting properties of vacuum-deposited layers of **CzPhPI** and **CzPhNI**. The results revealed a bipolar charge transporting ability of the layers of the materials. The transit times (t_{tr}) for both electrons and holes were easily recognized in the log-log graphs of current transients (Fig. 4.28. (a, b). The current transients were found to be very

dispersive. Drift mobilities of holes and electrons versus electric field for the layers of **CzPhPI** and **CzPhNI** are plotted in Fig 4.29. **CzPhPI** was characterized by hole mobility of 4.9×10^{-4} cm^{2}V^{-1}s^{-1} and electron mobility of 6.7×10^{-4} cm^{2}V^{-1}s^{-1} at an electric field of ca. 3×10^5 Vcm^{-1}. **CzPhNI** was characterized by much lower hole mobility of 8.9×10^{-5} cm^{2}V^{-1}s^{-1} and electron mobility of 2.2×10^{-5} cm^{2}V^{-1}s^{-1} at the same electric field (Fig 4.29.).

a)   b)
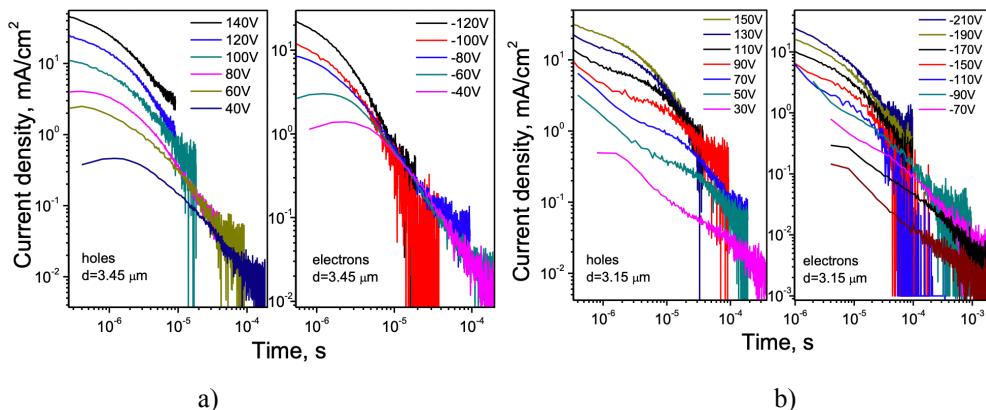
Fig. 4.28. Current transients for holes and electrons observed for the vacuum-deposited layers of **CzPhPI (a)** and **CzPhNI (b)**
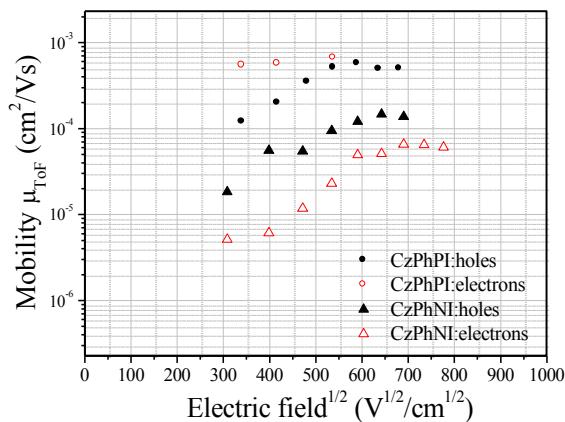
Fig. 4.29. Hole and electron drift mobilities versus electric field characteristics for **CzPhPI** and **CzPhNI**

4.2.6. Electroluminescent properties of CzPhPI

Since **CzPhPI** showed a relatively high PLQY in the solid state, its electroluminescent properties were investigated in a non-doped device A and in a doped device B, C and D using mCP, TCTA and oCzmOXD as the host, respectively. Studying **CzPhNI** as an emitter is unreasonable because of the extremely weak emission in a solid state. For comparison, the electroluminescent properties of **CzPhPI** as AIE/TADF emitter in different media, the same device structure

ITO/MoO$_3$(1 nm)/NPB(20 nm)/TCTA(20 nm)/mCP(10 nm)/light-emitting layer (30 nm)/TSPO1(10 nm)/TPBi(40 nm)/LiF(0.5 nm)/Al was used, except the light-emitting layers **CzPhPI**, **CzPhPI**(10 %):mCP, **CzPhPI**(10 %):TCTA or **CzPhPI**(10 %):oCzmOXD in devices A, B, C, or D, respectively (Fig. 4.30. (a)).

Taking into account the high ionization potential of 6.03 eV for **CzPhPI**, the hole-injection layer MoO$_3$ and hole-transporting layers NPB and TCTA were involved in the structure lowering energy barrier between anode and light-emitting layers (Fig. 4.30 (a)). Also, electron-injection layer LiF and electron-transporting layer TPBi were used lowering the energy barrier between the cathode and light-emitting layers due to the EA$_{PE}$ of 2.03 eV for **CzPhPI**. Additionally, exciton-blocking layers mCP and TSPO1 were used forbidding any leakage of triplet exactions from the emitter **CzPhPI** to the charge-transporting layers.

a)   b)

c)   d)
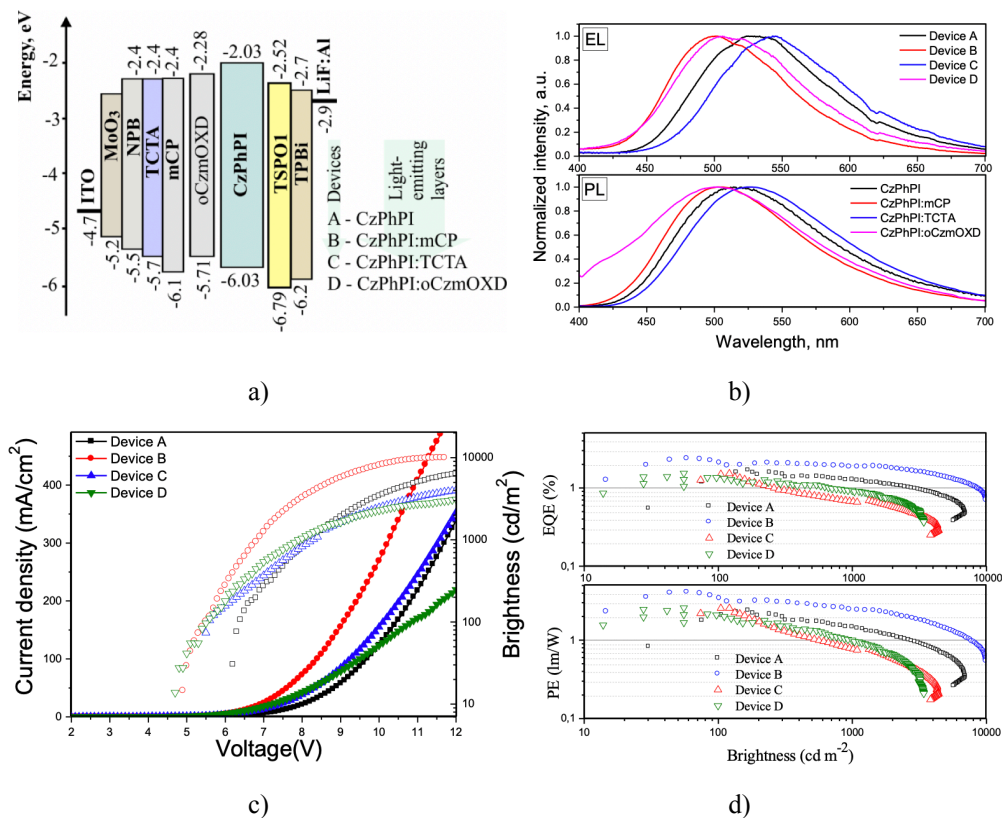
Fig. 4.30. Equilibrium energy diagrams (a), respectively, EL and PL spectra for devices and light-emitting layers (b), current density and brightness versus voltage characteristics (c), and EQEs and power efficiencies versus brightness (d) for the fabricated devices

A relatively strong effect of different hosts on the electroluminescence (EL) spectra of devices A–D was observed (Fig. 4.30. (b)). The non-doped device A was characterized by green emission with EL maximum at 529 nm and commission Internationale de l'Eclairage (CIE 1931) chromaticity coordinates (x, y) of (0.3, 0.51) (Fig. 4.32 (b)., Tab. 4.10.).

Due to the low-polarity of the used hosts mCP and oCzmOXD (ε=2.84 for mCP[133]), greenish-blue devices B and D were fabricated; while a yellow device C was obtained using a relatively high-polar host TCTA (ε=5.61 for TCTA[133]). The slight red shift of the EL spectra in comparison to the corresponding PL spectra can be explained by enhancing the delay fluorescence under electrical excitation. However, stable EL spectra were recorded at different voltages (Fig. 4.31.). The doped devices B–D were characterized by lower turn-on voltages (at 10 cd/m^2) in comparison to that of device A due to the lowering energy barriers between light-emitting layers and mCP and TSPO1 layers (Fig. 4.30. (a)). The best OLED performances were obtained for Device B, including the brightness (at 10 V) of 8300 cd/m^2, and current, power, external quantum efficiencies of 6.6 cd/A, 4.0 lm/W, and 2.4 %, respectively (Fig. 4.30. (c, d). This result is mainly related to the small ΔE_{S-T} of 0.03 eV for the **CzPhPI** in mCP host thus efficient TADF (Fig. 4.24.). As it was previously shown for TADF emitters including TADF emitters with the AIE phenomena, TADF properties of such emitters can be improved by using an appropriate host due to the host polarity giving high efficiency RISC and hence TADF[132,133]. Overall, mCP is the most appropriate host for **CzPhPI** among the tested ones (Fig. 4.32. (a)).
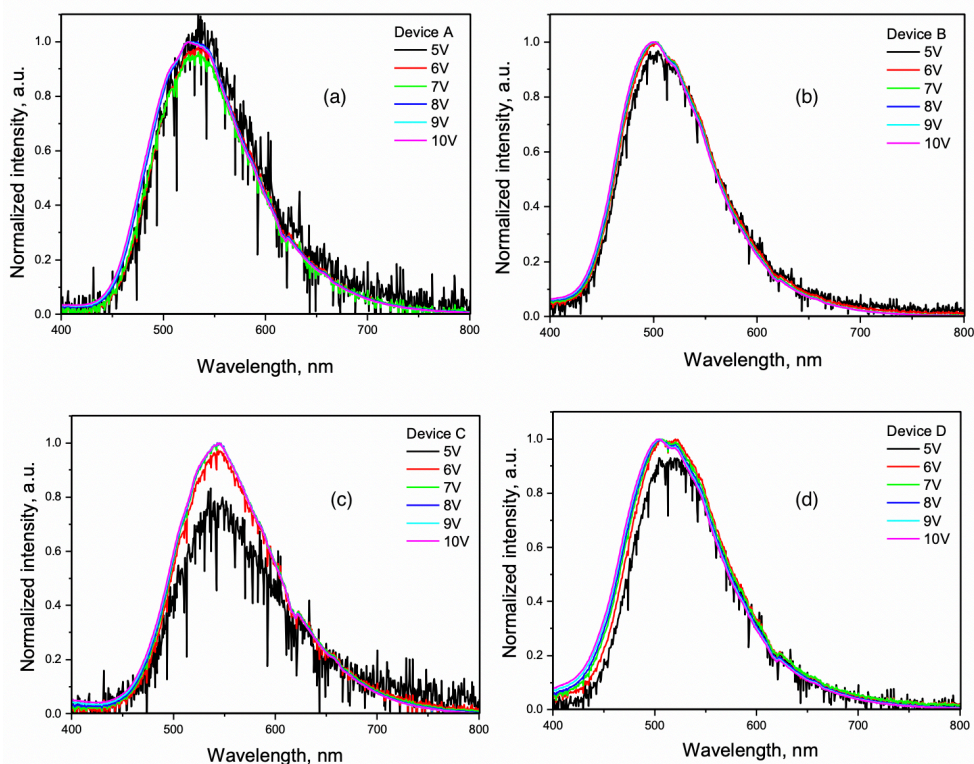
Fig. 4.31. El spectra of devices A **(a)**, B **(b)**, C **(c)**, D **(d)** at different voltages.

a)

b)
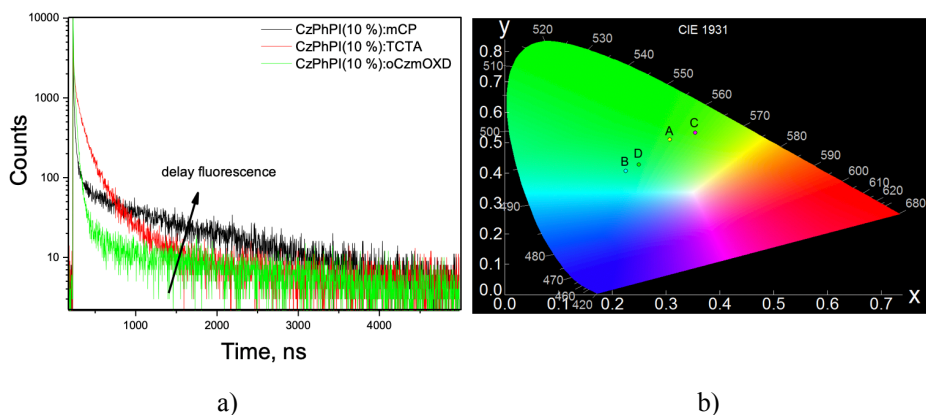
Fig. 4.32. PL decays of doped films **CzPhPI**(10%):mCP, **CzPhPI**(10%):TCTA, and **CzPhPI**(10%):oCzmOXD (a) and CIE coordinates for devices A–D at 8V (b)

Table 4.10. A summary of OLEDs parameters

Device	Light-emitting layers	EL max., nm	CIE 1931 (x, y)	Brightness,[a] cd/m²	V_{on},[b] V	CE_{max}, cd/A	PE_{max}, lm/W	EQE_{max}, %
A	**CzPhPI**	529	(0.3, 0.51)	3400	6.1	4.8	2.2	1.7
B	**CzPhPI**(10%):mCP	500	(0.23, 0.41)	8300	4.9	6.6	4.0	2.4
C	**CzPhPI**(10%):TCTA	504	(0.35, 0.53)	2400	4.7	4.5	2.6	1.5
D	**CzPhPI**(10%):oCzmOXD	544	(0.25, 0.46)	2300	5.0	3.8	2.4	1.5

[a] at 10 V CIE, CIE of EL spectrum for devices A–D recorded at 8 V, [b] at 10 cd/m².

To conclude, two new donor-acceptor compounds containing carbazole and imide units were synthesized by utilizing a simple and convenient three-step synthetic pathway. The carbazole-phthalimide luminophore demonstrated aggregation-induced emission enhancement in combination with thermally-activated delayed fluorescence implemented *via* through-space charge transfer mechanism. The compounds were found to have good thermal stability and decent semiconductor properties. Additionally, a carbazole-phthalimide derivative was examined as an emitter in doped and non-doped organic light-emitting diodes, exhibiting moderate efficiency and comparably high brightness of the fabricated devices.

These results can be characterized as a valuable contribution to the array of materials exhibiting AIE and TADF phenomena combination. The proposed design strategies can be a good background for the creation of inexpensive emitting materials for highly efficient OLEDs.

4.3. Donor-acceptor 1,3-thiazole-based organoboron complexes

The evolution of new technologies entails an intensive scientific research in the area of photo- and electroactive organic materials. The development of luminescent compounds which can serve as components of various optoelectronic devices such as organic light-emitting diodes (OLEDs)[134,135,136] or light-emitting electrochemical cells (OLECs)[137,138] optical sensing materials in biological[139,140] and supramolecular[141,142] systems is one of the biggest scientific challenges.

In this context, organoboron complexes have many advantages compared to other fluorophores (porphyrins, metal complexes, etc.) including strong absorption bands in UV and visible regions, high fluorescent quantum yields, photostability, good solubility in common organic solvents; insensitivity to the environment, e.g. pH[143]. Currently, the most investigated organoboron compounds are boron-dipyrromethene (BODIPY) derivatives[144,145]. Unfortunately, despite the intensive fluorescence of BODIPY dyes in a solution, their emission in the solid state is usually weak, which limits optoelectronic applications[146].

In the last few years, a study of different boron (III) organic complexes, including other than pyrrole heterocyclic units, was the subject of great research interest[146]. They are very attractive because of their optical variability and synthetic convenience. However, in contrast to boron complexes with *N,N*-chelating ligands[147,148,149] *N,O*-analogues were little investigated. Mainly those based on phenolic[150,151,152] or *β*-ketoiminate[153,154] ligands were reported, while the complexes formed from amid group containing ligands are presented only as pyridine and 1,8-naphthyridine derivatives[155,156]. The use of *N,O* *π*-conjugated ligands with carbonyl *O*- and heterocyclic *N*-coordinating centers can open the way to obtain various new boron (III) complexes with interesting properties. The design of the donor-acceptor type systems can lead to attractive electronic properties, such as chromism, charge transporting properties, *π*-conjugated electronic states recombination[157,158].

This chapter discusses the synthesis and investigation of physical properties and structure-properties relationship of thiazolo[3,2-c][1,3,5,2]oxadiazaborinine derivatives.

4.3.1. Synthesis and structural analysis

Synthesis work was performed by the scientific group of Potopnyk[98]. 2,2-Difluoro-1,3,5,2-oxadiazaborinine, which was selected as an acceptor unit, is a well-known electron-withdrawing moiety for the materials exhibiting intramolecular charge transfer[155,156]. As an electron-donor unit, 4-dimethylaminophenyl moiety was selected as an affordable and convenient starting material. Structures of the studied materials were carefully designed to investigate the influence of substituents at position 4 of the thiazole ring on photophysical properties of the corresponding boron dyes. All of the synthesized compounds were characterized by high-resolution mass spectrometry and the ^{1}H, ^{13}C, and ^{19}F NMR analysis. In addition, the structures of **5a** and **5c–e** were further confirmed by single-crystal X-ray analysis (Fig 4.34.). The general structure of the investigated compounds is depicted in Fig. 4.33.

X-ray analysis of complexes **5a** and **5c−5e** confirmed that the boron atom is coordinated in a tetrahedral geometry by nitrogen, oxygen, and two fluorine atoms.

In the solid state, compound **5a** definitely has a non-planar geometry. The dimetylaminophenyl group is twisted against the thiazolo- oxadiazaborinine unit: the torsion angle of C3−C4−C9−N2 is 24.2° (Fig 4.34.).
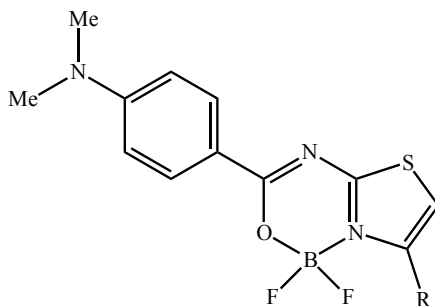
R = H (**5a**), Me (**5b**), CO₂Et (**5c**), Ph (**5d**), 4-C₆H₄-NMe₂ (**5e**),
4-C₆H₄-CN (**5f**), 4-C₆H₄-NO₂ (**5g**)

Fig. 4.33. The general structure of compounds **5a–5g**

However, complex **5c** exhibits an almost planar structure, including an ester group at the thiazole unit (the torsion angles of C7−C6−C9−N2 and O2−C13−C10−N3 are 4.0° and 5.1°, respectively) (Fig 4.34.). Another situation is observed in the case of compounds **5d** and **5e**: the main part of the molecules remains flat; however, the aryl substituents at position 4 of the thiazole ring are twisted to the rest of the molecules. For complex **5d**, the torsion angles of C16−C11−C10−N2 and C6−C1−C7−N1 are 4.3° and 59.2°, while the value of the corresponding angles of dye **5e** (C5−C6−C9−N4 and C18− C13−C12−N2) are 3.4° and 58.1°, respectively (Fig. 4.34.).
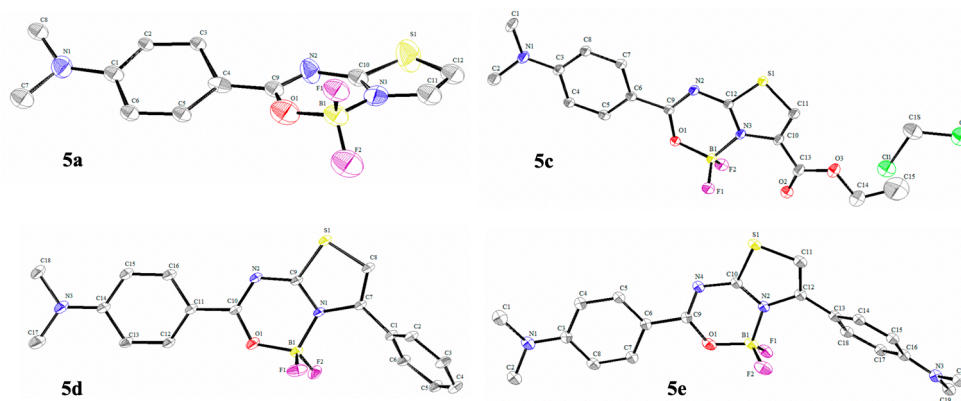
Fig. 4.34. ORTEP diagram of complexes **5a**, **5c**, **5d** and **5e**.

4.3.2. Electrochemical characterization

The cyclic voltammetry technique was used to explore the redox behaviour of dyes **5a−5g**. The oxidation and reduction scans were performed in a deoxygenated dichloromethane solution at room temperature with tetrabutylammonium

hexafluorophosphate (TBAPF$_6$) as the supporting electrolyte. Onset reduction and onset oxidation potentials, as well as the electron affinities (EA$_{CV}$) and the ionization potentials (IP$_{CV}$) of complexes are summarized in Table 4.11., and cyclic voltammograms are shown in Fig. 4.35.
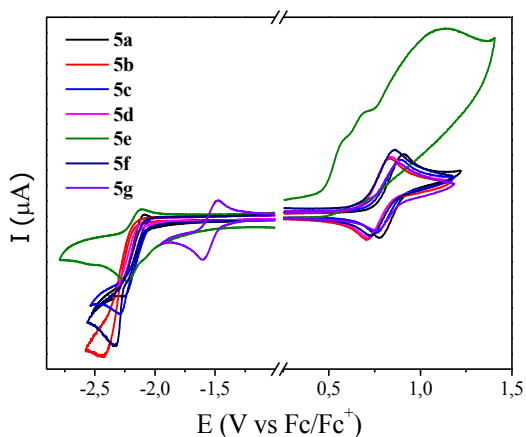
Fig. 4.35. Cyclic voltammograms of compounds **5a–5g**

The values of IP$_{CV}$ are mostly contained in a narrow range from 5.03 to 5.08 eV; however, for the compound with an additional donor (4-dimethylamino- phenyl) substituent at the thiazole ring (**5e**), the corresponding value is smaller (4.76 eV). Electron affinity changes to 2.20−2.35 eV and 2.59 eV for compounds **5a−d,f** and **5e**, respectively, and increases significantly to 2.95 eV for the complex with the 4-nitrophenyl substituent at the thiazole ring (**5g**).

Table 4.11. Onset reduction and onset oxidation potentials, electron affinities and ionization potentials of complexes 5a–g

Compound	E_{red}^{onset}, V	E_{ox}^{onset}, V	EA$_{CV}$, eV	IP$_{CV}$, eV
5a	-2.112	0.674	2.29	5.07
5b	-2.203	0.636	2.20	5.04
5c	-2.056	0.663	2.34	5.06
5d	-2.133	0.647	2.27	5.05
5e	-1.810	0.355	2.59	4.76
5f	-2.046	0.676	2.35	5.08
5g	-1.454	0.625	2.95	5.03

4.3.3. Photophysical properties of solutions

The absorption and fluorescence spectra of the solutions of compounds **5a−g** are demonstrated in Fig. 4.36. The obtained data are summarized in Table 4.12. The

characteristic absorption peak, with the maximum absorption wavelengths at 402−417 nm showed almost no variation with changing solvent polarity.
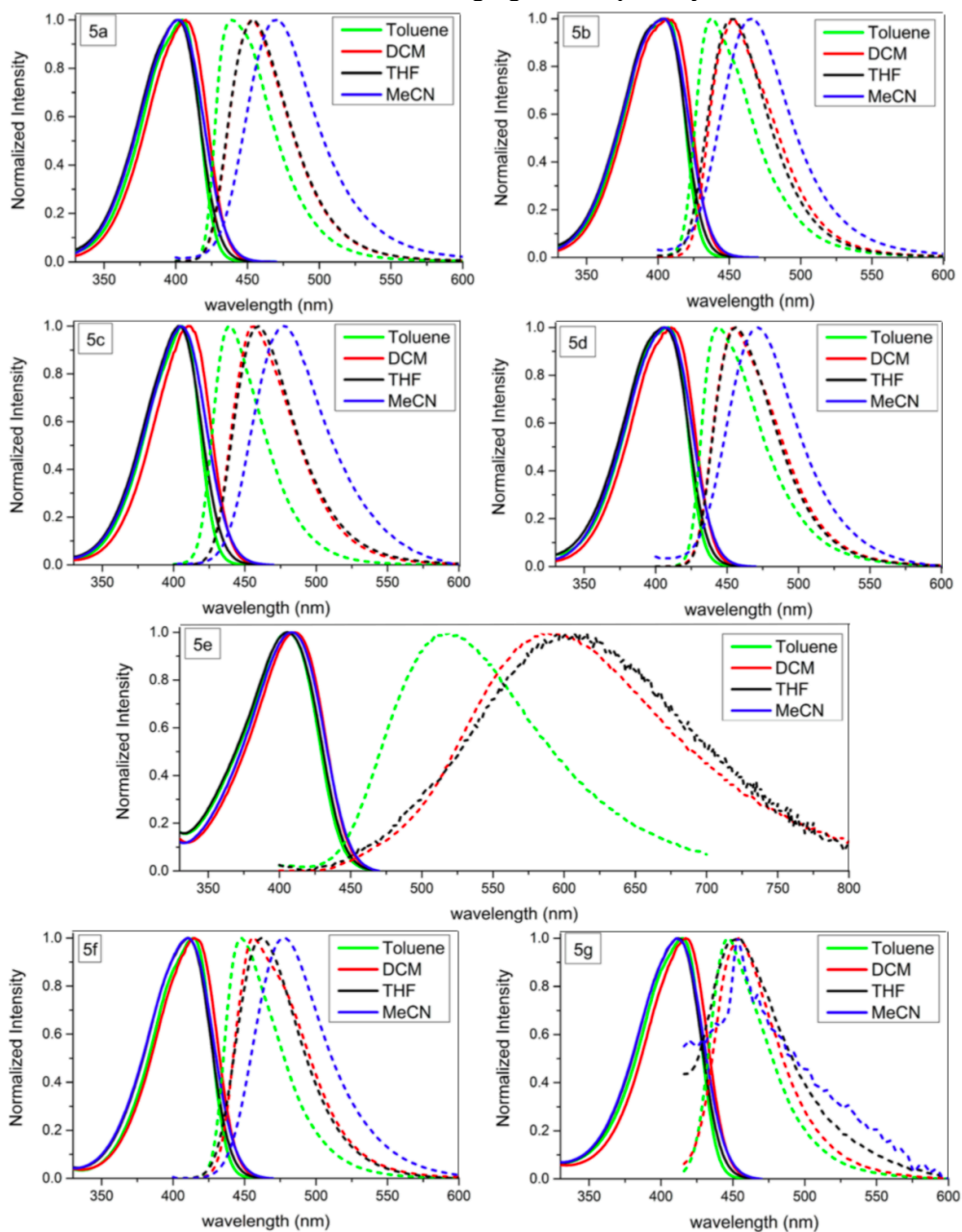
Fig. 4.36. Absorption (solid lines) and emission (dashed lines) spectra of **5a−g** recorded in different solvents

The molar absorption coefficient values change from the minimum for complex **5e** (46700−50600 M^{-1} cm^{-1}) to the maximum for **5g** (60100−67600 M^{-1} cm^{-1}). The

dilute solutions of **5a−d**, **f−g** show one very similar emission band centred with the maxima in toluene at 437−448 nm, in DCM at 453−456 nm, in THF at 453−462 nm, and in acetonitrile at 453−477 nm, while compound **5e** is characterized by a bathochromic shift (emission maximum in toluene at 518 nm, in DCM at 590 nm, and in THF at 616 nm). In acetonitrile, complex **5e** does not show essential fluorescence. The solvent effect on the fluorescence properties of **5a−g** manifests in increasing the value of λ_{em} and Stokes shift with the increase of solvent polarity, while fluorescence quantum yields decrease. These observations indicate that the fluorescence emission of dyes **5a−g** was partially or fully originated from the photoinduced intramolecular charge transfer (ICT) state.

Table 4.12. Photophysical properties of complexes **5a–g** in different solvents

| Compound	Solvent	λ_{abs}, nm	ε, M^{-1}cm^{-1}	λ_{em}, nm	Φ	Stokes shift, cm^{-1}
5a	toluene	405	56600	439	>0.99	1912
	DCM	407	54400	453	0.86	2495
	THF	402	55400	454	0.99	2849
	acetonitrile	402	49700	469	0.10	3553
5b	toluene	407	59300	437	>0.99	1687
	DCM	406	53300	453	0.87	2555
	THF	405	55100	453	>0.99	2616
	acetonitrile	403	52900	466	0.14	3355
5c	toluene	406	63100	439	0.94	1851
	DCM	412	60400	456	0.84	2342
	THF	404	60700	459	0.56	2966
	acetonitrile	405	60600	477	0.09	3727
5d	toluene	409	56600	444	0.94	1927
	DCM	411	57000	454	0.89	2304
	THF	406	57300	456	0.75	2701
	acetonitrile	406	58700	471	0.08	3399
5e	toluene	405	47300	518	0.66	5386
	DCM	411	50600	590	0.04	7382
	THF	406	47800	616	<0.01	8397
	acetonitrile	409	46700	–	–	–
5f	toluene	414	59900	448	0.62	1833
	DCM	415	56500	456	0.61	2167
	THF	411	53800	462	0.23	2686
	acetonitrile	411	55000	477	0.11	3366
5g	toluene	415	62900	447	0.02	1725
	DCM	417	67600	454	<0.01	1954
	THF	412	60100	454	<0.01	2245
	acetonitrile	411	63300	453	<0.01	2256

Complexes **5a−d**, **f** showed very high fluorescent quantum yields in non-polar solvents, while these parameters in acetonitrile are considerably lower. Other properties were observed for complexes **5e** and **5g**. Complex **5e** showed a comparatively good quantum yield in toluene (0.66) but a very small one in DCM, THF, and MeCN. Complex **5g** exhibited a very weak emission in every investigated solvent. For the THF solutions of the investigated complexes, the lifetime of the excited state was measured (Fig. 4.39., Table 4.13.). It is worth noting that the value of the lifetime of compound **5e** (0.21 ns) is considerably lower than for the rest of the complexes (1.39−2.24 ns).

Table 4.13. Lifetime of the exited state of complexes **5a–g** in DCM

Comp.	**5a**	**5b**	**5c**	**5d**	**5e**	**5f**	**5g**
τ, ns	2.22	2.24	2.10	2.06	0.64	1.39	1.64

4.3.4. Theoretical calculations

To understand the absorption properties of the synthesized complexes, density functional theory (DFT) calculations were performed using the Gaussian 09 software package[94]. All geometrical structures are optimized and molecular orbitals calculated at the B3LYP/6-31G* level. The calculated HOMO-LUMO plots are given in Fig. 4.37., while theoretical HOMO and LUMO values are summarized in Table 4.14.
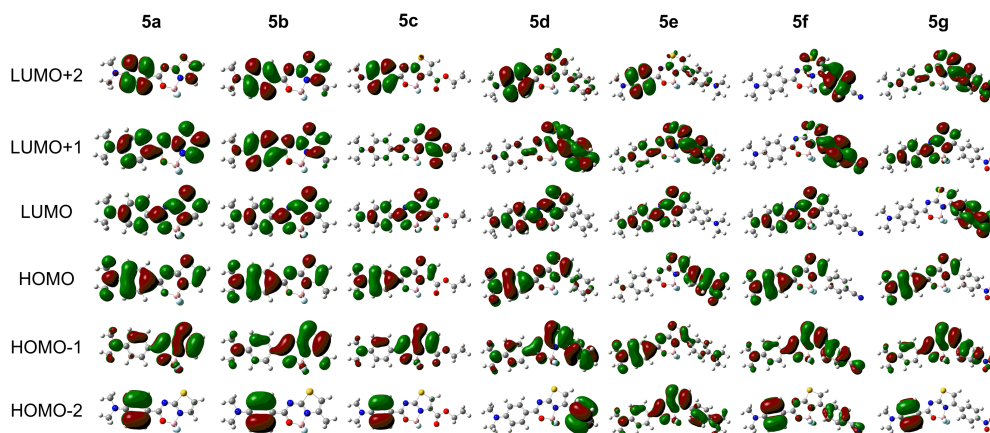
Fig. 4.37. Frontier molecular orbitals of complexes **5a–g**.

Table 4.14. Calculated HOMO-LUMO energy levels of **5a–5g**

Comp.	**5a**	**5b**	**5c**	**5d**	**5e**	**5f**	**5g**
E_{LUMO}, eV	-1.82	-1.75	-1.89	-1.78	-1.99	-2.04	-2.42
E_{HOMO}, eV	-5.47	-5.42	-5.54	-5.42	-5.09	-5.62	-5.64

In compounds **5d–g**, the aryl groups at position 4 of the thiazole ring are twisted in the ground state, what is agreed with X-ray analysis of **5d** and **5e** (Fig. 4.34.). Thus, these substituents are deconjugated with the rest of the molecule. The electron distribution of the HOMOs and LUMOs for **5a–g** is subjected to the general rule that the HOMO electrons are predominantly located on the dimethylaminophenyl group while LUMO electrons are mainly located on thiazolo-oxadiazaborinine moiety. The exceptions are compounds with weak emission properties (**5e** and **5g**). In the case of complex **5e**, there are two donor (dimethylaminophenyl) groups and in HOMO the electron distribution is shifted to donor substituent at thiazole ring, while HOMO-1 is very similar to HOMO of compounds **5a-d** and **5f-g**. The specific situation is observed for compound **5g**: LUMO is shifted from fluorophore unit and preferably located on the nitro-phenyl group. However, LUMO+1 has an analogical shape comparably with LUMO of the rest of complexes.

To calculate singlet transitions, time-dependent DFT (TD-DFT) computations were also performed at the B3LYP/6-31G* level, using the previously obtained optimized structures. The calculated excitation energies for the six lowest singlet excited states, maximum absorption wavelengths (λ_{max}), oscillator strengths (f) and molecular contribution of the leading configurations are shown in Table 4.15. For the compounds **5a–d, f** the excitation to the first singlet excited state ($S_0 \rightarrow S_1$) is preferable ($f \sim 1$, $\lambda_{max} = 381 \div 391$ nm). Then, these complexes exhibit reverse transition $S_1 \rightarrow S_0$, which is accompanied by light emission.

Table 4.15. Calculated properties of the 6 lowest singlet excited states for **5a–g** determined through TD-DFT

Comp.	Transition	Energy (eV)	Wavelength (nm)	Oscillator strength	Molecular contribution of the leading configurations*
5a	$S_0 \rightarrow S_1$	3.2465	381.90	0.9695	100% H→L
	$S_0 \rightarrow S_2$	4.1453	299.10	0.0755	93% H-1→L / 4% H-2→L / 3% H→L+1
	$S_0 \rightarrow S_3$	4.2872	289.19	0.0000	100% H-3→L
	$S_0 \rightarrow S_4$	4.2908	289.95	0.0138	84% H-2→L / 8% H→L+2 / 5% H→L+1 / 3% H-1→L
	$S_0 \rightarrow S_5$	4.8671	254.74	0.0625	52% H→L+2 / 36% H→L+1 / 12% H-2→L
	$S_0 \rightarrow S_6$	4.9118	252.42	0.0002	88% H→L+3 / 12% H-1→L+3
5b	$S_0 \rightarrow S_1$	3.2452	382.05	1.0066	100% H→L
	$S_0 \rightarrow S_2$	4.0785	304.00	0.0472	98% H-1→L / 2% H→L+1
	$S_0 \rightarrow S_3$	4.2945	288.71	0.0000	100 % H-3→L
	$S_0 \rightarrow S_4$	4.3081	287.80	0.0039	86% H-2→L / 9% H→L+1 / 5% H→L+2

| | S$_0$→S$_5$ | 4.8659 | 254.80 | 0.0572 | 55% H→L+1 / 31% H→L+2 / 14% H-2→L |
	S$_0$→S$_6$	4.9588	250.03	0.0003	85% H→L+3 / 15% H-1→L+3
5c	S$_0$→S$_1$	3.2300	383.85	0.9362	100% H→L
	S$_0$→S$_2$	3.7014	334.97	0.1443	97% H→L+1 / 3% H-1→L
	S$_0$→S$_3$	4.1694	297.37	0.0491	87% H-1→L / 8% H-2→L / 3% H→L+1 / 2% H→L+4
	S$_0$→S$_4$	4.2696	290.39	0.0001	75% H-4→L / 25% H-3→L
	S$_0$→S$_5$	4.2942	288.73	0.0175	82% H-2→L / 11% H→L+2 / 7% H-1→L
	S$_0$→S$_6$	4.4585	278.09	0.0001	75% H-3→L+1 / 13% H-3→L / 7% H-4→L / 5% H-4→L+1
5d	S$_0$→S$_1$	3.1962	387.91	1.0611	100% H→L
	S$_0$→S$_2$	3.7454	331.03	0.0141	100% H-1→L
	S$_0$→S$_3$	4.1206	300.89	0.0009	100% H-2→L
	S$_0$→S$_4$	4.2725	290.19	0.0101	61% H-5→L / 33% H-3→L / 6% H-4→L
	S$_0$→S$_5$	4.2994	288.37	0.0005	47% H-4→L / 31%H-5→L / 15% H-3→L / 7% H→L+2
	S$_0$→S$_6$	4.4114	281.06	0.1296	58% H→L+1 / 21% H-3→L / 13% H-4→L / 8% H-5→L
5e	S$_0$→S$_1$	2.5323	489.61	0.0536	100% H→L
	S$_0$→S$_2$	3.2636	379.90	1.1481	100% H-1→L
	S$_0$→S$_3$	4.0330	307.43	0.0544	73% H-2→L / 17% H-3→L / 10% H→L+1
	S$_0$→S$_4$	4.0851	303.50	0.0463	82% H-3→L / 10 % H-2→L / 8% H→L+1
	S$_0$→S$_5$	4.2751	290.02	0.2432	70% H→L+1 / 11% H-2→L / 10% H-5→L / 7% H-4→L / 2% H-3→L
	S$_0$→S$_6$	4.2957	288.62	0.0131	72% H-5→L / 16% H-6→L / 6% H-4→L / 4% H→L+1 / 2% H-2→L
	S$_0$→S$_1$	3.1727	390.78	1.1352	100% H→L
	S$_0$→S$_2$	3.6960	335.45	0.0499	88% H→L+1 / 12% H-1→L

5f	$S_0 \rightarrow S_3$	3.8846	319.17	0.0219	87% H-1$\rightarrow$L / 13%H$\rightarrow$L+1
	$S_0 \rightarrow S_4$	4.2400	292.41	0.0029	84% H-2$\rightarrow$L / 9% H-5$\rightarrow$L / 5% H$\rightarrow$L+4 / 2% H$\rightarrow$L+3
	$S_0 \rightarrow S_5$	4.2768	289.90	0.0029	86% H-5$\rightarrow$L / 9% H-3$\rightarrow$L / 5%H-2$\rightarrow$L
	$S_0 \rightarrow S_6$	4.5155	274.58	0.1289	69% H-3$\rightarrow$L / 15% H-1$\rightarrow$L+1 / 7% H-5$\rightarrow$L / 6% H-2$\rightarrow$L / 3%H$\rightarrow$L+3)
5g	$S_0 \rightarrow S_1$	2.7122	457.14	0.0388	100% H$\rightarrow$L
	$S_0 \rightarrow S_2$	3.1573	392.69	1.1688	96% H$\rightarrow$L+1 / 4% H-1$\rightarrow$L
	$S_0 \rightarrow S_3$	3.3133	374.20	0.0014	94% H-5$\rightarrow$L / 3% H-5$\rightarrow$L+2 / 3% H-4$\rightarrow$L
	$S_0 \rightarrow S_4$	3.6103	343.42	0.0874	96% H-1$\rightarrow$L / 4% H$\rightarrow$L+1
	$S_0 \rightarrow S_5$	3.8157	324.93	0.0014	97% H-8$\rightarrow$L / 3% H-8$\rightarrow$L+2
	$S_0 \rightarrow S_6$	3.9477	314.06	0.0269	97% H-1$\rightarrow$L+1 / 3% H$\rightarrow$L+2

*H – HOMO, L – LUMO.

On the other hand, compound **5e** absorbs light preferably by transition $S_0 \rightarrow S_2$ (f = 1.1481, λ_{max} = 380 nm), when an electron moves from HOMO-1 to LUMO. For compound **5g**, excitation also occurs dominantly by $S_0 \rightarrow S_2$ transition (f = 1.1688, λ_{max} = 393 nm). However, in this case the electron moves from HOMO to LUMO+1. Probably, the de-excitation of molecules **5e** and **5g** include several transitions ($S_2 \rightarrow S_1/S_2 \rightarrow T_1$ and following $S_1 \rightarrow S_0/T_1 \rightarrow S_0$), which finally provide to the quenching of fluorescence.

4.3.5. Photophysical characterization of neat films

To study the solid-state photophysical properties of the synthesized complexes, the thin films were obtained by using the spin-coating technique from DCM solutions. The emission maxima of the solid samples of all of the studied thiazole-boron complexes are red-shifted with respect to those of the corresponding solutions (Fig 4.38., Table 4.16.).
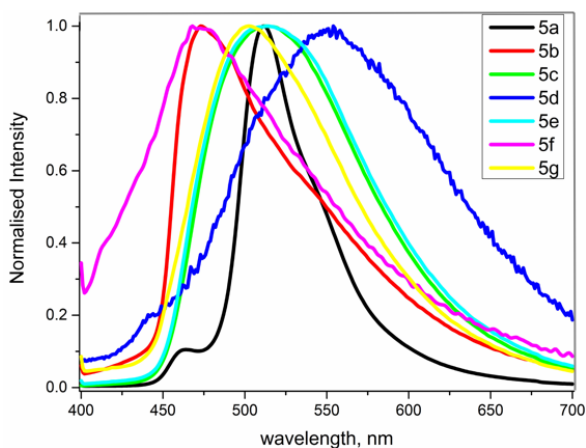
Fig 4.38. Overlaid normalized emission spectra of **5a–g** in the solid state

Also, excited-state lifetimes of neat films are established to have two lifetime components as compared to the single component demonstrated in solutions (Fig. 4.39.)
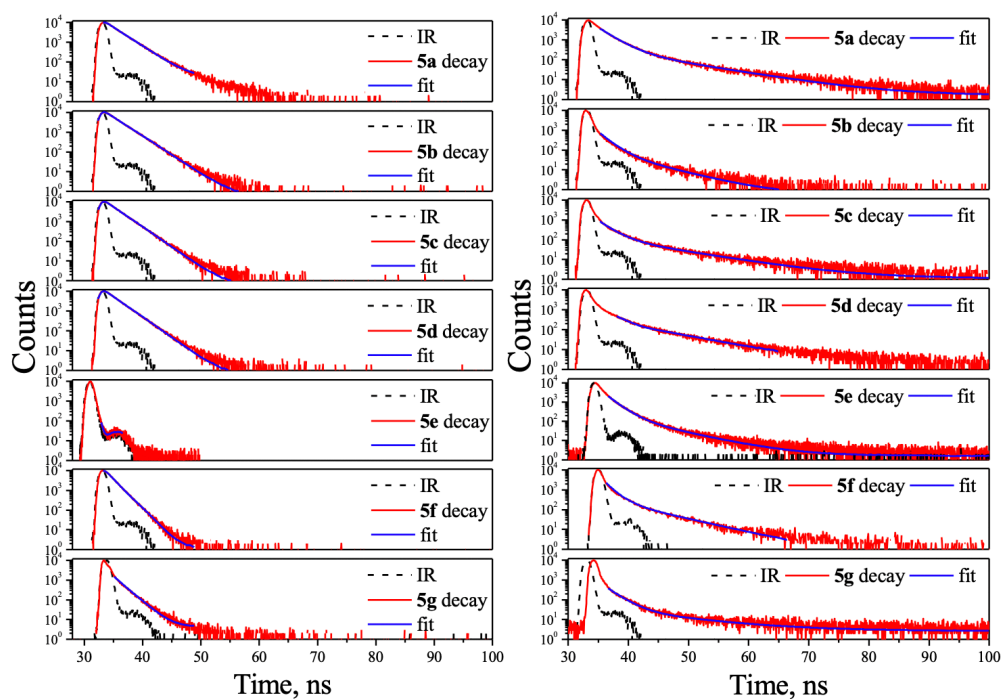
Fig. 4.39. Excited-state lifetimes of compounds **5a–5g** in a THF solution (left) and a solid neat film (right)

The films of most of the investigated dyes showed relatively weak fluorescence quantum yields ($\Phi = 0.07-0.25$), which were predetermined by aggregation-induced quenching. Compound **5g** in the solid state as well as in the dilute solution was almost

non-emissive ($\Phi < 0.01$). In contrast, the thin film of compound **5a** exhibited a very high fluorescence quantum yield (0.94), which is comparable with that of dilute solutions in non-polar solvents (toluene, DCM, and THF).

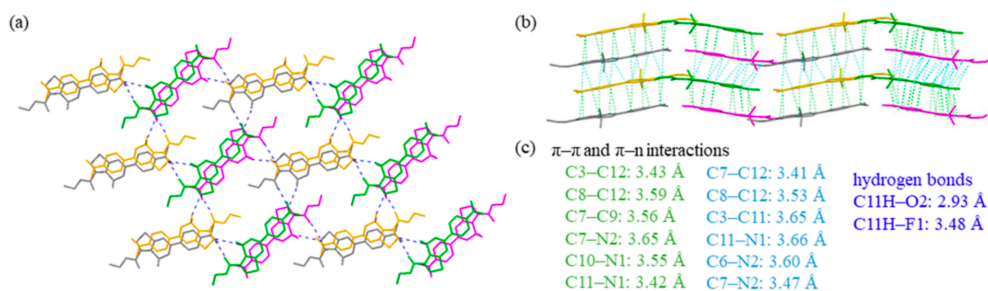The value of the fluorescent quantum yield in the solid state largely depends on interactions between the molecules in the crystal packing. In this context, $\pi-\pi$ intermolecular interactions can inhibit fluorescence[159].

Table 4.16. Photophysical data of complexes **5a–g** in the solid samples

Compound	λ_{em}, nm	Φ	τ, ns
5a	512	0.94	2.08, 8.83
5b	473	0.12	1.56, 5.66
5c	502	0.09	1.85, 8.79
5d	513	0.25	0.73, 7.51
5e	554	0.10	1.62, 6.11
5f	514	0.07	1.33, 6.35
5g	468	<0.01	1.94, 10.27

To consider the differences, the quantum yield, the molecular packing of complexes **5a, c−e** were carefully analyzed.

(a)

(b)

(c) $\pi-\pi$ and $\pi-n$ interactions

C3–C12: 3.43 Å C7–C12: 3.41 Å hydrogen bonds
C8–C12: 3.59 Å C8–C12: 3.53 Å C11H–O2: 2.93 Å
C7–C9: 3.56 Å   C3–C11: 3.65 Å C11H–F1: 3.48 Å
C7–N2: 3.65 Å   C11–N1: 3.66 Å
C10–N1: 3.55 Å C6–N2: 3.60 Å
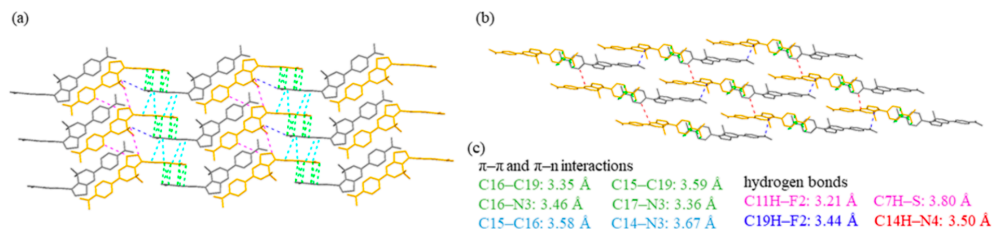C11–N1: 3.42 Å C7–N2: 3.47 Å

Fig. 4.40. Molecular packing of complex **5c**: (a) top view, (b) side view, and (c) list of intermolecular interactions. The green and light blue dotted lines show $\pi-\pi$ and $\pi-n$ interactions; the blue dotted lines show hydrogen bonds

As shown in Fig. 4.40., molecules in **5c** are linked by CH−O (2.93 Å) and CH−F (3.48 Å) hydrogen bonds forming the dimers in the top view. However, these molecules are organized in the dimers by $\pi-\pi$ and $\pi-n$ interactions (C−C, 3.43−3.59 Å; C−N, 3.42−3.65 Å) in the side view. Additionally, $\pi-\pi/\pi-n$ interactions were observed for each of these dimers (C−C, 3.41−3.65 Å; C−N, 3.47−3.66 Å), forming stoking columns. Because of the relatively effective $\pi-\pi/\pi-n$ interactions, compound **5c** exhibits a weak fluorescent quantum yield (9%) in the solid state.

Complex **5e** also exhibits well-ordered packing. The molecules form a net-type structure by a connection via CH−N (3.50 Å), CH−S (3.80 Å), and two CH−F (3.21 and 3.44 Å) hydrogen bonds. Moreover, the dimethylaminophenyl groups at position 4 of the thiazole ring demonstrate $\pi-\pi$ and $\pi-n$ interactions (C−C, 3.35−3.59 Å; C−N,

3.36−3.67 Å) (Fig. 4.41.). As a result, in this case, the relatively strong $\pi-\pi/\pi-n$ interactions provide weak fluorescence in the solid state ($\Phi = 10\%$).

(a)

(b)

(c)
$\pi-\pi$ and $\pi-n$ interactions
C16−C19: 3.35 Å   C15−C19: 3.59 Å
C16−N3: 3.46 Å   C17−N3: 3.36 Å
C15−C16: 3.58 Å   C14−N3: 3.67 Å

hydrogen bonds
C11H−F2: 3.21 Å   C7H−S: 3.80 Å
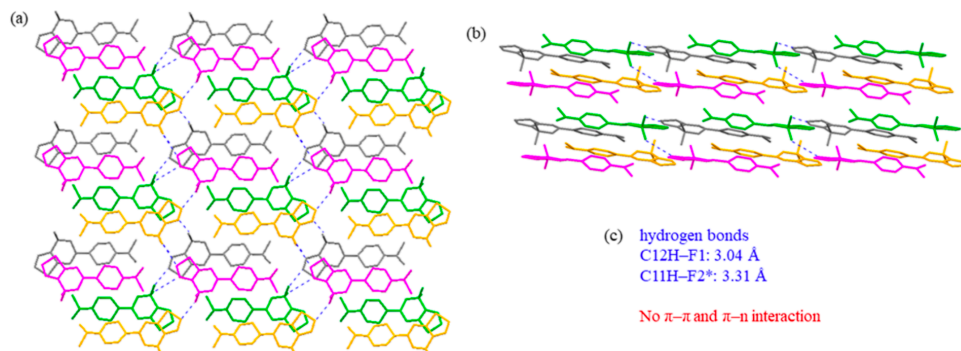C19H−F2: 3.44 Å   C14H−N4: 3.50 Å

Fig. 4.41. Molecular packing of complex **5e**: (a) top view, (b) side view, and (c) list of intermolecular interactions. The green and light blue dotted lines show $\pi-\pi$ and $\pi-n$ interactions; the magenta, blue, and red dotted lines show hydrogen bonds

As shown in Fig. 4.42., boron derivative **5d** forms layers consisting of dimers interacting via a parallel CH−π interaction (CH−C, 3.33−3.49 Å). However, in this structure, effective $\pi-\pi/\pi-n$ interactions are not observed (Fig. 4.42.). Therefore, compound **5d** is considered to have weaker intermolecular interactions than **5c** and **5e**, and a slightly higher fluorescent quantum yield of **5d** ($\Phi = 25\%$) is probably owing to the non-availability of $\pi-\pi$ and $\pi-n$ interactions.

(a)

(b)

(c) CH−π interactions in dimers
C8H−C2: 3.49 Å
C8H−C3: 3.33 Å

No hydrogen bond and π−π interaction
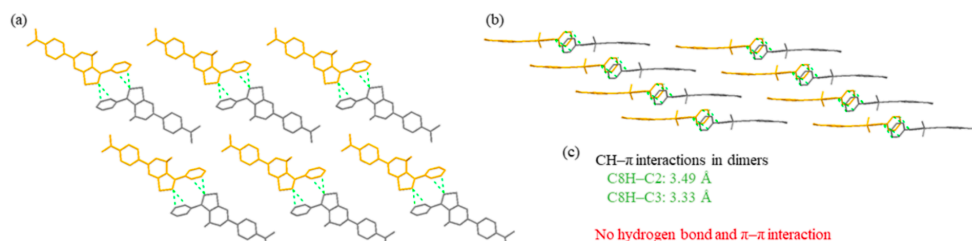
Fig. 4.42. Molecular packing of complex **5d**: (a) top view, (b) side view, and (c) list of intermolecular interactions. The green dotted lines show CH−π interactions in dimers

(a)

(b)

(c) hydrogen bonds
C12H−F1: 3.04 Å
C11H−F2*: 3.31 Å

No π−π and π−n interaction

Fig. 4.43. Molecular packing of complex **5a**: (a) top view, (b) side view, and (c) list of intermolecular interactions. The blue dotted lines show hydrogen bonds

For complex **5a**, the molecular packing is definitely different than for dyes **5c−e** (Fig. 4.43.). In this case, neighboring molecules are connected by weak CH−F

hydrogen bonds (3.04 and 3.31 Å). The dimethylaminophenyl groups are twisted and orientated at some angle toward each other. The molecules do not make any effective π−π or π−n interactions. Because of the inhibition of effective π−π/π−n interactions, the quantum yield of complex **5a** in the solid state is very high (94%).

Additionally, the fluorescence properties of **5a** were investigated in THF-water mixtures of various ratios (**5a** is soluble in THF but not soluble in water). The fluorescence intensity decreased with increasing water content to 80%. However, when the water content was increased to 90%, a dramatic increase of fluorescence intensity and a change of emission color from blue (λ_{em} = 454 nm) to green (λ_{em} = 508 nm) were observed (Fig 4.44.). These changes resulted from the formation of aggregates in the THF-water mixtures, which definitely indicates the effect of aggregation-induced emission (AIE)[78] for **5a**.
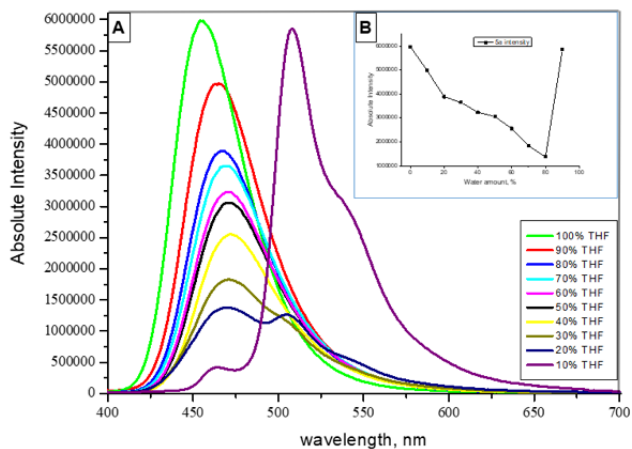
Fig. 4.44. (A) Emission spectra of **5a** in THF/water mixture with different fractions of water and (B) change of emission intensity of **5a** with water fraction.
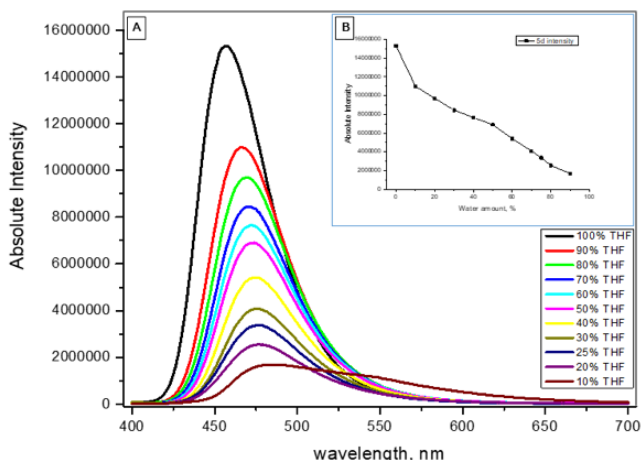
Fig. 4.45. (A) Emission spectra of **5d** in THF/water mixture with different fraction of water and (B) change of emission intensity of **5d** with water fraction.

An analogical investigation of emission activity of complex **5d** ($\Phi = 25\%$ in the solid state) in THF/H$_2$O solutions demonstrated an absence of the AIE effect (Fig 4.45.). This result can be explained by specific molecular packing of **5d**. It is possible that the reason for the deficiency of the AIE effect in this case is the formation of the dimer molecules in **5d** in the solid state (Fig 4.44.), which is not observed for the boron complex **5a**.

To conclude, novel *N,O* π-conjugated donor−acceptor organoboron complexes containing thiazole building blocks were synthesized and investigated. The examined compounds mostly exhibit a very high emission in the solutions. Structure-properties relationship and the influence of the functional group at position 4 of the thiazole ring on electronic and photophysical properties was studied. It was found that the incorporation of methyl or ethoxycarbonyl groups into the molecular structure does not significantly affect the photophysical parameters in the solution. A detailed investigation of structure and properties of unsubstituted thiazole complex revealed a very high fluorescence quantum yield in the solid state and the presence of aggregation-induced emission, which apparently are related to the unusual molecular packing and inhibition of π−π/π−n interactions.

5. CONCLUSIONS

1. A series of deep-blue emitting twisted donor-acceptor carbazole-chloropyridine conjugates were designed, theoretically investigated, synthesized and characterized. Their photophysical, thermal, electrochemical, photoelectrical and charge-transporting properties were investigated.

1.1. Simple, convenient and cost-effective design strategy based on single-step catalyst-free nucleophilic aromatic substitution was proposed to achieve yields up to 77%.

1.2. The materials demonstrated moderate to excellent thermal stability (up to $T_d = 380°C$) and a glass-forming ability with glass transition temperatures in the range of 93°C–134°C.

1.3. Ionization potential values of the materials measured by photoelectron emission spectroscopy were found to be in range from 5.74 eV to 5.88 eV.

1.4. The layers of the compounds demonstrated hole drift mobility values of $1×10^{-5}$ cm^2/Vs at electric field $2×10^5$ V/cm.

1.5. Dilute solutions of the compounds demonstrated significant dependence of the photoluminescence wavelength on the solvent polarity and relatively low photoluminescence quantum yield (0.02–0.04) which, however, significantly increases in the solid state (up to 0.16) which indicates aggregation-induced emission enhancement; mono-substituted chloropyridine derivative exhibited deep blue thermally activated delayed fluorescence with emission intensity maximum at 430 nm.

2. Two new twisted donor-acceptor phenyl-linked carbazole-aromatic imide derivatives were designed, theoretically investigated, synthesized and characterized. Their thermal, electrochemical, photophysical, photoelectric and charge-transporting properties were examined. An organic light-emitting device was fabricated applying one of the materials as an emitter.

2.1. Inexpensive and simple synthetic pathway based on a three-step catalyst-free synthesis was implemented to obtain these materials with the yields up to 76%.

2.2. Structural analysis revealed uncommon charge transfer through space mechanism.

2.3. The materials exhibited good thermal stability with initial decomposition temperatures situated in the range of 280°C–310°C.

2.4. Ionization potentials and electron affinities of the materials were found to be in the range of 6.03 eV–6.09 eV and 2.03–2.44 eV, respectively.

2.5. The compounds exhibited the capability of transporting both holes and electrons with hole mobility of $4.9×10^{-4}$ cm^{2}V^{-1}s^{-1} and electron mobility of $6.7×10^{-4}$ cm^{2}V^{-1}s^{-1} at an electric field of ca. $3×10^5$ Vcm^{-1}.

2.6. Carbazole-phthalimide derivative demonstrated aggregation-induced emission enhancement and thermally activated delayed fluorescence with a very low value of singlet-triplet energy splitting of 0.03 eV.

2.7. Carbazole-phthalimide derivative was used as an emitter to fabricate a series of doped and non-doped organic light-emitting devices. The best device showed the turn-on voltage of 4.9 V, maximum external quantum efficiency of 2.4%,

maximum current efficiency of 6.6 cd/A and maximum power efficiency of 4.0 lm/W with maximum brightness of 8300 cd/m^2.

3. Seven donor-acceptor 1,3-thiazole-based organoboron complexes were theoretically and structurally investigated, their electrochemical and photophysical properties were examined.

3.1. Ionization potentials and electron affinities were established by cyclic voltammetry technique and ranged from 4.76 to 5.08 eV and from 2.20 to 2.95 eV, respectively.

3.2. Photophysical properties and structure-properties relationship of the materials were investigated and the following results were obtained:

- Compounds demonstrate strong and sharp photoluminescence, generally situated in blue and sky-blue region with very high quantum yields observed for dilute solutions, especially for those in non-polar solvents (up to 0.99). Photoluminescence quantum yields of the solid films were found to be from low to moderate (<0.01– 0.25), however for the unsubstituted 1,3-thiazole-based complex it was found to be very high (0.94). Such behavior can be analyzed and explained by structural analysis of molecular packing.

- In addition, unsubstituted 1,3-thiazole-based complex were examined on the presence of aggregation-induced emission, which was proved by corresponding measurements, while other materials did not demonstrate the presence of aggregation-induced emission.

- Excited-state lifetimes were found to be extremely low in dilute solutions (from 0.64 ns to 2.24 ns) and low in solid-state films (from 0.73 ns to 10.27 ns).

6. REFERENCES

[1] ROUTLEDGE, R., A popular history of science (2nd ed.). *G. Routledge and Sons* [interactive]. 1881, p. 553. ISBN 0-415-38381-1. Access via the Internet: <https://books.google.lt/books?id=VO1HAAAAIAAJ&pg=PA553&redir_esc=y&hl=lt>

[2] STEUART, W., et al. Special Reports: Telephones and Telegraphs 1902. *Washington D.C.: U.S. Bureau of the Census* [interactive]. 1906, pp. 118–119. Access via the Internet: <https://books.google.lt/books?id=x-cpAAAAYAAJ&pg=PA118&dq=%22wireless+telegraphy&redir_esc=y#v=onepage&q=%22wireless%20telegraphy&f=false>

[3] GUARNIERI, M., Trailblazers in Solid-State Electronics [Historical]. *IEEE Industrial Electronics Magazine* [interactive]. 2011, Vol. 5(4), 46–47. Access via the Internet: <https://doi.org/10.1109/mie.2011.943016>

[4] TYNE, G., The Saga of the Vacuum Tube, Part 6. *Radio News. Chicago, IL: Ziff-Davis.* 1943, Vol. 30 (3): 26–28, 91.

[5] LOSSEV, O., (1928). CII. Luminous carborundum detector and detection effect and oscillations with crystals. *The London, Edinburgh, and Dublin Philosophical Magazine and Journal of Science* [interactive]. 1928, Vol. 6(39), 1024–1044. Access via the Internet: < https://doi.org/10.1080/14786441108564683>

[6] November 17 – December 23, 1947: Invention of the First Transistor. *American Physical Society News* [interactive]. 2000, Vol. 9, 10. Access via the Internet: <https://www.aps.org/publications/apsnews/200011/history.cfm>

[7] KUEHNE, A.J.C., and GATHER, M.C. (2016). Organic Lasers: Recent Developments on Materials, Device Geometries, and Fabrication Techniques. *Chemical Reviews* [interactive]. Vol. 116 (21), 12823–12864. Access via the Internet: <https://doi.org/10.1021/acs.chemrev.6b00172>

[8] BERGGREN, M., et al. Organic materials for printed electronics. *Nature Materials* [interactive]. 2007, Vol. 6 (1), 3–5. Access via the Internet: <http://www.nature.com/doifinder/10.1038/nmat1817>.

[9] Embracing the organics world. *Nature Materials* [interactive]. 2013, Vol. 12 (7), 591–591. Access via the Internet: <http://www.nature.com/doifinder/10.1038/nmat3707>.

[10] TANG, C.W., and VANSLYKE, S.A. Organic electroluminescent diodes. *Applied Physics Letters* [interactive]. 1987, Vol. 51 (12), 913. Access via the Internet: <http://scitation.aip.org/content/aip/journal/apl/51/12/10.1063/1.98799>

[11] TAKIMIYA, K., et al. π-Building Blocks for Organic Electronics: Revaluation of "Inductive" and "Resonance" Effects of π-Electron Deficient Units. *Chemistry of Materials* [interactive]. 2014, Vol. 26 (1), 587–593. Access via the Internet: <http://pubs.acs.org/doi/abs/10.1021/cm4021063>

[12] KO, C.W., and TAO, Y.T. Bright white organic light-emitting diode. *Applied Physics Letters* [interactive]. 2001, Vol. 79 (25), 4234. Access via the Internet: <http://scitation.aip.org/content/aip/journal/apl/79/25/10.1063/1.1425454>

[13] KULKARNI, A.P., et al. Electron Transport Materials for Organic Light-Emitting Diodes. *Chemistry of Materials* [interactive]. 2004, Vol. 16 (23), 4556–4573. Access via the Internet: <http://pubs3.acs.org/acs/journals/doilookup?in_doi=10.1021/cm049473l>

[14] TAO, Y., et al. Organic host materials for phosphorescent organic light-emitting diodes. *Chemical Society Reviews* [interactive]. 2011, Vol. 40 (5), 2943. Access via the Internet: <http://xlink.rsc.org/?DOI=c0cs00160k>

[15] LUNDIN, N.J., et al. Synthesis and Characterization of a Multicomponent Rhenium(I) Complex for Application as an OLED Dopant. *Angewandte Chemie International Edition* [interactive]. 2006, Vol. 45 (16), 2582–2584. Access via the Internet: <http://doi.wiley.com/10.1002/anie.200504532>

[16] KLESSINGER, M., and MICHL, J. Excited states and photochemistry of organic molecules, *VCH publishers* (1995)

[17] BALDO, M. A., et al. Highly efficient phosphorescent emission from organic electroluminescent devices. *Nature* [interactive]. 1998, Vol. 395 (6698), 151. Access via the Internet: <https://www.nature.com/articles/25954>

[18] ADACHI, C., et al. High-efficiency red electrophosphorescence devices. *Applied Physics Letters*. [interactive]. 2001, Vol. 78 (11), 1622. Access via the Internet: <https://doi.org/10.1063/1.1355007>

[19] MEERHEIM, R., et al. Ultrastable and efficient red organic light emitting diodes with doped transport layers *Applied Physics Letters*. [interactive]. 2006, Vol. 89 (6), 061111. Access via the Internet: <https://doi.org/10.1063/1.2268354 >

[20] ADACHI, C., et al. Endothermic energy transfer: A mechanism for generating very efficient high-energy phosphorescent emission in organic materials *Applied Physics Letters*. [interactive]. 2001, Vol. 79 (13), 2082. Access via the Internet: < https://doi.org/10.1063/1.1400076 >

[21] YEH, S.-J., et al. New Dopant and Host Materials for Blue-Light-Emitting Phosphorescent Organic Electroluminescent Devices. *Advanced Materials* [interactive]. 2005, Vol. 17 (3), 285–289. Access via the Internet: <http://doi.wiley.com/10.1002/adma. 200401373>.

[22] TANAKA, D., et al. High Luminous Efficiency Blue Organic Light-Emitting Devices Using High Triplet Excited Energy Materials. *Jpn. Japanese Journal of Applied Physics* [interactive]. 2007, Vol. 46 (2) L117. Access via the Internet: <http://iopscience.iop.org/article/10.1143/JJAP.46.L117/meta>

²³ ADACHI, C., et al. Nearly 100% internal phosphorescence efficiency in an organic light-emitting device. *Journal of Applied Physics* [interactive]. 2001, Vol. 90 (10), 5048. Access via the Internet: <http://scitation.aip.org/content/aip/journal/jap/90/10/10.1063/1. 1409582>.

²⁴ ADACHI, C., et al. High-efficiency organic electrophosphorescent devices with tris(2-phenylpyridine)iridium doped into electron-transporting materials. *Applied Physics Letters* [interactive]. 2000, Vol. 77 (6), 904. Access via the Internet: <http://scitation.aip.org/content/aip/journal/apl/77/6/10.1063/1.1306639>.

²⁵ CHOU, P.-T., and CHI, Y. Osmium- and Ruthenium-Based Phosphorescent Materials: Design, Photophysics, and Utilization in OLED Fabrication. *European Journal of Inorganic Chemistry. European Journal of Inorganic Chemistry* [interactive]. 2006, Vol. 2006 (17), 3319–3332. Access via the Internet: <https://doi.org/10.1002/ejic.200600364>

²⁶ NIU, Y.-H., et al. Highly Efficient Electrophosphorescent Devices with Saturated Red Emission from a Neutral Osmium Complex. *Chemistry of Materials* [interactive]. 2005, Vol. 17 (13), 3532–3536. Access via the Internet: <https://dx.doi.org/10.1021/cm047709f>

²⁷ TUNG, Y.-L., et al. Organic Light-Emitting Diodes based on Charge-Neutral RuII Phosphorescent Emitters. *Advanced Materials* [interactive]. 2005, Vol. 17 (8), 1059. Access via the Internet: <https://doi.org/10.1002/adma.200401806>

²⁸ NITSCH, J., et al. Cuprophilic interactions in highly luminescent dicopper(i)–NHC–picolyl complexes – fast phosphorescence or TADF? *Chemical Communications* [interactive]. 2016, Vol. 52(14), 2932–2935. Access via the Internet: <https://dx.doi.org/10.1039/C5CC09659F>

²⁹ WU, F., et al. Phosphorescent Cu(I) complexes based on bis(pyrazol-1-yl-methyl)-pyridine derivatives for organic light-emitting diodes. *Journal of Materials Chemistry C* [interactive]. 2015, Vol. 3 (1), 138–146. Access via the Internet: <https://dx.doi.org/10.1039/c4tc01885k>

³⁰ YANG, X., et al. Functionalization of phosphorescent emitters and their host materials by main-group elements for phosphorescent organic light-emitting devices. *Chemical Society Reviews* [interactive]. 2015, Vol. 44 (23), 8484–8575. Access via the Internet: <https://dx.doi.org/10.1039/c5cs00424a>

³¹ NODA, T., and SHIROTA, Y. 5,5'-Bis(dimesitylboryl)-2,2'-bithiophene and 5,5''-Bis(dimesitylboryl)-2,2':5',2''-terthiophene as a Novel Family of Electron-Transporting Amorphous Molecular Materials. *Journal of the American Chemical Society* [interactive]. 1998, Vol. 120 (37), 9714–9715. Access via the Internet: <https://dx.doi.org/10.1021/ja9817343>

³² ZHANG, T., et al. Fluorene/tridurylborane hybrids as solution-processible hosts for phosphorescent organic light-emitting diodes. Dyes and Pigments

[interactive]. 2013, Vol. 97 (1), 155–161. Access via the Internet: <https://dx.doi.org/10.1016/j.dyepig.2012.11.022>

[33] REN, X., et al. Ultrahigh Energy Gap Hosts in Deep Blue Organic Electrophosphorescent Devices. *Chemistry of Materials* [interactive]. 2004, Vol.16 (23), 4743–4747. Access via the Internet: <https://dx.doi.org/10.1021/cm049402m>

[34] HOLMES, R. J., et al. Efficient, deep-blue organic electrophosphorescence by guest charge trapping. *Applied Physics Letters* [interactive]. 2003 Vol. 83 (18), 3818-3820. Access via the Internet: <https://doi.org/10.1063/1.1624639>

[35] LIN, J.-J., et al. A Highly Efficient Host/Dopant Combination for Blue Organic Electrophosphorescence Devices. *Advanced Functional Materials* [interactive]. 2008, Vol. 18 (3), 485–491. Access via the Internet: <https://doi.org/10.1002/adfm.200700537>

[36] 'BRIEN, D. F., et al. Improved energy transfer in electrophosphorescent devices. *Applied Physics Letters* [interactive]. 1999, Vol. 74 (3), 442–444. Access via the Internet: <https://doi.org/10.1063/1.123055>

[37] TOKITO, S., et al. Confinement of triplet energy on phosphorescent molecules for highly-efficient organic blue-light-emitting devices. *Applied Physics Letters* [interactive]. 2003, Vol. 83 (3), 569–571. Access via the Internet: <https://doi.org/10.1063/1.1594834>

[38] GONG, S., et al. Simple CBP isomers with high triplet energies for highly efficient blue electrophosphorescence. *Journal of Materials Chemistry* [interactive]. 2012, Vol. 22 (7), 2894–2899. Access via the Internet: <https://dx.doi.org/10.1039/c1jm14903b>

[39] JANG, S. E., et al. High power efficiency in simplified two layer blue phosphorescent organic light-emitting diodes. *Organic Electronics* [interactive]. 2010, Vol. 11(6), 1154–1157. Access via the Internet: <https://dx.doi.org/10.1016/j.orgel.2010.04.004>

[40] HUDSON, Z. M., et al. N-Heterocyclic Carbazole-Based Hosts for Simplified Single-Layer Phosphorescent OLEDs with High Efficiencies. *Advanced Materials* [interactive]. 2012, Vol. 24 (21), 2922–2928. Access via the Internet: <https://doi.org/10.1002/adma.201200927>

[41] LIN, M.-S., et al. Incorporation of a CN group into mCP: a new bipolar host material for highly efficient blue and white electrophosphorescent devices. *Journal of Materials Chemistry* [interactive]. 2012, Vol. 22 (31), 16114. Access via the Internet: <https://dx.doi.org/10.1039/c2jm32717a>

[42] ZHANG, T., et al. A CBP derivative as bipolar host for performance enhancement in phosphorescent organic light-emitting diodes. *Journal of Materials Chemistry C* [interactive]. (2013), Vol. 1 (4), 757–764. Access via the Internet: <https://dx.doi.org/10.1039/c2tc00305h>

[43] CHO, Y. J., and LEE, J. Y. Modified N,N′-Dicarbazolyl-3,5-benzene as a High Triplet Energy Host Material for Deep-Blue Phosphorescent Organic Light-Emitting Diodes. *Chemistry - A European Journal* [interactive]. 2011, Vol. 17 (41), 11415–11418. Access via the Internet: <https://doi.org/10.1002/chem.201101095>

[44] JEON, S. O., et al. External Quantum Efficiency Above 20% in Deep Blue Phosphorescent Organic Light-Emitting Diodes. *Advanced Materials* [interactive]. 2011, Vol. 23 (12), 1436–1441. Access via the Internet: <https://doi.org/10.1002/adma.201004372>

[45] JEON, S. O., and LEE, J. Y. Comparison of symmetric and asymmetric bipolar type high triplet energy host materials for deep blue phosphorescent organic light-emitting diodes. *Journal of Materials Chemistry* [interactive]. 2012, Vol. 22 (15), 7239. Access via the Internet: <https://dx.doi.org/10.1039/c2jm30742a>

[46] HUANG, H., et al. Optimizing the conjugation between N,N′-dicarbazolyl-3,5-benzene and triphenylphosphine oxide as bipolar hybrids for highly efficient blue and single emissive layer white phosphorescent OLEDs. *Organic Electronics* [interactive]. 2013, Vol. 14 (10), 2573–2581. Access via the Internet: <https://dx.doi.org/10.1016/j.orgel.2013.06.011>

[47] UOYAMA, H., et al. Highly efficient organic light-emitting diodes from delayed fluorescence. *Nature* [interactive]. 2012, Vol. 492 (7428), 234–238. Access via the Internet: <http://www.nature.com/doifinder/10.1038/nature11687>.

[48] PARTEE, J., et al. Delayed Fluorescence and Triplet-Triplet Annihilation in pi-Conjugated Polymers. *Physical Review Letters* [interactive]. 1999, Vol. 82 (18), 3673–3676. Access via the Internet: <http://link.aps.org/doi/10.1103/PhysRevLett.82.3673>.

[49] JOU, J.-H., et al. Approaches for fabricating high efficiency organic light emitting diodes. *J. Mater. Chem. C* [interactive]. 2015, Vol. 3 (13), 2974–3002. Access via the Internet: <http://xlink.rsc.org/?DOI=C4TC02495H>.

[50] DIAS, F.B., et al. Triplet Harvesting with 100% Efficiency by Way of Thermally Activated Delayed Fluorescence in Charge Transfer OLED Emitters. *Advanced Materials* [interactive]. 2013, Vol. 25 (27), 3707–3714. Access via the Internet: <http://www.ncbi.nlm.nih.gov/pubmed/23703877>.

[51] SANTOS, P.L., et al. Engineering the singlet–triplet energy splitting in a TADF molecule. *J. Mater. Chem. C* [interactive]. 2016, Vol. 4 (17), 3815–3824. Access via the Internet: <http://xlink.rsc.org/?DOI=C5TC03849A>.

[52] NOBUYASU, R.S., et al. Rational Design of TADF Polymers Using a Donor-Acceptor Monomer with Enhanced TADF Efficiency Induced by the Energy Alignment of Charge Transfer and Local Triplet Excited States. *Advanced Optical Materials* [interactive]. 2016, Vol. 4 (4), 597–607. Access via the Internet: <http://doi.wiley.com/10.1002/adom.201500689>.

⁵³ ZHANG, Q., et al. Design of Efficient Thermally Activated Delayed Fluorescence Materials for Pure Blue Organic Light Emitting Diodes.*Journal of the American Chemical Society* [interactive]. 2012, Vol. 134 (36), 14706–14709. Access via the Internet: <http://pubs.acs.org/doi/abs/10.1021/ja306538w>.

⁵⁴ TAO, Y., et al. Thermally Activated Delayed Fluorescence Materials Towards the Breakthrough of Organoelectronics. *Advanced Materials* [interactive]. 2014, Vol. 26 (47), 7931–7958. Access via the Internet: <https://doi.org/10.1002/adma.201402532>

⁵⁵ YANG, Z., et al. Recent advances in organic thermally activated delayed fluorescence materials. *Chemical Society Reviews* [interactive]. 2017, Vol. 46 (3), 915–1016. Access via the Internet: <https://dx.doi.org/10.1039/c6cs00368k>

⁵⁶ KOMATSU, R., et. al. Light-blue thermally activated delayed fluorescent emitters realizing a high external quantum efficiency of 25% and unprecedented low drive voltages in OLEDs. *Journal of Materials Chemistry C* [interactive]. 2016, Vol. 4(12), 2274–2278. Access via the Internet: < https://dx.doi.org/10.1039/c5tc04057d>

⁵⁷ KIM, M., et al. Correlation of Molecular Structure with Photophysical Properties and Device Performances of Thermally Activated Delayed Fluorescent Emitters. *The Journal of Physical Chemistry C* [interactive]. 2016, Vol.120 (5), 2485–2493. Access via the Internet: <https://dx.doi.org/10.1021/acs.jpcc.5b09114>

⁵⁸ DATA, P., et al. Dibenzo[a,j]phenazine-Cored Donor-Acceptor-Donor Compounds as Green-to-Red/NIR Thermally Activated Delayed Fluorescence Organic Light Emitters. *Angewandte Chemie International Edition* [interactive]. 2016, Vol. 55 (19), 5739–5744. Access via the Internet: < https://doi.org/10.1002/anie.201600113>

⁵⁹ ZHANG, Q., et al. Efficient blue organic light-emitting diodes employing thermally activated delayed fluorescence. *Nature Photonics* [interactive]. 2014, Vol. 8 (4), 326–332. Access via the Internet: <https://dx.doi.org/10.1038/nphoton.2014.12>

⁶⁰ ZHANG, Q., et al. Nearly 100% Internal Quantum Efficiency in Undoped Electroluminescent Devices Employing Pure Organic Emitters. *Advanced Materials* [interactive]. 2015, Vol. 27 (12), 2096–2100. Access via the Internet: <https://doi.org/10.1002/adma.201405474>

⁶¹ LEE, S. Y., et al. Luminous Butterflies: Efficient Exciton Harvesting by Benzophenone Derivatives for Full-Color Delayed Fluorescence OLEDs. *Angewandte Chemie International Edition* [interactive]. 2014, Vol. 53 (25), 6402–6406. Access via the Internet: <https://dx.doi.org/10.1002/anie.201402992>

⁶² RAJAMALLI, P., et al. (2016). A New Molecular Design Based on Thermally Activated Delayed Fluorescence for Highly Efficient Organic Light Emitting Diodes.

Journal of the American Chemical Society [interactive]. 2016, Vol. 138 (2), 628–634. Access via the Internet: <https://dx.doi.org/10.1021/jacs.5b10950>

[63] RAJAMALLI, P., et al. A thermally activated delayed blue fluorescent emitter with reversible externally tunable emission. *Journal of Materials Chemistry C* [interactive]. 2016, Vol. 4 (5), 900–904. Access via the Internet: <https://dx.doi.org/10.1039/c5tc03943f>

[64] HUDSON, Z. M., and WANG, S. (2009). Impact of Donor−Acceptor Geometry and Metal Chelation on Photophysical Properties and Applications of Triarylboranes. *Accounts of Chemical Research* [interactive]. 2009, Vol. 42 (10), 1584–1596. Access via the Internet: <https://dx.doi.org/10.1021/ar900072u>

[65] SHUTO, A., et al. π-Extended Planarized Triphenylboranes with Thiophene Spacers. *Organic Letters* [interactive]. 2013, Vol. 15 (24), 6234–6237. Access via the Internet: <https://dx.doi.org/10.1021/ol403084x>

[66] NUMATA, M., et al. High efficiency pure blue thermally activated delayed fluorescence molecules having 10H-phenoxaborin and acridan units. *Chemical Communications* [interactive]. 2015, Vol. 51 (46), 9443–9446. Access via the Internet: <https://dx.doi.org/10.1039/c5cc00307e>

[67] KITAMOTO, Y., et al. (2015). Light blue and green thermally activated delayed fluorescence from 10H-phenoxaborin-derivatives and their application to organic light-emitting diodes. *Journal of Materials Chemistry C* [interactive]. 2015, Vol. 3 (35), 9122–9130. Access via the Internet: <https://dx.doi.org/10.1039/c5tc01380a>

[68] KITAMOTO, Y., et al. Dimesitylarylborane-based luminescent emitters exhibiting highly-efficient thermally activated delayed fluorescence for organic light-emitting diodes. *Organic Electronics* [interactive]. 201, Vol. 34, 208–217. Access via the Internet: <https://dx.doi.org/10.1016/j.orgel.2016.04.030>

[69] HENDSBEE, A. D., et al. Phthalimide-based π-conjugated small molecules with tailored electronic energy levels for use as acceptors in organic solar cells. *Journal of Materials Chemistry C* [interactive]. 2015, Vol. 3 (34), 8904–8915. Access via the Internet: <https://dx.doi.org/10.1039/c5tc01877c>

[70] LI, M., et al. Aromatic-Imide-Based Thermally Activated Delayed Fluorescence Materials for Highly Efficient Organic Light-Emitting Diodes. *Angewandte Chemie International Edition* [interactive]. 2017, Vol. 56 (30), 8818–8822. Access via the Internet: < https://doi.org/10.1002/anie.201704435 >

[71] JANG, M. E., et al. Organic Light-emitting Diodes Based on Donor-substituted Phthalimide and Maleimide Fluorophores. *Chemistry Letters*, [interactive]. 2015, Vol. 44 (9), 1248–1250. Access via the Internet: <https://doi.org/10.1246/cl.150454>

[72] FÖRSTER T. and KASPER, K. Ein konzentrationsumschlag der fluoreszenz. *Z. Phys. Chem. (Muenchen, Ger.)* 1954, Vol. 1, 275−277. Access via the Internet: <https://doi.org/10.1002/bbpc.19550591018>

[73] LUO, J., et al. Aggregation-induced emission of 1-methyl-1,2,3,4,5-pentaphenylsilole. *Chemical Communications* [interactive]. 2001, Vol. 0 (18), 1740–1741. Access via the Internet: <https://dx.doi.org/10.1039/b105159h>

[74] TANG, B. Z., et al. Efficient blue emission from siloles. *Journal of Materials Chemistry* [interactive]. 2001, Vol. 11 (12), 2974–2978. Access via the Internet: <https://dx.doi.org/10.1039/b102221k>

[75] HONG, Y., et al. Aggregation-induced emission: phenomenon, mechanism and applications. *Chemical Communications* [interactive]. 2009, Vol. 0 (29), 4332. Access via the Internet: <https://dx.doi.org/10.1039/b904665h>

[76] LUO, J., et al. Switching of non-helical overcrowded tetrabenzoheptafulvalene derivatives. *Chemical Science* [interactive]. 2011, Vol. 2 (10), 2029. Access via the Internet: <https://dx.doi.org/10.1039/c1sc00340b>

[77] LEUNG, N. L. C., et al. (2014). Restriction of Intramolecular Motions: The General Mechanism behind Aggregation-Induced Emission. *Chemistry - A European Journal* [interactive]. 2014, Vol. 20(47), 15349–15353. Access via the Internet: <https://dx.doi.org/10.1002/chem.201403811>

[78] MEI, J., et al. Aggregation-Induced Emission: Together We Shine, United We Soar! *Chemical Reviews* [interactive]. 2015, Vol. 115 (21), 11718–11940. Access via the Internet: <https://dx.doi.org/10.1021/acs.chemrev.5b00263>

[79] WANG, H., et al. Novel Thermally Activated Delayed Fluorescence Materials-Thioxanthone Derivatives and Their Applications for Highly Efficient OLEDs. Advanced Materials, [interactive]. 2014, Vol. 26 (30), 5198–5204. Access via the Internet: <https://doi.org/10.1002/adma.201401393>

[80] LEE, I. H., et al. Aggregation-induced emission type thermally activated delayed fluorescent materials for high efficiency in non-doped organic light-emitting diodes. *Organic Electronics* [interactive]. 2016, Vol. 29 (22), 22–26. Access via the Internet: <https://dx.doi.org/10.1016/j.orgel.2015.11.019>

[81] HUANG, J., et al. Highly Efficient Nondoped OLEDs with Negligible Efficiency Roll-Off Fabricated from Aggregation-Induced Delayed Fluorescence Luminogens. *Angewandte Chemie International Edition* [interactive]. 2017, Vol. 56 (42), 12971–12976. Access via the Internet: <https://doi.org/10.1002/anie.201706752>

[82] AIZAWA, N., et al. Aggregation-induced delayed fluorescence from phenothiazine-containing donor–acceptor molecules for high-efficiency non-doped organic light-emitting diodes. *Polymer Journal* [interactive]. 2016, Vol. 49 (1), 197–202. Access via the Internet: <https://dx.doi.org/10.1038/pj.2016.82>

[83] HUANG, B., et al. Simple aggregation–induced delayed fluorescence materials based on anthraquinone derivatives for highly efficient solution–processed red OLEDs. *Journal of Luminescence* [interactive]. 2017, Vol. 187, 414–420. Access via the Internet: <https://dx.doi.org/10.1016/j.jlumin.2017.03.038>

[84] PARK, J., et al. Synthesis, characterization of the phenylquinoline-based on iridium(III) complexes for solution processable phosphorescent organic light-emitting diodes. *Organic Electronics* [interactive]. 2013, Vol. 14 (9), 2114–2123. Access via the Internet: <https://dx.doi.org/10.1016/j.orgel.2013.05.013>

[85] PIETRASZKIEWICZ, M., et al. Highly photo- and electroluminescent 1,3-diketonate Eu(III) complexes with spiro-fluorene-xantphos dioxide ligands: synthesis and properties. *Journal of Materials Chemistry C* [interactive]. 2013, Vol. 1(48), 8028. Access via the Internet: <https://dx.doi.org/10.1039/c3tc30783b>

[86] DE MELLO, J.C., et al. An improved experimental determination of external photoluminescence quantum efficiency. In *Advanced Materials* [interactive]. 1997. Vol. 9, no. 3, p. 230–232. Access via the Internet: <http://doi.wiley.com/10.1002/adma.19970090308>.

[87] GRITZNER, G., and KUTA, J. Recommendations on reporting electrode potentials in nonaqueous solvents. *Pure and Applied Chemistry*. 1984, Vol. 56 (4), 461–466. [interactive] Access via the Internet: <https://dx.doi.org/10.1351/pac198456040461>

[88] POMMEREHNE, J., et al. Efficient two layer leds on a polymer blend basis. *Advanced Materials* [interactive]. 1995, Vol. 7 (6), 551–554. Access via the Internet: <https://dx.doi.org/10.1002/adma.19950070608>

[89] MIYAMOTO, E., et al. Ionization potential of organic pigment film by atmospheric photoelectron emission analysis. In *Electrophotography* [interactive]. 1989. Vol. 28, no. 4, p. 364–370. Access via the Internet: <https://astp.jst.go.jp/modules/search/ DocumentDetail/0387-916X_28_4_Ionization+potential+of+organic+pigment+film+by+ atmospheric+photoelectron+emission+analysis._N%252FA>.

[90] KUKHTA, N. A., et al. Structure–property relationships of star-shaped blue-emitting charge-transporting 1,3,5-triphenylbenzene derivatives. *Dyes and Pigments* [interactive]. 2015, Vol. 117, 122–132. Access via the Internet: <https://dx.doi.org/10.1016/j.dyepig.2015.02.013>

[91] JUŠKA, G., et al. New method of drift mobility evaluation in μc-Si:H, basic idea and comparison with time-of-flight. *Journal of Non-Crystalline Solids* [interactive]. 2000, Vol. 266-269, 331–335. Access via the Internet: <https://dx.doi.org/10.1016/s0022-3093(99)00720-6>

[92] MIMAITE, V., et al. Can hydrogen bonds improve the hole-mobility in amorphous organic semiconductors? Experimental and theoretical insights. *Journal*

of Materials Chemistry C [interactive]. 2015, Vol. 3 (44), 11660–11674. Access via the Internet: <https://dx.doi.org/10.1039/c5tc02534f>

[93] PIVRIKAS, A., et al. A review of charge transport and recombination in polymer/fullerene organic solar cells. *Progress in Photovoltaics: Research and Applications* [interactive]. 2007, Vol. 15 (8), 677–696. Access via the Internet: <https://dx.doi.org/10.1002/pip.791>

[94] FRISCH, M.J.. et al. 2009. Gaussian 16, Revision A.03; Gaussian, Inc.: Wallingford, CT, 2016.

[95] SPARTAN'14 for windows version 1.1.4. 1840 Von Karman avenue, suite 370, Irvine, CA, 92612. Wavefunction, Inc.; 2013.

[96] HARWOOD, L.M., an MOODY, C.J. *Experimental organic chemistry: principles and practice* [interactive]. [s.l.]: Oxford: Blackwell scientific, 1990. ISBN 0632020164 ; 0632020172 pbk.

[97] WHARTON, et al. The Production and Characterisation of Novel Conducting Redox-Active Oligomeric Thin Films From Electrooxidised Indolo[3,2,1-jk]carbazole. *Chemistry - A European Journal* [interactive]. 2009, Vol. 15 (22), 5482–5490. Access via the Internet: <https://doi.org/10.1002/chem.200900097 >

[98] POTOPNYK, M. A., et al. N,O π-Conjugated 4-Substituted 1,3-Thiazole BF2 Complexes: Synthesis and Photophysical Properties. *The Journal of Organic Chemistry* [interactive]. 2018, Vol. 83 (3), 1095–1105. Access via the Internet: < http://dx.doi.org/10.1021/acs.joc.7b02239>

[99] FARINOLA, G. M., and RAGNI, R. Electroluminescent materials for white organic light emitting diodes. *Chemical Society Reviews* [interactive]. 2011, Vol. 40 (7), 3467. Access via the Internet: <https://doi.org/10.1039/C0CS00204F >

[100] DUAN, L., et al. Strategies to Design Bipolar Small Molecules for OLEDs: Donor-Acceptor Structure and Non-Donor-Acceptor Structure. *Advanced Materials* [interactive]. 2011, Vol. 23 (9), 1137–1144. Access via the Internet: <https://doi.org/10.1002/adma.201003816 >

[101] TANG, J., et al. New starburst sensitizer with carbazole antennas for efficient and stable dye-sensitized solar cells. *Energy & Environmental Science* [interactive]. 2010, Vol. 3 (11), 1736. Access via the Internet: <https://doi.org/10.1039/C0EE00008F >

[102] JIAO, C.-X., et al. Conjugated carbazole dimer as fluorescence carrier for preparation of iodine-sensitive chemical sensor. *Analytica Chimica Acta* [interactive]. 2005, Vol. 528 (2), 229–234. Access via the Internet: <https://doi.org/10.1016/j.aca.2004.04.061>

[103] SATO, K., et al. (2013). Organic Luminescent Molecule with Energetically Equivalent Singlet and Triplet Excited States for Organic Light-Emitting Diodes.

Physical Review Letters [interactive]. 2013, Vol. 110 (24). Access via the Internet: <https://doi.org/10.1103/PhysRevLett.110.247401>

[104] BUČINSKAS, A., et al. N-annelated perylenes as effective green emitters for OLEDs. *RSC Advances* [interactive]. 2015, Vol. 5 (95), 78150–78159. Access via the Internet: <https://doi.org/10.1039/C5RA15075B>

[105] SKUODIS, E., et al. OLEDs based on the emission of interface and bulk exciplexes formed by cyano-substituted carbazole derivative. *Dyes and Pigments* [interactive]. 2017, Vol. 139, 795–807. Access via the Internet: <https://doi.org/10.1016/j.dyepig.2017.01.016>

[106] YANG, Z., et al. Recent advances in organic thermally activated delayed fluorescence materials. *Chemical Society Reviews* [interactive]. 2017, Vol. 46 (3), 915–1016. Access via the Internet: <https://doi.org/10.1039/C6CS00368K >

[107] LO, D., et al. Sky-blue aggregation-induced emission molecules for non-doped organic light-emitting diodes. *Journal of Materials Chemistry C* [interactive]. 2017, Vol. 5 (24), 6054–6060. Access via the Internet: <https://doi.org/10.1039/C7TC01659J >

[108] FURUE, R. et. al. Aggregation-Induced Delayed Fluorescence Based on Donor/Acceptor-Tethered Janus Carborane Triads: Unique Photophysical Properties of Nondoped OLEDs. *Angewante Chemie Intnational Edition* [interactive]. 2016, Vol. 55 (25), 7171. Access via the Internet: <https://doi.org/10.1002/anie.201603232>

[109] LI, J., and GRIMSDALE, A. C. Carbazole-based polymers for organic photovoltaic devices. *Chemical Society Reviews* [interactive]. 2010, Vol. 39 (7), 2399. Access via the Internet: <https://doi.org/10.1039/B915995A>

[110] SEIDLER, N., et al. Influence of the hole blocking layer on blue phosphorescent organic light-emitting devices using 3,6-di(9-carbazolyl)-9-(2-ethylhexyl)carbazole as host material. *Applied Physics Letters* [interactive]. 2010, Vol. 96 (9), 093304. Access via the Internet: <https://doi.org/10.1063/1.3350890>

[111] KROTKUS, S., et al. Pyrenyl-Functionalized Fluorene and Carbazole Derivatives as Blue Light Emitters. *The Journal of Physical Chemistry C* [interactive]. 2012, Vol. 116 (13), 7561–7572. Access via the Internet: <https://dx.doi.org/10.1021/jp300161k >

[112] TANG, C., et al. A versatile efficient one-step approach for carbazole–pyridine hybrid molecules: highly efficient host materials for blue phosphorescent OLEDs. *Chemical Communications* [interactive]. 2015, Vol. 51 (9), 1650–1653. Access via the Internet: <https://doi.org/10.1039/C4CC08335K >

[113] KULKARNI, A. P., et al. Electron Transport Materials for Organic Light-Emitting Diodes. *Chemistry of Materials* [interactive]. 2004, Vol. 16 (23), 4556–4573. Access via the Internet: <http://dx.doi.org/10.1021/cm049473l >

[114] LI, B., et al. Dicarbazolyldicyanobenzenes as Thermally Activated Delayed Fluorescence Emitters: Effect of Substitution Position on Photoluminescent and Electroluminescent Properties. *Chemistry Letters* [interactive]. 2014, Vol. 43 (3), 319–321. Access via the Internet: <https://doi.org/10.1246/cl.130907>

[115] ISHIMATSU, R., et al. Electrogenerated Chemiluminescence of Donor-Acceptor Molecules with Thermally Activated Delayed Fluorescence. *Angewandte Chemie International Edition* [interactive]. 2014, Vol. 53 (27), 6993–6996. Access via the Internet: <https://doi.org/10.1002/anie.201402615 >

[116] AMBROSE, J. F., and NELSON, R. F. Anodic Oxidation Pathways of Carbazoles. *Journal of The Electrochemical Society* [interactive]. 1968, Vol. 115 (11), 1159. Access via the Internet: <http://dx.doi.org/10.1149/1.2410929>

[117] IRGASHEV, R. A., et al. Synthesis and properties of new π-conjugated imidazole/carbazole structures. Dyes and Pigments [interactive]. 2017, Vol.141, 512–520. Access via the Internet: <https://doi.org/10.1016/j.dyepig.2017.03.008>

[118] REIG, M., et al. Easy accessible blue luminescent carbazole-based materials for organic light-emitting diodes. *Dyes and Pigments* [interactive]. 2017, Vol. 137, 24–35. Access via the Internet: <https://doi.org/10.1016/j.dyepig.2016.09.062>

[119] KARPICZ, R., et al. Impact of intramolecular twisting and exciton migration on emission efficiency of multifunctional fluorene-benzothiadiazole-carbazole compounds. *The Journal of Chemical Physics* [interactive]. 2011, Vol. 134 (20), 204508. Access via the Internet: <https://doi.org/10.1063/1.3594047>

[120] HONG, Y., et al. Aggregation-induced emission. *Chemical Society Reviews* [interactive]. 2011, Vol. 40 (11), 5361. Access via the Internet: <https://doi.org/10.1039/C1CS15113D >

[121] KUKHTA, N. A., et al. Can Fluorenone-Based Compounds Emit in the Blue Region? Impact of the Conjugation Length and the Ground-State Aggregation. *Chemistry of Materials* [interactive]. 2017, Vol. 29 (4), 1695–1707. Access via the Internet: <http://dx.doi.org/10.1021/acs.chemmater.6b05158>

[122] XU, S., et al. An Organic Molecule with Asymmetric Structure Exhibiting Aggregation-Induced Emission, Delayed Fluorescence, and Mechanoluminescence. *Angewandte Chemie International Edition* [interactive]. 2014, Vol. 54 (3), 874–878. Access via the Internet: <https://doi.org/10.1002/anie.201409767 >

[123] CHO, D. W., et al. Intramolecular Exciplex and Intermolecular Excimer Formation of 1,8-Naphthalimide−Linker−Phenothiazine Dyads. *The Journal of Physical Chemistry B* [interactive]. 2006, Vol. 110 (10), 4576–4582. Access via the Internet: <https://doi.org/10.1021/jp056078p>

[124] HUNG, W.-Y., et al. Highly Efficient Bilayer Interface Exciplex For Yellow Organic Light-Emitting Diode. *ACS Applied Materials & Interfaces* [interactive].

2013, Vol. 5 (15), 6826–6831. Access via the Internet: <https://doi.org/10.1021/am402032z>

[125] HIGASHINO, T., et al. Air-stable n-channel organic field-effect transistors based on charge-transfer complexes including dimethoxybenzothienobenzothiophene and tetracyanoquinodimethane derivatives. *Journal of Materials Chemistry C* [interactive]. 2016, Vol. 4 (25), 5981–5987. Access via the Internet: <https://doi.org/10.1039/c6tc01532h>

[126] SARMA, M., and WONG, K.-T. Exciplex: An Intermolecular Charge-Transfer Approach for TADF. *ACS Applied Materials & Interfaces* [interactive]. 2018, Vol. 10 (23), 19279–19304. Access via the Internet: <https://doi.org/10.1021/acsami.7b18318>

[127] BRETON, G. W., and CRASTO, C. J. Substituted 2-(Dimethylamino)biphenyl-2′-carboxaldehydes as Substrates for Studying n→π* Interactions and as a Promising Framework for Tracing the Bürgi–Dunitz Trajectory. *The Journal of Organic Chemistry* [interactive]. 2015, Vol. 80 (15), 7375–7384. Access via the Internet: <http://dx.doi.org/10.1021/acs.joc.5b00766>

[128] SHIMIZU, M., et al. Twisting strategy applied to N,N-diorganoquinacridones leads to organic chromophores exhibiting efficient solid-state fluorescence. *Tetrahedron Letters* [interactive]. 2011, Vol. 52 (32), 4084–4089. Access via the Internet: < https://doi.org/10.1016/j.tetlet.2011.05.087>

[129] SHIMIZU, M., et al. 1,4-Bis(alkenyl)-2,5-dipiperidinobenzenes: Minimal Fluorophores Exhibiting Highly Efficient Emission in the Solid State. *Angewandte Chemie International Edition* [interactive]. 2009, Vol. 48 (20), 3653–3656. Access via the Internet: <https://doi.org/10.1002/anie.200900963>

[130] SWORAKOWSKI, J. How accurate are energies of HOMO and LUMO levels in small-molecule organic semiconductors determined from cyclic voltammetry or optical spectroscopy? *Synthetic Metals* [interactive]. 2018, Vol. 235, 125. Access via the Internet: <https://doi.org/10.1016/j.synthmet.2017.11.013>

[131] ZHAO, G.-J., and HAN, K.-L. Hydrogen Bonding in the Electronic Excited State. *Accounts of Chemical Research* [interactive]. 2011, Vol. 45 (3), 404–413. Access via the Internet: < https://doi.org/10.1021/ar200135h >

[132] ETHERINGTON, M. K., et al .Revealing the spin–vibronic coupling mechanism of thermally activated delayed fluorescence, *Nature Communications* [interactive], 2016, Vol. 7, 13680 1−7. Access via the Internet: <https://doi.org/10.1038/ncomms13680>

[133] SKUODIS, E., et al. Aggregation, thermal annealing, and hosting effects on performances of an acridan-based TADF emitter. *Organic Electronics* [interactive]. 2018, Vol. 63, 29–40. Access via the Internet: <https://doi.org/10.1016/j.orgel.2018.09.002>

[134] YANG, X., et. al. Functionalization of phosphorescent emitters and their host materials by main-group elements for phosphorescent organic light-emitting devices. *Chemical Society Reviews* [interactive]. 2015, Vol. 44 (23), 8484. Access via the Internet: <https://doi.org/10.1039/C5CS00424A>

[135] LI, X.-L., et. al. High-Efficiency WOLEDs with High Color-Rendering Index based on a Chromaticity-Adjustable Yellow Thermally Activated Delayed Fluorescence Emitter. *Advanced Materials* [interactive]. 2016, Vol. 28 (23), 4614. Access via the Internet: <https://doi.org/10.1002/adma.20150596>

[136] GANSCHOW, M. et. al. Dibenzobarrelene-Based Azaacenes: Emitters in Organic Light-Emitting Diodes. *Chemistry-A Europian Journal* [interactive]. 2017, Vol. 23 (18), 4415. Access via the Internet: < https://doi.org/10.1002/chem.201605820>

[137] COSTA, R. D. et. al. Luminescent ionic transition-metal complexes for light-emitting electrochemical cells. *Angewante Chemie Intnational Edition* [interactive]. 2012, Vol. 51 (33), 8178. Access via the Internet: <https://doi.org/10.1002/anie.201201471>

[138] SUBEESH, M. S. et. al. Phenanthroimidazole Derivative as an Easily Accessible Emitter for Non-Doped Light-Emitting Electrochemical Cells.The *Journal of Physical Chemistry C* [interactive]. 2015, Vol. 119 (41), 23676. Access via the Internet: <https://doi.org/10.1021/acs.jpcc.5b07871>

[139] FERNANDEZ, A. and VENDRELL, M. Smart fluorescent probes for imaging macrophage activity. *Chemical Society Reviews* [interactive]. 2016, Vol. 45 (5), 1182. Access via the Internet: <https://doi.org/10.1039/c5cs00567a>

[140] DE MOLINER et. al. Modern Synthetic Avenues for the Preparation of Functional Fluorophores. *Angewante Chemie International Edition* [interactive]. 2017, Vol. 56 (14), 3758. Access via the Internet: <https://doi.org/10.1002/anie.201609394>

[141] SAHOO, S. K. et. al. Iron(III) selective molecular and supramolecular fluorescent probes. *Chemical Society Reviews* [interactive]. 2012, Vol. 41 (21), 7195. Access via the Internet: <https://doi.org/10.1039/c2cs35152h>

[142] CAUSA, F. et. al. Supramolecular Spectrally Encoded Microgels with Double Strand Probes for Absolute and Direct miRNA Fluorescence Detection at High Sensitivity. *Journal of The American Chemical Society* [interactive]. 2015, Vol. 137 (5), 1758. Access via the Internet: <https://doi.org/10.1021/ja511644b>

[143] LOUDET, A. and BURGESS, K. BODIPY Dyes and Their Derivatives: Syntheses and Spectroscopic Properties. *Chemical Reviews* [interactive]. 2007, Vol. 107 (11), 4891. Access via the Internet: <https://doi.org/10.1021/cr078381n>

[144] KOWADA, T. et. al. BODIPY-based probes for the fluorescence imaging of biomolecules in living cells. *Chemical Society Reviews* [interactive]. 2015, Vol. 44 (14), 4953. Access via the Internet: <https://doi.org/10.1039/c5cs00030k>

[145] ZHAO, J., et al. The triplet excited state of Bodipy: formation, modulation and application. *Chemical Society Reviews* [interactive]. 2015, Vol. 44 (24), 8904–8939. Access via the Internet: <https://doi.org/10.1039/C5CS00364D >

[146] FRATH, D., et al. Luminescent Materials: Locking π-Conjugated and Heterocyclic Ligands with Boron(III). *Angewandte Chemie International Edition* [interactive]. 2014, Vol. 53 (9), 2290–2310. Access via the Internet: < https://doi.org/10.1002/anie.201305554>

[147] GLOTZBACH, C., et al. Fluorescent Modular Boron Systems Based on NNN- and ONO-Tridentate Ligands: Self-Assembly and Cell Imaging. *The Journal of Organic Chemistry* [interactive]. 2013, Vol. 78 (9), 4410–4418. Access via the Internet: <https://dx.doi.org/10.1021/jo4003745>

[148] MARKS, T., et al. Azacyanines of the Pyrrolopyrrole Series. *Chemistry - A European Journal* [interactive]. 2014, Vol. 20 (21), 6494–6504. Access via the Internet: <https://doi.org/10.1002/chem.201304235>

[149] LIU, Q., et al. Benzothiazole-enamide-based BF2 complexes: luminophores exhibiting aggregation-induced emission, tunable emission and highly efficient solid-state emission. *Journal of Materials Chemistry C* [interactive]. 2015, Vol. 3 (12), 2953–2959. Access via the Internet: <https://doi.org/10.1039/C4TC02876G >

[150] ZHOU, Y., et al. Novel binaphthyl-containing bi-nuclear boron complex with low concentration quenching effect for efficient organic light-emitting diodes. *Chemical Communications* [interactive]. 2010, Vol. 46 (35), 6512. Access via the Internet: <https://doi.org/10.1039/C0CC01715A >

[151] FRATH, D., et al. Chemistry on Boranils: An Entry to Functionalized Fluorescent Dyes. *Organic Letters* [interactive]. 2012, Vol. 14 (18), 4774–4777. Access via the Internet: <http://doi.org/10.1021/ol3020573>

[152] BENELHADJ, K., et al. 2-(2′-Hydroxyphenyl)benzimidazole and 9,10-Phenanthroimidazole Chelates and Borate Complexes: Solution- and Solid-State Emitters. *Organic Letters* [interactive]. 2013, Vol. 15 (12), 2918–2921. Access via the Internet: <http://doi.org/10.1021/ol400849a>

[153] KUBOTA, Y., et al. Synthesis and Fluorescence Properties of Thiazole–Boron Complexes Bearing a β-Ketoiminate Ligand. *Organic Letters* [interactive]. 2012, Vol. 14 (17), 4682–4685. Access via the Internet: <http://doi.org/10.1021/ol302179r>

[154] GRABARZ, A. M., et al. Photophysical Properties of Phenacylphenantridine Difluoroboranyls: Effect of Substituent and Double Benzannulation. *The Journal of*

Organic Chemistry [interactive]. 2017, Vol. 82 (3), 1529–1537. Access via the Internet: <http://dx.doi.org/10.1021/acs.joc.6b02732>

[155] WU, Y.-Y., et al. Large Stokes Shift Induced by Intramolcular Charge Transfer in N,O-Chelated Naphthyridine–BF2 Complexes. *Organic Letters* [interactive]. 2012, Vol. 14 (20), 5226–5229. Access via the Internet: <http://doi.org/10.1021/ol302347m>

[156] GRABARZ, A. M., et al. The Influence of the π-Conjugated Spacer on Photophysical Properties of Difluoroboranyls Derived from Amides Carrying a Donor Group. *The Journal of Organic Chemistry* [interactive]. 2016, Vol. 81(6), 2280–2292. Access via the Internet: <http://dx.doi.org/10.1021/acs.joc.5b02691>

[157] BEDNARSKA, J., et al. Two-photon absorption of BF2-carrying compounds: insights from theory and experiment. *Physical Chemistry Chemical Physics* [interactive]. 2017, Vol. 19 (8), 5705–5708. Access via the Internet: <https://doi.org/10.1039/C7CP00063D >

[158] FIN, A., et al. Oligothiophene Amphiphiles as Planarizable and Polarizable Fluorescent Membrane Probes. *Angewandte Chemie International Edition* [interactive]. 2012, Vol. 51 (51), 12736–12739. Access via the Internet: <https://doi.org/10.1002/anie.201206446 >

[159] KUBOTA, Y., et al. Synthesis and Fluorescence Properties of Pyrimidine Mono- and Bisboron Complexes. *The Journal of Organic Chemistry* [interactive]. 2013, Vol. 78 (14), 7058–7067. Access via the Internet: <https://doi.org/10.1021/jo400879g>

[160] PANDER, P., et. al. Thermally activated delayed fluorescence with a narrow emission spectrum and organic room temperature phosphorescence by controlling spin–orbit coupling and phosphorescence lifetime of metal-free organic molecules. *The Journal of Materials Chemistry C* [interactive]. 2018, Vol. 6 (20), 5434-5443. Access via the Internet: <https://doi.org/10.1039/c8tc00175h >

LIST OF PUBLICATIONS

Papers in the journals inscribed into the list approved by *Clarivate Analytics*:

1. Y. Danyliv, R. Lytvyn, D. Volyniuk, O. Bezvikonnyi, I. Hladka, J. V. Gražulevičius. Derivatives of carbazole and chloropyridine exhibiting aggregation induced emission enhancement and deep-blue delayed fluorescence. Dyes. Pigm., 2018; 149, 588–596. DOI: https://doi.org/10.1016/j.dyepig.2017.11.027
2. M. Potopnyk, R. Lytvyn, Y. Danyliv, M. Ceborska, O. Bezvikonnyi, D. Volyniuk, J. V. Gražulevičius. N,O π-Conjugated 4-Substituted 1,3-Thiazole BF2 Complexes: Synthesis and Photophysical Properties. J. Org. Chem., 2018; 83 (3), 1095–1105. DOI: https://doi.org/10.1021/acs.joc.7b02239
3. Y. Danyliv, D. Volyniuk, O. Bezvikonnyi, I. Hladka, K. Ivaniuk, I. Helzhynskyy, P. Stakhira, A. Tomkevičienė, L. Skhirtladze, J. V. Gražulevičius. Through-space charge transfer in luminophore based on phenyl-linked carbazole- and phthalimide moieties utilized in cyan-emitting OLEDs. Dyes. Pigm., 2020; 107833. DOI: https://doi.org/10.1016/j.dyepig.2019.107833

Attendance of international conferences:
1. Danyliv, Yan; Volyniuk, Dmytro; Gražulevičius, Juozas Vidas. Carbazolyl-containing imides as emitters with through-space charge-transfer: synthesis and properties // The 5th International Conference on the Physics of Optical Materials and Devices, Igalo, Montenegro, August 27-31, 2018 : Book of abstracts / 2018. p. 140.

2. Danyliv, Yan; Lytvyn, R.; Volyniuk, Dmytro; Bezvikonnyi, Oleksandr; Gražulevičius, Juozas Vidas. Novel donor-acceptor-donor materials based on difluorobenzene acceptor unit // Baltic polymer symposium 2017, Tallinn, Estonia, 20-22 September, 2017 / Tallinn : TTU. 2017, p. 77.

3. Danyliv, Yan; Lytvyn, Roman; Volyniuk, Dmytro; Hladka, Iryna; Bezvikonnyi, Oleksandr; Gražulevičius, Juozas Vidas. Hexafluorobenzene donor-acceptor-donor materials: synthesis and properties // State of the Art in Organic-only TADF OLEDs. From Theory to Applications: XXIInd International Krutyn Summer School 2017 Krutyń, Masurian Lake District, Poland, May 21-27, 2017 / 2017, p. 45.

4. Danyliv, Yan; Lytvyn, Roman; Volyniuk, Dmytro; Bezvikonnyi, Oleksandr; Gražulevičius, Juozas Vidas. One-step synthesis of donor-acceptor derivatives of pentachloropyridine, their modification and photophysical properties // Baltic polymer symposium 2016 : Klaipeda, September 21-24, 2016 : programme and abstracts / 2016. ISBN 9786090212356. p. 80.

5. Danyliv, Yan; Lytvyn, Roman; Bagdžiūnas, Gintautas; Volyniuk, Dmytro; Gražulevičius, Juozas Vidas. Synthesis and properties of 2-(9h-carbazol-9-yl)aniline imides : Y. Danyliv, R. Lytvyn, G. Bagdžiūnas, D. Volynyuk, J.V. Gražulevičius // Molecular crystals and liquid crystals : the jubilee 10th international conference on electronic processes in organic and inorganic materials, ICEPOM-10, May 23- 27, 2016, Ternopol, Ukraine. Oxon : Taylor & Francis. ISSN 1542-1406. 2016, p. 48.

6. Danyliv, Yan; Lytvyn, Roman; Bagdžiūnas, Gintautas; Kostiv, Nataliya; Volyniuk, Dmytro; Gražulevičius, Juozas Vidas. The convenient synthesis of carbazole substituted pyridines and their photophysical properties // Baltic polymer symposium 2015 : Sigulda, Latvia, September 16-18 : programe and proceedings / 2015. ISBN 9789934542121. p. 155.

ACKNOWLEDGMENTS